



National Library  
of Canada

Acquisitions and  
Bibliographic Services Branch

395 Wellington Street  
Ottawa, Ontario  
K1A 0N4

Bibliothèque nationale  
du Canada

Direction des acquisitions et  
des services bibliographiques

395, rue Wellington  
Ottawa (Ontario)  
K1A 0N4

*Your file    Votre référence*

*Our file    Notre référence*

## NOTICE

The quality of this microform is heavily dependent upon the quality of the original thesis submitted for microfilming. Every effort has been made to ensure the highest quality of reproduction possible.

If pages are missing, contact the university which granted the degree.

Some pages may have indistinct print especially if the original pages were typed with a poor typewriter ribbon or if the university sent us an inferior photocopy.

Reproduction in full or in part of this microform is governed by the Canadian Copyright Act, R.S.C. 1970, c. C-30, and subsequent amendments.

## AVIS

La qualité de cette microforme dépend grandement de la qualité de la thèse soumise au microfilmage. Nous avons tout fait pour assurer une qualité supérieure de reproduction.

S'il manque des pages, veuillez communiquer avec l'université qui a conféré le grade.

La qualité d'impression de certaines pages peut laisser à désirer, surtout si les pages originales ont été dactylographiées à l'aide d'un ruban usé ou si l'université nous a fait parvenir une photocopie de qualité inférieure.

La reproduction, même partielle, de cette microforme est soumise à la Loi canadienne sur le droit d'auteur, SRC 1970, c. C-30, et ses amendements subséquents.

End Depth and Flow Relationships for Smooth Open Trapezoidal  
and Circular Channels

Karl Ahlen

A Thesis  
in  
The Department  
of  
Civil Engineering

Presented in Partial Fulfilment of the Requirement for the  
degree of Master of Applied Science at Concordia University,  
Montreal Quebec Canada.

February 1994

©Karl Ahlen



National Library  
of Canada

Bibliothèque nationale  
du Canada

Acquisitions and  
Bibliographic Services Branch

Direction des acquisitions et  
des services bibliographiques

395 Wellington Street  
Ottawa, Ontario  
K1A 0N4

395, rue Wellington  
Ottawa (Ontario)  
K1A 0N4

*Your file    Votre référence*

*Our file    Notre référence*

The author has granted an irrevocable non-exclusive licence allowing the National Library of Canada to reproduce, loan, distribute or sell copies of his/her thesis by any means and in any form or format, making this thesis available to interested persons.

L'auteur a accordé une licence irrévocable et non exclusive permettant à la Bibliothèque nationale du Canada de reproduire, prêter, distribuer ou vendre des copies de sa thèse de quelque manière et sous quelque forme que ce soit pour mettre des exemplaires de cette thèse à la disposition des personnes intéressées.

The author retains ownership of the copyright in his/her thesis. Neither the thesis nor substantial extracts from it may be printed or otherwise reproduced without his/her permission.

L'auteur conserve la propriété du droit d'auteur qui protège sa thèse. Ni la thèse ni des extraits substantiels de celle-ci ne doivent être imprimés ou autrement reproduits sans son autorisation.

ISBN 0-315-90814-9

Name Karl Ahlen

Dissertation Abstracts International is arranged by broad, general subject categories. Please select the one subject which most nearly describes the content of your dissertation. Enter the corresponding four-digit code in the spaces provided.

Civil Engineering

SUBJECT TERM

0543 U·M·I

SUBJECT CODE

## Subject Categories

### THE HUMANITIES AND SOCIAL SCIENCES

#### COMMUNICATIONS AND THE ARTS

Architecture ..... 0729  
Art History ..... 0377  
Cinema ..... 0900  
Dance ..... 0378  
Fine Arts ..... 0357  
Information Science ..... 0723  
Journalism ..... 0391  
Library Science ..... 0399  
Mass Communications ..... 0708  
Music ..... 0413  
Speech Communication ..... 0459  
Theater ..... 0465

#### EDUCATION

General ..... 0515  
Administration ..... 0514  
Adult and Continuing ..... 0516  
Agricultural ..... 0517  
Art ..... 0273  
Bilingual and Multicultural ..... 0282  
Business ..... 0688  
Community College ..... 0275  
Curriculum and Instruction ..... 0727  
Early Childhood ..... 0518  
Elementary ..... 0524  
Finance ..... 0277  
Guidance and Counseling ..... 0519  
Health ..... 0680  
Higher ..... 0745  
History of ..... 0520  
Home Economics ..... 0278  
Industrial ..... 0521  
Language and Literature ..... 0279  
Mathematics ..... 0280  
Music ..... 0522  
Philosophy of ..... 0998  
Physical ..... 0523

Psychology ..... 0525  
Reading ..... 0535  
Religious ..... 0527  
Sciences ..... 0714  
Secondary ..... 0533  
Social Sciences ..... 0534  
Sociology of ..... 0340  
Special ..... 0529  
Teacher Training ..... 0530  
Technology ..... 0710  
Tests and Measurements ..... 0288  
Vocational ..... 0747

#### LANGUAGE, LITERATURE AND LINGUISTICS

Language  
General ..... 0679  
Ancient ..... 0289  
Linguistics ..... 0290  
Modern ..... 0291  
Literature  
General ..... 0401  
Classical ..... 0294  
Comparative ..... 0295  
Medieval ..... 0297  
Modern ..... 0298  
African ..... 0316  
American ..... 0591  
Asian ..... 0305  
Canadian (English) ..... 0352  
Canadian (French) ..... 0355  
English ..... 0593  
Germanic ..... 0311  
Latin American ..... 0312  
Middle Eastern ..... 0315  
Romance ..... 0313  
Slavic and East European ..... 0314

#### PHILOSOPHY, RELIGION AND THEOLOGY

Philosophy ..... 0422  
Religion  
General ..... 0318  
Biblical Studies ..... 0321  
Clergy ..... 0319  
History of ..... 0320  
Philosophy of ..... 0322  
Theology ..... 0469

#### SOCIAL SCIENCES

American Studies ..... 0323  
Anthropology  
Archaeology ..... 0324  
Cultural ..... 0326  
Physical ..... 0327  
Business Administration  
General ..... 0310  
Accounting ..... 0272  
Banking ..... 0770  
Management ..... 0454  
Marketing ..... 0338  
Canadian Studies ..... 0385  
Economics  
General ..... 0501  
Agricultural ..... 0503  
Commerce-Business ..... 0505  
Finance ..... 0508  
History ..... 0509  
Labor ..... 0510  
Theory ..... 0511  
Folklore ..... 0358  
Geography ..... 0366  
Gerontology ..... 0351  
History  
General ..... 0578

Ancient ..... 0579  
Medieval ..... 0581  
Modern ..... 0582  
Black ..... 0328  
African ..... 0331  
Asia, Australia and Oceania ..... 0332  
Canadian ..... 0334  
European ..... 0335  
Latin American ..... 0336  
Middle Eastern ..... 0333  
United States ..... 0337  
History of Science ..... 0585  
Law ..... 0398  
Political Science  
General ..... 0615  
International Law and Relations ..... 0616  
Public Administration ..... 0617  
Recreation ..... 0814  
Social Work ..... 0452  
Sociology  
General ..... 0626  
Criminology and Penology ..... 0627  
Demography ..... 0938  
Ethnic and Racial Studies ..... 0631  
Individual and Family Studies ..... 0628  
Industrial and Labor Relations ..... 0629  
Public and Social Welfare ..... 0630  
Social Structure and Development ..... 0700  
Theory and Methods ..... 0344  
Transportation ..... 0709  
Urban and Regional Planning ..... 0999  
Women's Studies ..... 0453

### THE SCIENCES AND ENGINEERING

#### BIOLOGICAL SCIENCES

Agriculture  
General ..... 0473  
Agronomy ..... 0285  
Animal Culture and Nutrition ..... 0475  
Animal Pathology ..... 0476  
Food Science and Technology ..... 0359  
Forestry and Wildlife ..... 0478  
Plant Culture ..... 0479  
Plant Pathology ..... 0480  
Plant Physiology ..... 0817  
Range Management ..... 0777  
Wood Technology ..... 0746  
Biology  
General ..... 0306  
Anatomy ..... 0287  
Biostatistics ..... 0308  
Botany ..... 0309  
Cell ..... 0379  
Ecology ..... 0329  
Entomology ..... 0353  
Genetics ..... 0369  
Limnology ..... 0793  
Microbiology ..... 0410  
Molecular ..... 0307  
Neuroscience ..... 0317  
Oceanography ..... 0416  
Physiology ..... 0433  
Radiation ..... 0821  
Veterinary Science ..... 0778  
Zoology ..... 0472  
Biophysics  
General ..... 0786  
Medical ..... 0760

#### EARTH SCIENCES

Biogeochemistry ..... 0425  
Geochemistry ..... 0996

Geodesy ..... 0370  
Geology ..... 0372  
Geophysics ..... 0373  
Hydrology ..... 0388  
Mineralogy ..... 0411  
Paleobotany ..... 0345  
Paleoecology ..... 0426  
Paleontology ..... 0418  
Paleozoology ..... 0985  
Palynology ..... 0427  
Physical Geography ..... 0368  
Physical Oceanography ..... 0415

#### HEALTH AND ENVIRONMENTAL SCIENCES

Environmental Sciences ..... 0768  
Health Sciences  
General ..... 0566  
Audiology ..... 0300  
Chemotherapy ..... 0992  
Dentistry ..... 0567  
Education ..... 0350  
Hospital Management ..... 0769  
Human Development ..... 0758  
Immunology ..... 0982  
Medicine and Surgery ..... 0564  
Mental Health ..... 0347  
Nursing ..... 0569  
Nutrition ..... 0570  
Obstetrics and Gynecology ..... 0380  
Occupational Health and Therapy ..... 0354  
Ophthalmology ..... 0381  
Pathology ..... 0571  
Pharmacology ..... 0419  
Pharmacy ..... 0572  
Physical Therapy ..... 0382  
Public Health ..... 0573  
Radiology ..... 0574  
Recreation ..... 0575

Speech Pathology ..... 0460  
Toxicology ..... 0383  
Home Economics ..... 0386

#### PHYSICAL SCIENCES

Pure Sciences  
Chemistry  
General ..... 0485  
Agricultural ..... 0749  
Analytical ..... 0486  
Biochemistry ..... 0487  
Inorganic ..... 0488  
Nuclear ..... 0738  
Organic ..... 0490  
Pharmaceutical ..... 0491  
Physical ..... 0494  
Polymer ..... 0495  
Radiation ..... 0754  
Mathematics ..... 0405  
Physics  
General ..... 0605  
Acoustics ..... 0986  
Astronomy and Astrophysics ..... 0606  
Atmospheric Science ..... 0608  
Atomic ..... 0748  
Electronics and Electricity ..... 0607  
Elementary particles and High Energy ..... 0798  
Fluid and Plasma ..... 0759  
Molecular ..... 0609  
Nuclear ..... 0610  
Optics ..... 0752  
Radiation ..... 0756  
Solid State ..... 0611  
Statistics ..... 0463  
Applied Sciences  
Applied Mechanics ..... 0346  
Computer Science ..... 0984

Engineering  
General ..... 0537  
Aerospace ..... 0538  
Agricultural ..... 0539  
Automotive ..... 0540  
Biomedical ..... 0541  
Chemical ..... 0542  
Civil ..... 0543  
Electronics and Electrical ..... 0544  
Heat and Thermodynamics ..... 0348  
Hydraulic ..... 0545  
Industrial ..... 0546  
Marine ..... 0547  
Materials Science ..... 0794  
Mechanical ..... 0548  
Metallurgy ..... 0743  
Mining ..... 0551  
Nuclear ..... 0552  
Packaging ..... 0549  
Petroleum ..... 0765  
Sanitary and Municipal ..... 0554  
System Science ..... 0790  
Geotechnology ..... 0428  
Operations Research ..... 0796  
Plastics Technology ..... 0795  
Textile Technology ..... 0994

#### PSYCHOLOGY

General ..... 0621  
Behavioral ..... 0384  
Clinical ..... 0622  
Developmental ..... 0620  
Experimental ..... 0623  
Industrial ..... 0624  
Personality ..... 0625  
Physiological ..... 0989  
Psychobiology ..... 0349  
Psychometrics ..... 0632  
Social ..... 0451



This is to certify the thesis prepared

and submitted in partial fulfilment of the requirements for  
the degree of

Signed by the final examining committee:

Supervisor \_\_\_\_\_  
Co-Supervisor \_\_\_\_\_

Don Kene  
Dean of Faculty

# ABSTRACT

## End Depth and Flow relationships for Smooth Open Trapezoidal and Circular Channels

Karl Ahlen

The current study's objective was to obtain an accurate relationship between the end depth  $Y_e$  and the discharge rate for smooth open channels with trapezoidal and circular cross sections. To accomplish this, the momentum equation was used. The velocity and pressure head distributions at the end depth  $Y_e$  were determined to obtain the corresponding velocity and pressure coefficients, ( $\alpha$ ,  $\beta$  and  $K$ ).

The pressure head readings were obtained through the use of a static Pitot tube. Velocity readings were obtained through the use of a Pitot tube and a Laser Doppler Anemometer(LDA) system. The velocity measurements with the Pitot tube utilised procedures to take into account the curvilinear nature of the flow in the  $Y_e$  region.

The present investigation improves on existing studies in several ways.

- (1) The velocities over the entire end depth and critical depth sections for circular and trapezoidal cross sectional channels were measured over a range of flow conditions.
- (2) The pressure distribution at the end depth section

for circular and trapezoidal cross sectional channels were measured to incorporate the pressure force term in the momentum analysis.

- (3) The pressure and velocity coefficients  $K$ ,  $\alpha$ , and  $\beta$  were evaluated based on the velocity and pressure distribution data.
- (4) Pressure head values were also calculated indirectly at the end depth section using velocity distribution data for circular and trapezoidal cross sectional channels.

Another aspect of the study was the improved analysis of the momentum equation with the calculation of  $\alpha$  and  $\beta$  coefficients for both circular and trapezoidal channels.

The improved analysis of the momentum equation provides for a more accurate functional relationship between the two flow variables. This would permit the establishment of a simple method for monitoring the flow rate in existing channels at their discharge point.

## Acknowledgements

I would like to thank Dr. Balachandar for suggesting the topic and agreeing to be my supervisor. For providing me with advice and being my co-supervisor, I would like to thank Dr. Ramamurthy. In helping me with the installation of laboratory equipment I would like to thank Messrs N.Lang Vo, and Danny Roy of the Hydraulics Lab. For help in fabricating the experimental equipment used in this thesis, I would like to thank Mr. Paul Scheiwiller and the machine shop staff of the engineering faculty.

For giving me financial and emotional support over the years to help me finish my studies, I would like to thank my parents Anna and Arne Ahlen.



## Table of Contents

List of Figures . . . . .	ix
List of Tables . . . . .	xi
Symbols and Abbreviations . . . . .	.xiii
Chapter 1 Introduction	
1.0 General Remarks . . . . .	1
1.1 Scope of Study . . . . .	2
Chapter 2 Literature Review	
2.0 Introduction . . . . .	4
2.1 Literature Review Trapezoidal Channel . . . . .	4
2.2 Literature Review Circular Channel. . . . .	5
2.3 Theoretical Considerations . . . . .	7
Chapter 3 Equipment and Procedure	
3.0 Introduction . . . . .	9
3.1 Trapezoidal Equipment Set up . . . . .	9
3.1.1 Laser Doppler Anemometer(LDA) Probe Positioning . . . . .	.10
3.2 Circular Equipment Setup . . . . .	.10
3.2.1 Laser Doppler Anemometer(LDA) Probe Positioning . . . . .	.11
3.3 Laser . . . . .	.11
3.4 Experimental Procedure . . . . .	.13
3.4.1 Critical Depth( $Y_c$ )/End depth( $Y_e$ ) measurements . . . . .	.13

3.4.2 Pressure Head measurements . . . . .	.13
3.4.3 Velocity measurements by a Pitot Tube in Curvilinear flow . . . . .	.14
3.4.3.1 Calculation of $U_x, U_r$ and $U_y$ . . . . .	15
3.4.4 LDA Measurements . . . . .	.16
3.4.5 Determination of Coefficients . . . . .	.17
3.4.6 Verification of Momentum Equation . . . . .	.19
3.4.7 Energy Equation . . . . .	.20

## Chapter 4 Results

4.0 Introduction . . . . .	22
4.1 Observations . . . . .	22
4.1.1 Pressure Head measurements. . . . .	22
4.1.2 $Y_a/Y_c$ vs Q Comparisons. . . . .	24
4.1.3 Velocity Measurements (Pitot Tube). . . . .	25
4.1.4 (a) Velocity Measurements Trapezoidal Channel using LDA . . . . .	25
4.1.4 (b) Laser Velocity Measurements Circular Channel using LDA . . . . .	26
4.1.5 Comparisons between pitot tube and laser measurements . . . . .	28
4.1.6 Flow Profile . . . . .	28
4.2 Calculated Pressure Coefficients . . . . .	29
4.3 Calculated Velocity Coefficients, $\alpha$ and $\beta$ . . . . .	31
4.4 The Momentum Discussion . . . . .	32
4.5 Discussion on Energy Equation. . . . .	34

4.5.1 Application from the critical section to end depth section . . . . .	34
4.5.2 Application over the vertical end depth section . . . . .	35
4.6 Momentum Discussion with Calculated Pressure Data for Circular Channel . . . . .	36
4.7 Discussion using Free Vortex . . . . .	37
Chapter 5 Conclusions	
5.0 General Remarks . . . . .	39
5.0.1 Trapezoidal Channel . . . . .	39
5.0.2 Circular Channel . . . . .	39
5.0.3 Calculated $P/\gamma$ values . . . . .	40
5.0.4 Concluding Remarks . . . . .	40
5.1 Recommendations . . . . .	40
References . . . . .	41
Appendix A Figures . . . . .	44
Appendix B Computer Program. . . . .	77
Appendix C Sample Calculations . . . . .	89
Appendix D Uncertainty Analysis . . . . .	105
Appendix E Sample Results. . . . .	107

## List of Figures

Fig. 2.1 ( Chart on Previous Studies (a), (b), (c)) . . . . .	45
Fig. 3.1 ( Trapezoidal channel set up) . . . . .	48
Fig. 3.2 ( Circular Channel set up ) . . . . .	49
Fig. 3.3 ( Laser Stand set up for Trapezoidal Channel) .	50
Fig. 3.4 ( Pressure Taps on Circular Channel) . . . . .	51
Fig. 3.5 ( Laser stand set up for circular channel (a), (b) ) . . . . .	52
Fig. 3.6 ( Location of Pressure Taps ) . . . . .	54
Fig. 3.7 ( Pitot Tube Mounting ) . . . . .	55
Fig. 4.1 ( Pressure Field for Trapezoidal Channel) . . .	56
Fig. 4.2 ( Pressure Field for Circular Channel) . . . .	57
Fig. 4.3 ( Variation of P with $Y_1/Y$ :centre line ) . . . .	58
Fig. 4.4 ( Variation of P with $Y_1/Y$ :Wall Pressure Head ) . . . . .	59
Fig. 4.5 ( Pressure comparisons ) . . . . .	60
Fig. 4.6 ( Definition Sketch used by Keller) . . . . .	61
Fig. 4.7 ( Variation of $nY_e/b$ vs $Q^2m^3/gB^5$ ) . . . . .	62
Fig. 4.8 ( End depth comparisons for Circular Channel ) .	63
Fig. 4.9 ( Comparisons with Smith(1962) Data ) . . . .	64
Fig. 4.10 ( Velocity Profile For Pitot Tube(a) (b)) (+ Comparisons with Velocity Profiles of Different Channels(c)) . . . . .	65
Fig. 4.11 ( Velocity Profile for Laser Trapezoidal Measurements(a), (b), (c)) . . . . .	68

Fig. 4.12 ( Velocity Profile for Circular Laser	
Measurements (a), (b), (c)) . . . . .	.71
Fig. 4.13 ( Variation of K ) . . . . .	.74
Fig. 4.14 ( Comparing K Values ) . . . . .	.75
Fig. 4.15 (Comparisons of Velocity Distribution at $Y_e$	
and $Y_c$ ) . . . . .	.76

## List of Tables

Table 3.1 Pressure Coefficients . . . . .	.18
Table 3.2 Velocity Coefficients. . . . .	.19
Table 4.1 Calculated Pressure Coefficients . . . . .	.30
Table 4.2 Momentum Analysis for Trapezoidal Channel. . . . .	.33
Table 4.3 Momentum Analysis for Circular Channel . . . . .	.33
Table 4.4 Comparisons of Calculated and Measured $P/\gamma$ values . . . . .	.35
Table 4.5 Momentum Analysis with calculated Pressures for Circular Channel . . . . .	.36
Table C.1 Calculation Table . . . . .	.94
Table C.2 Converting Cylindrical Coordinates to Rectangle Coordinates for $Y_e=11.91$ . . . . .	.97
Table C.3 Sample Data For Calculating Pressure Heads(Circular) . . . . .	.99
Table C.4 Sample Data For Calculating Pressure Heads(Trapezoidal) . . . . .	.99
Table C.5 Pressure Force Calculation . . . . .	101
Table E.1 Results from Laser Readings for Trapezoidal Channel . . . . .	.108
Table E.2 Velocity at Critical Section for Trapezoidal Channel . . . . .	.110
Table E.3 LDA Readings for Circular Channel, $Q=40.71$ l/s .	.111
Table E.4 LDA Readings for Circular Channel, $Q=31.74$ l/s .	.112
Table E.5 Pressure Field Data for Circular Pipes. . . . .	.113

Table E.6 Sample Manometer Data for Circular Channel. . .	.114
Table E.7 Pressure Field Data for Trapezoidal Channel . .	.115
Table E.8 Manometer Data For $Q=34.32$ l/s . . . . .	.116

## Symbols and Abbreviations

A = cross sectional area

B = Width of Channel.

D and  $D_o$  = Diameter of Pipe

G =  $9.81 \text{ m/s}^2$  (gravitational constant)

H = Pressure head  $P/\gamma$

K = pressure coefficient

M = momentum

Q = Flow rate

P = pressure

V or v = velocity

Y = Depth

Subscript e = end depth section

Subscript c = critical depth section

$r = Y_e/Y_c$

$v_m$  = maximum velocity

z = elevation

$\gamma = 9870 \text{ N/m}^3$

$\alpha'$  = Pressure distribution coefficient

$\beta'$  = Pressure distribution coefficient

$\alpha$  = Corolis coefficient

$\beta$  = Momentum Coefficient



# Chapter 1 Introduction

## 1.0 General Remarks

To predict the discharge in open channels, earlier studies have been conducted to determine a functional relationship between the flow rate  $Q$  and end depth  $Y_e$ . End depth relationships have been studied more extensively for the rectangular cross sectional channels than for circular and trapezoidal cross section channels. See Fig. 2.1 for a summary of previous studies.

End depth pressure and velocity fields are also available for rectangular, (Rajaraman et al 1968)) and triangular, (Repologle(1962)) cross sectional channels. Keller et al (1989) generated a pressure coefficient  $K$ , from data of the previous authors who investigated triangular and rectangular channels. The present investigation has attempted to validate the assumptions utilised in the above mentioned study. It may be noted that none of the earlier investigations had determined the nature of alpha ( $\alpha$ ) and beta ( $\beta$ ) coefficient (Table 3.2) for circular and trapezoidal channels.

This study aims to verify basic assumptions in formulating the governing equations relating the main geometric and hydrodynamic parameters. The refinement of existing relationships between parameters was done with the

use of data collected with an Laser Doppler Anemometer (LDA) system. It should be noted that the  $\alpha$  and  $\beta$  coefficients have not been evaluated for either the circular or trapezoidal channels in previous studies. These coefficients were determined experimentally in the current study and used to accurately evaluate the momentum equation (Eq 2.3).

### 1.1 Scope of Study

The present study was mainly experimental and the analysis is limited to the interpretation of test data collected. The objectives of the study were as follows;

- (1) Using the Pitot and Static Pitot tube
  - (a) The pressure field for both the circular and trapezoidal open channels at the end depth and critical depth sections were measured.
  - (b) The velocities for both channels at the end depth and critical sections were measure.
- (2) Using the Laser Doppler Anemometer (LDA) data
  - (a) The three main velocity components in the trapezoidal and circular open channels were determined
  - (b) The  $\alpha$  and  $\beta$  coefficients for both the trapezoidal and circular open channels were evaluated and the assumptions made in some of

the previous studies were validated.

- (c) The momentum equation (Eq 2.3) was used to refine the  $Q=F(Y_o)$  more accurately based on the velocity and pressure distribution data.
- (d) The Pressure head ( $P/\gamma$ ) values were calculated from the measured velocity distribution data and compared it with the direct static probe pressure measurements.

# Chapter 2 Literature Review

## 2.0 Introduction

To predict discharge in horizontal circular or trapezoidal channels, it is desirable to have a simple and accurate method. This method could use the end depth as a single measurement to evaluate the discharge and reduce errors. Several studies have been carried out on this topic for both channels.

## 2.1 Literature Review on Trapezoidal Channels

There have been numerous studies on end depths in rectangular channels while fewer studies related to trapezoidal channels. The first study into end depth relationships in rectangular channels was done by Rouse (1936) for which the  $Y_e/Y_c$ , end depth vs critical depth, ratio 0.72 was determined. Diskin(1961) performed experiments on trapezoidal channels relating  $Y_e$  to the discharge. Charts describing some of the previous studies on end depths in various types of channels are shown in Fig. 2.1.

Rajaratnam et al (1968) and Replogle (1962) performed velocity measurements in the vicinity of the end depth section in open channels with various geometries. Replogle(1962) measured the velocity profile in rectangular and triangular

sections. Rajaratnam et al (1968) measured velocity distributions in rectangular channels and calculated the  $\beta$  coefficient. The coefficient  $\beta$  ranged from 1.074 to 1.148.

There have been several recent studies to determine the nature of the  $Y_e/Y_c$  ratio for trapezoidal channels. For instance, Keller et al (1989) assumed a pressure distribution coefficient,  $K$ , (Table 3.1) from previously measured data for rectangular and triangular channels. For a rectangle channel of width  $B$ , Ferro (1992) showed that for  $0.8 < B/Y_e < 17.9$  the ratio  $Y_e/Y_c$  did not change. Gupta et al (1993) obtained a dimensionless calibration curve relating  $(Qm^{1.5}/g^{0.5}B^{2.5})$  with  $(e^{5.5(S_0)}mY_e/B)$  for predicting the discharge  $Q$  with  $Y_e$  known.  $B$  was the bottom width of the channel,  $m$  was the slope of the side walls and  $S_0$  was the slope of the channel. For the present investigation,  $S_0$  was always zero. See Fig 3.1 for definition sketch.

## 2.2 Literature Review on Circular Channels

Both Smith 1962, and Rajaratnam et al 1964(b) investigated the end depth in horizontal circular channels. The studies were based solely on end depth to discharge measurements.

Smith (1962) investigated the relationship between end depth and discharge. A relationship between  $A_e/A_c$ , ratios of areas of the end depth and critical sections, and  $Y_e/D$  was

found.

Rajaratnam et al (1964) (b) investigation determined that the  $Y_e/Y_c$  ratio for horizontal circular channels was 0.725. The  $Y_e/Y_c$  ratio remained constant until the  $Y_c/D$  ratio was greater than 0.9. Rajarantam et al(1964) performed a theoretical analysis to determine a pressure factor to account for nonhydrostatic conditions. This factor was not verified through experimental investigations.

Diskin(1962) stated that a linear relationship could be generated by comparing  $Y_e/D$  vs  $Q/G^{0.5}D^{2.5}$ . An equation illustrating the relationship was generated(Eq 2.1).

$$\frac{Q}{(gD^5)^{0.5}} = 1.82 \left( \frac{Y_e}{D_o} \right)^{1.96} \quad 2.1$$

Eq 2.2 shows a relationship of  $Y_e/Y_c$  with changing pipe diameter.

$$\left( \frac{Y_e}{Y_c} \right) = \frac{0.72}{\left( \frac{Y_c}{D_o} \right)^{0.005}} \quad 2.2$$

Diskin(1963) observed the  $Y_e/Y_c$  ratio to be higher than that obtained by Rajaratnam et al (1964) (b). For a ten inch diameter pipe, Diskin(1963) found the ratio  $Y_e/Y_c$  ranged from 0.785 to 1, when the  $Y_c/D_o$  ratio ranged from 0.5 to 0.132. Diskin (1963) also noted several objections to using the end depth as a measuring device. These were the existence of cross waves and a hump in the transverse section. Measuring the depth further upstream was proposed as an alternative device.

Other authors, (Argyropouls et al (1964)), expanded further on equations developed by Rajaratnam et al(1964) and Smith(1962). Compared using the end depth ratio to different formulas developed earlier for predicting the flow rates.

## 2.3 Theoretical Considerations

The governing equation for the end depth problem for both the trapezoidal and circular channel is the momentum equation. Eq 2.3.

$$P_e + M_e = P_c + M_c - F_L \quad 2.3$$

Here the pressure and momentum terms are represented by P and M. The suffixes e and c denote the end depth and critical sections(see Fig 3.1 for definitions).  $F_L$  represents the friction force. A thorough presentation of the derivation and analysis of the governing equation is presented by the several earlier investigators;( Rouse 1936, Diskin 1964, Rajaratnam 1962, and Neogy 1972).

The components of pressure and momentum at the end depth could not be evaluated easily on the basis of test data, as the flow is highly curvilinear at the end depth section. Since the stream lines were curvilinear, hydrostatic rules could not be applied. To evaluate the component terms, the following equations had to be used, (Rajarantam et al 1964 and 1968).

$$P_o = 0.5 K_1 Y_o \gamma A_o \quad 2.4$$

$$M_o = \frac{\gamma Q^2}{g} \frac{1}{A_o} \beta \quad 2.5$$

For an accurate evaluation of  $P_o$  and  $M_o$ ,  $K_1$ , a coefficient to account for nonhydrostatic conditions, and  $\beta$  had to be evaluated. To accurately evaluate  $K_1$  and  $\beta$ , experiments had to be performed. The  $\beta$  coefficient in previous studies had been assumed to be 1.0. This assumption would be examined in this study.

The  $\alpha$  coefficient for the velocity had to be determined for use in the energy equation. The true velocity head is denoted by,  $\alpha V^2/2g$ . Alpha is known as the energy coefficient (Coriolis coefficient). It is generally not equal to unity when the flow is curvilinear.



# Chapter 3 Equipment and Procedure

## 3.0 Introduction

The experiment was performed on two different apparatus. A diagram of each experimental layout is shown in Fig. 3.1, Trapezoidal channel, and 3.2, Circular channel.

## 3.1 Trapezoidal channels Equipment Set up

The smooth stainless steel horizontal channel used in this experiment had a bottom width (B) of 0.127 m, side slopes (m) of 1:1 and a height of 0.334 m (see Fig. 3.1). It was 6.85 meters long. The end section (0.70 m long) was constructed of clear plexiglass to facilitate Laser Doppler Anemometer (LDA) measurements.

Screens and a fine mesh were set up 0.50 m before the entrance to the channel to reduce large scale turbulence. A low resistance mesh, (1cm by 1cm), was placed just in the entrance to the trapezoidal channel and 0.52 m into the channel to reduce scalar turbulence in the channel. The discharge was measured with the use of a standard V-notch.

### 3.1.1 Laser Doppler Anemometer (LDA) Probe Positioning

A diagram of the laser mount is shown in Fig. 3.3. The moving mechanism as illustrated in Fig. 3.3 was used to move the laser probe in steps of 1mm. The probe was placed in two different orientations and was always normal to the channel walls. When the probe was placed in position 1 (Fig 3.3) the axial velocity  $U_z$  and lateral velocity  $U_x$  were measured in the rectangular sub section of the trapezoidal channel. In position 2 (Fig 3.3) the probe measured the axial velocities  $U_z$  in the triangular sub section of the channel.

### 3.2 Circular Channel Equipment Setup

A diagram of the circular channel is shown in Fig. 3.2. It consisted of a head tank that funnelled water into a horizontal circular pipe. The pipe was 10 meters long and 0.3048 m in diameter. At the end depth section water flowed into a tail gate box and was then channelled into a standard V-notch.

A square to circular transition section was placed at the channel entrance to greatly reduce turbulence and entrance head losses. Sufficient damping devices (screens, honeycombs) were placed in the head box to reduce larger scale turbulence.

### 3.2.1 Laser Doppler Anemometer (LDA) Probe Positioning

For laser measurements in a circular pipe, the laser probe had to be positioned perpendicular to the channel axis to reach locations along a radial axis. Along with this requirement, the probe also had to be moved parallel to the channel axis. The LDA probe measured velocities in the  $\theta$  and  $z$  directions (Fig 3.4). The velocities in the radial ( $r$ ) direction were calculated using the  $U_z$  and  $U_\theta$  data because  $U_r$  could not be measured. (Appendix C)

Diagrams of the laser probe mount are shown in Fig. 3.5(a) & (b). The mount consisted of a circular sleeve that was concentric to the channel and had two flanges attached to it. The two flanges were for circular rotation around the pipe at a fixed axial location. A mechanism was attached to the outer flange to allow for radial motion of the probe.

The laser mount could be moved accurately to the nearest 1 mm for linear motion and 2 degrees for circular motion.

### 3.3 Laser Doppler Anemometer (LDA)

The laser doppler anemometer (LDA) system used in this study was supplied by Dantec Inc. It consisted of an argon ion laser that measured velocity in two directions. The power of

the laser was 300 mw. The laser light was first directed through a transmitter that split the beam in two. After the laser beams had gone through the transmitter, they were directed through fibre optic cables to the probe. There were four laser beams coming out of the probe. Two of them were blue and the other two were green. The diameter of the beams were 1.35 mm and their wave lengths were 488.0 nm(blue) and 514.5 nm(green). The beam spacing was 38 mm and there were 35 fringes. The probe system had a light transmitting efficiency caused by the interference phenomena of about 70%.

Velocity was calculated by measuring the light scattered when extraneous particles crossed the fringe. The fringes were located in the measuring volume at the focal point of the beams. Velocity was calculated by the following equation based on manufactures calibration data.

$$U = f_d d_f = f_d \frac{\lambda}{2 \sin(\frac{\theta}{2})} \quad 3.1$$

U= Component of velocity in the plane of the two laser beams and perpendicular to their bisector.

$f_d$ = Doppler frequency,  $d_f$ = fringe spacing

$\lambda$  = Wavelength of laser light,  $\theta$  = beam intersection angle

In the current study the collection and transmitting of light was done with one probe operating in the backward scatter mode.

### 3.4 Experimental Procedure

#### 3.4.1 Critical Depth( $Y_c$ )/End depth( $Y_e$ ) measurements

End depths, surface water profiles and side water profiles, were measured by a metric depth gauge which had an resolution of 0.10 mm. The total flow rate was measured by passing flow over a standard V-notch and using standard procedures to calculate the flow rate( $Q$ ). Critical depths ( $Y_c$ ) were calculated by using standard methods(Chow 1959). The equations used are listed below.

For Circular Channels;

$$Y_c = 0.325 \left( \frac{Q}{D_o} \right)^{\frac{2}{3}} + 0.083 (D_o) \quad 3.2$$

For Trapezoidal Channels

$$\frac{0.5(0.127 + Y_c) Y_c}{0.127 + 2Y_c} = \frac{\left( \frac{Q}{(0.127 + Y_c) Y_c} \right)^2}{2g} \quad 3.3$$

#### 3.4.2 Pressure Head Measurements

Wall pressure heads were measured using manometers. A diagram of pressure tap locations are shown in Fig. 3.4 and 3.6. The pressure taps were 1.6 mm in diameter. The manometers could measure the pressure head to the nearest 0.1 mm.

The manometers displayed the static head  $((P/\gamma)+z)$ . To obtain the true  $(P/\gamma)$  value, a datum was established. The datum was the bottom elevation of the channels when  $(P/\gamma)=0$ .

To determine the pressure distribution in the channel flow, a static pitot tube was used. The static pitot tube measured the static head  $(P/\gamma+z)$  at any point. Used the same datum established for wall pressure head readings.

A diagram showing the set up for the Pitot tube is shown in Fig.3.7.

### 3.4.3 Velocity Measurements by a Pitot Tube in Curvilinear Flow.

A static pitot tube, in conjunction with a pitot tube, was used to measure the velocity in curvilinear flow. The pitot tube was used to measure the dynamic head,  $(P/\gamma + z + U_z^2/2g)$ . Velocity head was calculated by subtracting the static head,  $(P/\gamma + z)$  from the dynamic head,  $(P/\gamma + z + U_z^2/2g)$ , to get  $U_z^2/2g$  and subsequently  $U_z$ . Additional details on the orientation of the axis are provided in Fig. 3.4 and 3.6.

When taking velocity measurements at the end depth, the static and dynamic pressure readings were taken at the exact same location.

### 3.4.3.1 Calculation of $U_y$ , $U_x$ , and $U_z$

The velocity  $U_y$  had to be calculated in both the circular and trapezoidal channels using both LDA and pitot tube data by the following procedure:

- (1) The slope of the water surface at the end depth section was measured. The  $y$  and  $z$  components of the velocity at any point at the end depth section were related by the following relationship,  $dy/dz = U_y/U_z$  along any stream line. The  $dy/dz$  ratio was determined by measuring the slope of the water surface and then fitting an equation to the profile by the least square method.
- (2) The slope  $dy/dz$  of stream lines was assumed to linearly increase from zero at the channel bottom, to a maximum at the water surface.
- (3)  $Dy/dz$  was obtained by multiplying the elevation of pitot tube measurement by the  $dy/dz/y$  ratio. Then multiplied the  $dy/dz$  ratio by  $U_z$ , which was measured, to obtain  $U_y$ .

For calculating  $U_r$  in the circular channel, the continuity relation was used. An initial value of  $U_r$  near the core of the channel was calculated by relating  $U_r$  to  $U_y$  by the following equation  $U_r = U_y/\cos \theta$ . The rest of the values for  $U_r$  were calculated using the continuity relationship. (Appendix

C Sample Calculations).

Used the measured value of  $U_z$  and the calculated value of  $U_y$  along with the continuity principle to determine  $U_x$  in the triangular section( Fig. 4.6) of the trapezoidal channel.

### 3.4.4 LDA Measurements

The process of measuring velocities with the laser was more involved than with the pitot tube. First the velocities could not be measured exactly at the end depth due to the disposition of the laser beams. To measure the velocity with the beams, both beams had to pass through a nearly flat surface. At the end depth section, both beams do not traverse the fluid through similar paths. Velocities at several axial locations  $z=1.5, 3, 6$  cm upstream of the end depth section had were measured. Extrapolation techniques were then used to calculate the end depth velocities. Three locations upstream of the end depth section were considered a minimum for extrapolation purposes.

For the LDA system, continuous and repetitive modes were available. When running on continuous mode, data was saved to a file. In the repetitive mode, the average velocity on the screen along with a histogram were displayed. Both modes were used in this study. A typical velocity histogram is shown in Appendix E.



### 3.4.5 Determination of Pressure and Velocity Coefficients

In analyzing the results, several coefficients had to be determined due to the nonuniform velocity and pressure distributions. These included the  $\alpha$ ,  $\alpha'$ ,  $\beta$  and  $\beta'$  coefficients (Table 3.1-3.2) for velocity and pressure distributions. Other pressure coefficients were calculated ( $K, K_a$ ), and used in calculating the pressure force. The pressure force is used in the momentum equation. The coefficients were used to account for non hydrostatic conditions at the end depth.

To calculate these coefficients, two different computer programs were written. One was for calculating the velocity coefficients and the other for pressure coefficients. (Table 3.1).

The source code and flow charts for all the programs are included in Appendix B. All programs were written in Turbo Pascal 6.0.

Table 3.1 (Pressure Coefficients)

Author	Formula	Computer Method
Chow (1959)	$\alpha^1 = 1 + \frac{1}{Qy} \int_0^A cv da$ $\beta^1 = \frac{1}{AZ} \int_0^A cdA + 1$	A = Total area of the integral dA $v = Q/A$ $C = v^2/g$ $z = 2/3 Y_e$
Rajaratnam (1968) Rouse (1936) and more	$P_e = AK_e \frac{\gamma Y_e}{2}$	$P = (p/\gamma) * \gamma * A * 0.5$ $K1 = P / (A * 0.5 * Y_e * \gamma)$
Keller (1989)	$K = \frac{4}{3} \frac{0.215 + 0.175 X_e}{1 + X_e} = \frac{4}{3} K_e$	Follow equation as written

Appendix B shows a flow chart of the program for calculating the velocity coefficients. The program used a grid to determine all the incremental areas. These areas were then multiplied by the corresponding velocity component and summed up. See Table 3.2 for the procedure for calculating  $\alpha$  and  $\beta$  coefficients.

Table 3.2 (Velocity Coefficients)

Coefficients	Formula
Alpha	$\alpha = \frac{\int_0^A v^3 dA}{V^3 A}$
Beta	$\beta = \frac{\int_0^A v^2 dA}{V^2 A}$

### 3.4.6 Verification of the Momentum Equation

To verify the momentum equation, the terms at each end of a control volume were calculated. (Fig. 3.1 and 3.2) The control volume was bound by the end depth section at the down stream location and the critical section at the up stream section. Boundary friction was neglected when balancing the momentum relation (Eq 2.3)

For calculating the pressure force at the end depth section, the following procedure was used;

- (1) Symmetry of flow was assumed and verified.
- (2) The areas at the end depth section and critical section were calculated. The area at the end depth section was divided into sub areas where the pressure head was measured or calculated.
- (3) The average pressure over a sub area was multiplied

by the sub area to obtain the pressure force.

- (4) All pressure forces over the entire end depth section were summed.
- (5) Standard procedures and formulas were used to calculate other terms in the momentum equation.

Appendix C provides for more details on the calculations related to the momentum analysis.

### 3.4.7 Energy equation

The main equation used for the energy analysis is the energy equation. This equation together with the continuity equation is shown below.

$$\frac{P}{\gamma} + z + \frac{V^2}{2g} = \text{constant} \quad 3.4$$

$$Q = V_1 A_1 = V_2 A_2 \quad 3.5$$

The continuity equation Eq 3.5 was used to check for continuity of flow. Eq 3.4 was used to calculate  $P/\gamma$  at the end depth section where  $V^2/2g + z$  values were known.

When Eq 3.4 was used to calculate  $P/\gamma$  values at a vertical end depth location, the following procedure was used.

- (1) A location on the water surface across the cross section was used as the reference point to calculate  $P/\gamma$  for the a vertical cross section

because  $P/\gamma=0$  and  $z$  and  $V^2/2g$  were known at the reference point.  $V$  is the total velocity and is defined by the following equations.

For Trapezoidal Channels

$$V^2 = U_z^2 + U_x^2 + U_r^2 \quad 3.6$$

For Circular Channels

$$V^2 = U_z^2 + U_\theta^2 + U_r^2 \quad 3.7$$

- (2) The  $P/\gamma$  values were calculated over the entire end depth section at discrete locations outside the boundary layer where  $V^2$  and  $z$  are known.
- (3) The pressure distribution in the boundary layer was assumed to be linear.

# Chapter 4 Results

## 4.0 Introduction

For trapezoidal and circular channels the velocity and pressure head values at the end depth section were measured for a range of discharge values. With the measured data, the velocity coefficients were determined. The presentation and analysis of the results are presented in subsequent sections.

## 4.1 Observations

### 4.1.1 Pressure Head measurements

For both the circular and trapezoidal channels, the pressure along the perimeter of the end depth section was zero. In the interior of both channels, the pressure head was found to be greater than atmospheric. Figs 4.1 and 4.2 qualitatively illustrate the general pressure distributions in trapezoidal and circular channels.

Fig 4.3 illustrates a typical pressure head distribution pattern for a vertical section in a circular channel. Fig 4.4 illustrates the pressure head distribution along the periphery of the wall 3.2 mm upstream of the end depth section. Although both figures show pressure distributions in just circular channels, similar patterns were observed in trapezoidal channels.

To check that there was no sudden change of gradient in the pressure head measurements, the following ratios  $P/P_{ref}$  vs  $L/L_{ref}$  were compared (Fig. 4.5).  $P$  was the measured pressure at any given distance  $L$  from the end depth and  $P_{ref}$  was the pressure head at an arbitrary reference location  $L_{ref}$  distance from the end depth which was greater than the critical distance  $L_c$ .

Fig 4.5 shows that there is no sudden change in the gradient of pressure head measurements along the centre line. No sudden change in the gradient in the pressure head measurements across the end depth section was observed. This observation would contrast with an assumption by an earlier investigator, Keller et al (1989).

As shown earlier in this study, Keller et al (1989) obtained a pressure coefficient,  $K$  Table 3.1, for trapezoidal channels from combining previous data for triangular and trapezoidal channels. This procedure would result in an imaginary line (A-B Fig. 4.6) separating the rectangle and triangle sections. At this point the pressure head distribution assumed by Keller (1989) was discontinuous (Fig. 4.6). Measured pressure head data in this study indicated that the trapezoidal channel had to be treated as a whole unit to exclude discontinuity. There was no discontinuity observed in the pressure head measurements since pressure is always continuous. Keller's assumption would also affect the pressure coefficient ( $K$ ).

#### 4.1.2 $Y_e/Y_c$ vs $Q$ comparisons

For circular and trapezoidal channels, the variation of  $Y_e/Y_c$  vs  $Q$  for the present study was found to correspond to previous studies. (Fig 4.7 , 4.8 and 4.9) Similarly, Rajaratnam et al (1964) (b) presented a relationship  $Y_e/D$  vs  $Q/G^{0.5}D^{2.5}$  which was compared to existing data (Fig 4.8). In this study, the range of data presented, was  $0.22 < Y_e/D < 0.4$  and  $0.10 < Q/G^{0.5}D^{2.5} < 0.26$ . A regression by the least square method was performed using the present data. This resulted in a relation between  $Y_e/D$  with  $Q/G^{0.5}D^{2.5}$  (Eq 4.1).

$$\frac{Q}{(GD^5)^{1/2}} = 1.0213 \left( \frac{Y_e}{D_c} \right) - 0.12848 \quad 4.1$$

Correlation was found to be very good.

Fig 4.9 shows the variation of  $A_e/A_c$  with  $Y_e/d$  where  $A_e$  and  $A_c$  are the cross sectional areas at the critical and end depth sections. The present set of data follows the trend suggested by Smith (1962).

The above comparisons were used to calibrate the equipment used in this study. Because similar results were obtained, equipment and procedure was deemed proper.



#### **4.1.3 Velocity measurements with a Pitot tube**

The highest velocities at the end depth section were observed near the bottom of the channel which was consistent with earlier observations (Rajarantam et al 1968). The axial  $U_z$  velocity distribution along the centre line corresponded qualitatively with previously published data (Insert Fig. 4.10(a)). A typical velocity contour profile developed by measured velocity points is also shown in Fig. 4.10(a) along with sample measured data.

Fig 4.10 (b) shows the axial velocity contours for a circular channel using Pitot tube measurements

For a numeric comparison of the velocity profiles for both channels and with Rajarantam et al (1968), refer to Fig 4.10(c). This figure shows the profile developed from both pitot tube and LDA measurements.

#### **4.1.4(a) Laser Doppler Anemometer (LDA) Measurements for The Trapezoidal Channel**

Velocities were measured or calculated according to procedures laid out in section 3.4.3 The laser probe measured velocities in two directions.

Fig 4.11 (a)-(c) illustrates typical velocity contours for all 3 velocity components at  $Y_0$  for one given flow rate in

a trapezoidal channel. Sample velocity measurements are also included in Fig 4.11(a)-(c). Velocities were measured for six different flow rates. The contours for each velocity component of all flow rates showed similar patterns.

The axial velocity  $U_z$  for all flow rates where velocity measurements were taken, were multiplied by the incremental areas to directly calculate the flow rate. The difference between the calculated and measured flow rates was less than 5%. Irrotationality outside the boundary layer and continuity of the flow were also checked and confirmed through the use of basic principles (Appendix C).

In Keller et al (1989) study, the boundary line between the rectangle and triangle section was assumed to have a velocity of zero (line A-B, Fig 4.6). As can be seen in Fig 4.11(a), the velocity is not zero at this boundary line. This assumption would affect the value of the  $\alpha$  and  $\beta$  coefficients

#### **4.1.4(B) Velocity Measurements for Circular Channels**

The results of the LDA tube measurements for circular channels are shown in Fig. 4.12(a)-4.12(c). Velocity measurements were taken for six different flow rates. Fig 4.12(a)-4.12(c) show the three components of velocities for a given flow rate using LDA. All velocity profiles for all flow

rates showed similar patterns. For the circular channel, the  $\theta$ ,  $r$  and  $z$  cylindrical coordinate system is shown in Fig 3.4. The velocity in the  $\theta$  and  $z$  direction were measured while the velocity in the  $r$  direction was calculated using the  $z$  and  $\theta$  values, (Appendix C). The boundary layer was also found to be around  $0.1Y_0$  when  $\theta'$  was  $0^\circ$ .

Because of limitations with the range of the laser, the pitot tube had to be used for regions which were out of range of the LDA lens. At the higher flow rates, pitot data was used in the 10 to 15% of the centre region that was not covered by LDA data. Procedure to measure velocities with the pitot tube were described in section 3.4.

Velocities calculated by the pitot tube data in regions where the velocity was measured by the laser showed close correlation in the  $U_z$  direction. Could then use a hybrid set of data to generate the velocity contours.

Along the  $5^\circ$  radial line (Fig 4.12(a)), the velocities in the  $z$  direction showed the same characteristics as the results of Rajarantam et al (1968) (Fig 4.10 (c)).

The  $\theta$  velocity on any given radial line increased from zero at the centre line to a maximum. The maximum was at a given angular distance  $\theta'$  from the centre line from where it would decrease until the water surface. Fig 4.12(b) insert illustrates the above described relationship.

As in the trapezoidal channel, the axial velocity  $U_z$  for all flow rates were multiplied by incremental areas to

directly calculate the flow rate. The difference between the calculated and measured flow rates was less than 5%. Irrotationality outside the boundary layer and continuity of the flow were also checked and confirmed through the use of basic principles (Appendix C). Irrotationality was checked in three orthogonal directions ( $x, y, z$ ).

#### **4.1.5 Comparisons between pitot tube and laser measurements**

The LDA was able to measure the velocity more accurately than the pitot tube and could also measure the velocity in two directions. It was more sensitive to fluctuations of velocity, especially near the channel surface because it was non-intrusive. It could also measure velocities closer to the channel bottom than the pitot tube. The pitot tube was more sluggish in its response to velocity changes. Measuring, curvilinear flow posed no difficulties to LDA measurements.

#### **4.1.6 Flow Profile**

The slope of the water surface ( $dy/dz$ ) at the end depth increased as the discharge ( $Q$ ) decreased. This would indicate that the component  $U_y$  relative to  $U_z$  would increase as discharge decreased. When the end depth was approximately two

centimetres, the flow began to wrap around the end depth section. Data was not taken at these flow rates because surface tension forces became significant.

#### 4.2. Calculated pressure coefficients

There were several kinds of pressure coefficients that were evaluated. The most common definition of the pressure coefficient used is stated in Eq 3.5 and was used by Rouse(1936) and Rajarantam (1968). Another definition for the pressure coefficient was introduced by Replogle(1962) and is stated below;

$$K_r = [((P/\gamma) + z) - z] / Y]_{\max}$$

$K_r$  could be determined experimentally. Keller(1989) introduced a pressure coefficient  $K$ , (Table 3.1), which was based on the end depth. Two other coefficients, ( $\alpha'$  and  $\beta'$  Table 3.1), were used to analysis curvilinear flow (Chow 1955).

To calculate the above pressure coefficients for the trapezoidal channel, a computer program was written. Table 4.1 shows the pressure coefficients calculated for the trapezoidal channel. A graphical presentation of the results are shown in Fig 4.14.

Table 4.1 Calculated Pressure Coefficients For Trapezoidal Channel

$Y_e$ (cm)	$\alpha'$	$\beta'$	$K_1$	K	$K_r$
Set 1 $z = 0$ mm Location A Fig 4.14					
10.7	1.026	1.018	0.282	0.262	0.276
9.0	1.018	1.012	0.289	0.264	0.299
7.9	1.013	1.009	0.303	0.266	0.303
6.4	1.009	1.006	0.297	0.268	0.312
Set 2 $z = -5$ mm Location B Fig 4.14					
10.7	1.024	1.016	0.235	0.262	0.234
8.7	1.028	1.019	0.276	0.265	0.246
7.3	1.011	1.008	0.288	0.267	0.287
5.0	1.004	1.002	0.282	0.272	0.326
Set 3 $z = -7$ mm Location C Fig 4.14					
11.4	1.040	1.025	0.220	0.261	0.219
9.3	1.029	1.020	0.258	0.264	0.228
9.2	1.027	1.018	0.218	0.264	0.218
8.1	1.022	1.015	0.235	0.265	0.248
5.4	1.011	1.007	0.282	0.270	0.287

Caption

$Y_e$  = end depth

$\alpha', \beta'$  = Pressure coefficient (Chow 1955)

$K_1$  = coefficient as defined by Rajaratnam (1967)

(See Table 3.1)

K = coefficient as defined by Keller (1989). (See Table 3.1)

$K_r$  = coefficient as defined by

Replogle (1962) =  $(P/\gamma/y)_{\max}$

With respect to trapezoidal channels, there was an observable increase in  $\alpha'$  and  $\beta'$  with an increase in  $Y_e$ . Coefficient,  $K$ , determined by Keller(1989) increased with  $Y_e$ .

A similarity in values between  $K_1$  and  $K_r$  was observed. In Fig. 4.13 a comparison of pressure head coefficients,  $K_1$  for circular, trapezoidal and rectangle channels is shown. The pressure head coefficients for the circular and trapezoidal channels were determined in this study, using Repogle's definition, while earlier studies had determined the values for rectangle channels.

The values of  $K_1$  and  $K_r$  varied with the three sets as can be seen in Fig 4.14. The variation can be explained by the location of the Pitot tube. For set 3 (Location C) the pitot tube was 7 mm down stream of the end depth section and had the lowest pressure head distribution values. The trend of decreasing pressure head values at sections down stream of  $Y_e$  was expected because the pressure head distribution would eventually become atmospheric throughout the flow region.

#### **4.3 Calculated Velocity coefficients, $\alpha$ and $\beta$ .**

For both channels the  $\alpha$  and  $\beta$  velocity coefficients were calculated and found to range from 1.03 to 1.10 for trapezoidal channels and 1.03 to 1.07 for circular channels. The coefficients were calculated using the formulas in (Table 3.2). Eq 4.2 and 4.3 were also used to calculate the  $\alpha$  and  $\beta$  coefficients (Chow 1959).

$$\alpha = 1 + 3\epsilon^2 - 2\epsilon^3 \quad 4.2$$

$$\beta = 1 + \epsilon^2 \quad 4.3$$

$$\epsilon = (U_m/U) - 1 \quad 4.3(a)$$

$U_m$  = Maximum velocity

$U$  = Average velocity

Similar results were obtained from both formulas.

Rajarantam(1968) reported  $\beta$  values of 1.07 to 1.14 for rectangular channels.

#### 4.4 The Momentum Equation

The momentum equation used in this present analysis is shown in Eq 2.4-2.6. In this discussion the friction force  $F_1$  was neglected, since its value was found to be less than 1% of total forces.

The pressure force  $P_e$  was calculated with knowledge of measured pressure heads across the whole channel cross section. After determining the pressure force  $P_e$  at the end depth, the momentum equation was applied. Tables 4.2 and 4.3 show the results of applying the momentum equation at varying flow rates for the two different channel geometries used in this study. Refer to Appendix C for procedure used in



calculating the pressure force and other terms of the momentum Equation, (Eq 2.3), at the end depth section.

Table 4.2 Momentum Analysis for Trapezoidal Channels

Flow Rate	$Y_e$ (cm)	$Y_c$ (cm)	$M_e+P_e$ (N)	$M_c+P_c$ (N)	$M_e+P_e$ (N) *
33.96 (l/s)	10.16	13.97	52.8	57.0	56.62
27.46 (l/s)	9.17	12.69	39.7	43.5	41.02
26.60 (l/s)	8.87	11.94	39.5	41.2	40.5

Table 4.3 Momentum Analysis For Circular Channels

Flow Rate	$Y_e$ (cm)	$Y_c$ (cm)	$M_e+P_e$ (N)	$M_c+P_c$ (N)	$M_e+P_e$ (N) *
38.76 (l/s)	11.61	14.86	64.5	68.3	67.3
38.32 (l/s)	11.11	14.76	63.0	67.3	67.0
27.57 (l/s)	9.36	12.34	42.1	44.2	43.9
22.9 (l/s)	8.5	11.2	33.3	35.0	34.5

\* = analysis that include the  $\beta$  coefficient where  $\beta=1.05$  for the trapezoidal channel and 1.03 for the circular channel.

Two of the trials showed near exact matching of the sum of the components of the momentum equation for the end depth and the critical section. Theoretically this is what was expected. When the  $\beta$  was added the equations balanced.

The main objective of this study was to obtain an equation to calculate  $Q$  by measuring  $Y_e$ . This was done by using the total momentum calculated for the critical section and equations presented in section 2.3. It was done for all flow rates in table 4.2 and 4.3. The comparisons for the highest flow rate for both channels is presented below;

	Discharge Measured	Discharge Calculated
Trapezoidal Channel	33.96 l/s vs	34.39 l/s
Circular Channel	38.76 l/s vs	39.65 l/s

The flow rates were calculated considering  $\beta$  to be greater than unity.

#### 4.5 Discussion of energy equation

##### 4.5.1 Application of the energy equation from the critical section to end depth section.

The energy relation Eq 3.4 was used to indirectly calculate the pressure head distribution at the end depth section using the velocity distribution data. Velocity and pressure head readings at the critical section, where the pressure head distribution was hydrostatic, were measured so that the total head could be evaluated. Eq 3.4 was then applied from the critical section to the end depth section (Fig 3.2). The velocity used in the energy equation was always the total velocity  $U$  as defined in Eq 3.6 and 3.7. One could only apply Eq 3.4 outside the boundary layer region. Fig 4.15 shows the velocity distribution at the critical and end depth section and the approximate boundary layer location.

#### 4.5.2 Application of Energy Equation at the vertical End Depth section

The  $P/\gamma$  values at discrete locations over a vertical cross section at the end depth section were individually obtained by the measured velocity distribution at these points. The details of the procedure are explained in section 3.4.7. Close agreement with the indirectly calculated  $P/\gamma$  values and those directly measured by a pitot static probe was observed. Refer to Table 4.4 for a comparison of calculated  $P/\gamma$  values and measured values.

Table 4.4 Comparisons of calculated and measured  $P/\gamma$  values (Circular Channel) (Typical Test Condition)

Elevation (cm)	$(P/\gamma)/Y$ calculated [ $Y_a=6.98$ ] $Q=18$ l/s	$(P/\gamma)/Y$ Measured [ $Y_a=7.10$ ] $Q=18.4$ l/s
5.6	0.17	0.17
4.6	0.23	0.25
3.6	0.27	0.31

The differences in values can be attributed to the boundary layer effects

#### 4.6 Momentum Analysis with Calculated Pressure head data for Circular Channel

The momentum analysis was applied with the calculated pressure head data and compared with the data in Table 4.2 and 4.3. The results of the comparison show a similar correlation between the sum of  $M_o$  and  $P_o$  vs sum of  $M_c$  and  $P_c$  (Eq 2.3) which were based on the following;

- i) Measured  $P/\gamma$  values based on static probe data.
- ii) Calculated  $P/\gamma$  values based on the velocity distribution data.

In table 4.5 are the results of the momentum analysis with calculated pressure head values (Eq 3.4).

Appendix C shows the data and calculations used in the momentum analysis. The pressure heads were calculated with use of the energy equation.

Table 4.5 Momentum Analysis with Calculated Pressure Forces  
For Circular Pipes (High, Middle and Low Flow rates)

$Q$ (l/s)	$Y_o$ (cm)	$Y_c$ (cm)	$M_o + P_o$ (N)	$M_o + P_o$ ( $\beta$ )	$M_c + P_c$ (N)
40.71	11.91	15.88	70.62	72.52	73.12
31.74	9.66	13.6	51.05	52.41	53.48
18.0	6.98	9.83	25.68	26.36	25.53

$\beta=1.03$  , Calculated from velocity data measured by the laser. See Eq 2.3 for momentum equation.

Clearly the addition of the  $\beta$  coefficients did make a difference in the calculations. It accounted for an additional three percent difference in the sum of the  $P_e$  and  $M_e$  terms (Eq 3.3). As can be seen in Table 4.5, the  $\beta$  coefficient improve the balance of the momentum equation.

The coefficient  $\alpha$  was used in calculating  $P_e$ . The momentum analysis with calculated  $P/\gamma$  values and measured ones were compared. An improvement was observed (Tables 4.2-4.5), when the  $\alpha$  coefficient was incorporated into the momentum analysis.

#### 4.7 Discussion of Free vortex model of Ali (1972)

Ali (1972) analyzed the end depth problem on the basis of the free vortex theory. It was found that there could be a close correlation between experimentally determined end depths and the predicted end depths.

Ali (1972) derived two equations from the free vortex theory for the velocity of lower and upper stream lines. These formulas are shown below as in Eq 4.4 and 4.5

$$V_u = (2 * g (H - h_e))^{0.5} \quad 4.4$$

$$V_l = (2gH)^{0.5} \quad 4.5$$

$H$  = Height of water surface

$V_u$  = upper stream line

$V_l$  = lower stream line

$$H = H_c + A_c / 2T_c$$

The velocities calculated with the above equations did not correspond with measured data. Values calculated by Ali(1972) were either too high or too low. For example, at  $Y_e = 11.65$ , the lower velocity was measured as 1.67 m/s. Calculating this velocity from formula 4.5 resulted in a velocity of 2.3 m/s. The velocity for the upper stream section was lower than measured. However the difference was smaller. There were a couple of problems with the analysis related to the facts presented below;

- i) Stream lines in a vertical plane are not strictly circular.
- ii) The radius of curvature increases as one moves towards the interior of the flow region.

# Chapter 5 Conclusions

## 5.0 General Remarks

New information relating the flow rate ( $Q$ ) and end depth ( $Y_e$ ) in trapezoidal and circular channels smooth open channels was obtained.

### 5.0.1 Trapezoidal Channel

In the current study, the velocity and pressure distributions for the trapezoidal channel were obtained, considering the end depth and critical depth cross section as a whole unit. The three components of velocity were also determined. This enabled the accurate determination of the velocity and pressure coefficients ( $\alpha$ ,  $\beta$  and  $K$ ) from the velocity and pressure distribution data. The above coefficients were then used with the momentum equation to accurately evaluate the  $Q=F(Y_e)$  (Eq 2.3-2.5) relationship. The  $\alpha$  and  $\beta$  coefficients were found to range from 1.03-1.07.

### 5.0.2 Circular Channel

The velocity and pressure head distribution for the entire end depth cross section permitted the evaluation of the

velocity( $\alpha$  and  $\beta$ ) and pressure (K) coefficients. All other objectives laid out in section 1.1 were met. This enabled one to accurately balance the momentum equation and establish the  $Q=F(Y_e)$  relationship.

### 5.0.3 Calculated Pressure Head Values

The energy equation (Eq 2.3) was used successfully to determine the end depth pressure field at the end depth section using the measured velocity distribution at that section.

### 5.0.4 Concluding Remarks

The accurate determination of the  $Q=F(Y_e)$  relationship would permit a cost effective method of flow rate monitoring at point source discharge locations.

## 5.1 Recommendations

- Measure all 3-d component with an LDA system instead of calculating one component, knowing the other two components.
- Perform measurements on channels with variable slopes and roughness values



## References

- Ali. K., and Sykes, A., "Free-Vortex Theory Applied to Free Overfalls", ASCE, Vol.98, No. HY5 , May, 1972, pp 973-979.
- Argyropoulos, P., Advani, R., Campbell, F., Leutheusser, H., and Smith, P., "End Depth for Circular channels" , *Journal of the Hydraulics Division*, Discussion of Paper by Rajaratnam, N., and Muralidhar, D., March 1964., HY5 September., 64, pp. 261-270.
- Argyropoulos, P., Advani, R., Muralidhar, D., Rajaratnam, N., and Vennard J., "Brink Depth For a Circular Channel", *Journal of the Hydraulics Division*, Discussion of Paper by C.D. Smith, Nov., 62., HY3 May., 1963, pp.389-405.
- Bauer, S., and Graf, W., "Free OverFall as Flow Measuring Device", *Journal of the Irrigation and Drainage Division*, ASCE, Vol.97, No. IR1, March, 1971, pp 73-83.
- Christodoulou, G., "Brink Depth in Non Aerated Overfalls", *Journal of Irrigation and Drainage Engineering*, ASCE, Vol. 111, No. 4, Dec., 1985, pp 385-403.
- Chow V. T., *Open Channel Hydraulics*, McGraw-Hill Inc., New York, 1959.
- Currie I.G., *Fundamental Mechanics of Fluids*, McGraw-Hill Inc., New York, 1974.
- Delleur, J.W., Dooge J.C.I., and Gent K.W., "Influence of Slope and Roughness on the Free Overfall", *Proceedings, ASCE*, Vol. 82, No. HY 4, Aug., 1956, pp. 1038-30-1038-35.
- Diskin, M.H., "End Depth at a Drop in Trapezoidal Channels", *Journal of the Hydraulics Division*, ASCE, Vol.87, No. HY 4, July, 1961, pp.11-32.
- Diskin, M., "Brink Depth for Circular Channels", *Journal of the Hydraulics Division*, Discussion of Paper by CD Smith, Nov 62, HY2 March., 1963, pp. 203-210.
- Fathy, A., and Shaarawi, M., "Hydraulics of the Free Overfall", *Proceedings, ASCE*, Vol. 80, Proceedings -Separate No. 564, Dec 1954, pp. 564-1-564-12.
- Ferro, V., "Flow Measurement With Rectangular Free Overfall", *Journal of Irrigation and Drainage Engineering*, ASCE, Vol. 118, No. 6, Nov/Dec, 1992, pp 956-963.
- Gupta, R.D., Jamil, M., and Mohsin, M., "Discharge Prediction

- in Smooth Trapezoidal Free Overfall (Positive, Zero and Negative Slopes)", *Journal of Irrigation and Drainage Engineering*, ASCE, Vol. 119, No. 2, March/April, 1993, pp 215-223.
- Keller, R., and Fong, S., "Flow Measurement with Trapezoidal Free Overfall", *Journal of Irrigation and Drainage Engineering*, ASCE, Vol. 115, No. 1, Feb., 1989, pp 125-136.
- Khanna, S.D., "Method to Solve Cubic Equations For Depth Below Overfall", *Journal of Irrigation and Drainage Division*, ASCE, Vol. 100, No. IR1, March, 1974, pp. 103-106.
- Hager, W.H., "Hydraulics of Plane Free Overfall", *Journal of Hydraulic Engineering*, ASCE, Vol. 109, No. 12, Dec., 1983, pp. 1683-1697.
- Markland, E., "Calculation of Flow at a Free Overfall by Relaxation Method", *Proceedings of the Institution of Civil Engineers*, Paper 686, Nov., 1965, pp. 71-78
- Moore, W., "Energy Loss at the Base of Free Overfall", *Proceedings*, ASCE, Paper No. 2204, Nov., 1941, pp. 1343-1392.
- Neogy, B., "Brink Depth For Trapezoidal Broad-Crested Weir", *Journal of the Hydraulics Division*, ASCE, Vol. 98, No. HY 12, Dec., 1972, pp. 2171-2189.
- Nezu, I., "Open-Channel Flow Measurements with a Laser Doppler Anemometer", *Journal of Hydraulic Engineering*, ASCE, Vol. 112, No. 5, May, 1986, pp. 335-353.
- Noutsopoulos, G., and Chrisdoulou, C., "Discussion of Kellers and Fong's Article"
- Rouse, H., "Discharge Characteristics of the Free Overfall", *Civil Engineering*, ASCE, Vol., 6, No., 4, April, 1936, pp. 257-260.
- Rajaratnam, N., and Muralidhar, D., "End Depth for Exponential Channels", *Journal of the Irrigation and Drainage Division*, ASCE, Vol. 90, No. IR 1, March, 1964, pp. 17-39. (A)
- Rajaratnam, N., and Muralidhar, "Characteristics of the Rectangular Free Overfall", *Journal of Hydraulic Research*, Vol. 6, No. 3, 1968, pp. 233-258.
- Rajaratnam, N., and Muralidhar, "Pressure and Velocity Distribution for Sharp-Crested Weirs", *Journal of Hydraulic Research*, Vol. 9, No. 2, 1971, pp. 233-258.
- Rajaratnam, N., Muralidhar, and Beltaos, S., "Roughness Effects

on Rectangular Free Overfall", *Journal of the Hydraulics Division*, ASCE, Vol. 102, No. HY 5, May., 1976, pp. 599-614.

Rajaratnam, N., Kar, S., and Hamid, H.I., "End Depth at a Drop in Trapezoidal Channels", Discussion Of M.H. Diskin.

Rajaratnam, N., and Muralidhar, "End Depth for Circular Channels ", *Journal of the Hydraulics Division*, ASCE, Vol. 90, No. HY 2, March., 1964, pp. 99-119. (B)

Repplogle, J.A., "Disc. of The End Depth at a Drop in Trapezoidal Channels by M.H. Diskin", *Journal of the Hydraulics Division*, ASCE, Vol. 88, No. HY2, Proc. Paper 3087, March 1962, pp. 161-165.

Saatci, A, "Velocity of Flow Calculations in Partially Filled Pipes", *Journal of Environmental Engineering*, Vol. 116, No. 6, Nov/Dec, 1990, pp. 1202-1208.

Smith, C.D., "Brink Depth For a Circular Channel", *Journal of the Hydraulics Division*, ASCE, Vol. 88, No. HY 6, Nov. 1962, pp. 125-134.

Streeter V.L., and Wylie E. B., *Fluid Mechanics*, edition 8, McGraw-Hill Inc., New York, 1985.

Strelkoff, T., and Moayeri, M., "Pattern of Potential Flow in a Free Overfall", *Journal of the Hydraulics Division*, ASCE, Vol. 96, No. HY2, April, 1970, pp. 879-901.

Trezidlis, G., and Anastasiadou-Partheniou, L., "Discussion of Free Overfall by Keller and Fong",

Vallentine H.R., *Applied Hydrodynamics*, Butterworths, London, 1967.

## Appendix A





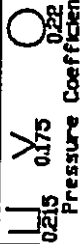
Investigators	Model	Results	Remarks
Rouse(1936)	Broad crested weir 	 Critical Section End Section Pressure distribution	First to investigate end depth to Discharge ratio $Y_e/Y_c = 0.72$
Shorawi & Fatih(1954)	Steel Flume $D=0.4m$ $L=3.0m$ $V=0.5m$ 	Performed pressure measurements	Theoretical investigation of $Y_e/Y_c$ vs S Only authors to find sub atmospheric Pressures
Delleur & Dooge & Gent(1956)	Theoretical+Experimental investigation Glass walled Tilling Flume $L = 9.144 m$ $V = 0.6096 m$	$S_o/S_{c0} = 0, Y_e/Y_c = 0.7$	Found relationship between slope and $Y_e/Y_c$ ratio decreased with increasing Slope Performed analysis on momentum equation Analytical determination of Pressure coefficients
Diskind(1961)	End depth in Trapezoidal Channel Channel 1 $b=0.1567m$ $n=1.5$ Channel 2 $b=0.125 m$ $n=2$ 	$0.67(Y_e/Y_c)0.735$	Theoretical investigation indicated $Y_e/Y_c = 0.67$
Replogle(1962)	End depths in channels	 0.215 0.175 Pressure Coefficients	Alpha and Beta coefficients = 1 Pressure coefficient = $Q/Y_{max}$
Hand(1962)	Trapezoidal Channel $n = 14.5$ and $12$	$Y_c$ to $Q$ relation	Confirmed previous results

Fig. 2.1(a): List of Previous Studies

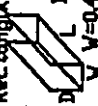
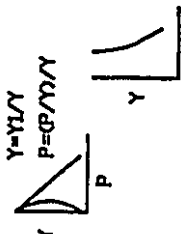

Investigators	Model	Results	Remarks
Rajaratnam & Muralidhar (1962)	Rectangular Flume Triangular & Exponential Channels Wooden Sides	Results Similar to Duller (56)	Direct solution of end depth problem found Solution used to predict discharge
Markland (1965)	Numerical	solved for various Fo number	Used relaxation method
Rajaratnam & Muralidhar (1968)	Rectangular Free Overfall  D=0.381m V=0.457m/s L=6.09m	$0.74 > Y_e/Y_c > 0.71$ Pressure Distribution $Y = Y_1/Y$ $P = \rho g Y_1/Y$ 	Pressure Distribution Parabolic at $Y_e$ Pressure coefficient = $P/(\rho g Y_1/Y)$ Velocity and Pressure distribution investigated
Rajaratnam & Muralidhar (1971)	Pressure & Velocity Distribution for Sharp-crested Viers	Results similar to 68 study Velocity Distribution	Pressure and velocity distribution similar to 68 study
Bauer & Graf (1971)	Rectangular channel Different Slopes and Materials  Constant Slope Variable Slope	Range Studied $0.6(Y_e/Y_c) < 0.8$ $0.7(Y_c/Y_c) < 0.11$ Channel surfaces Glass, Canvas and Sand Pumps	Rougher surface = lower $Y_e/Y_o$ Ratio Determination of Discharge at end Depth $Q = \sqrt{Y_c} \cdot Q \cdot b^{0.86}$ Good For Rectangular Channels

Fig. 2.1(b): List of Previous Studies



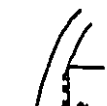

Investigators	Model	Results	Remarks
AU & Sykes (1972)	Used Rectangular+ Traingular Models Channel Length=6.1m	$Y_3/Y_c=0.703$  $Y_e/Y_c=0.793$ 	Compared results to momentum and free Vortex theory
Neogy (1972)	Trapezoidal Broad Crested Weir	$0.757 > Y_e/Y_c > 0.744$ 6.13 Breadth of wier Crest > 26.1m	$\log F_o$ vs $Y_e/Y_c$ = linear No variation of $Y_e/Y_c$ with breadth of weir crest
Rajaratnam & Muralidhar (1976)	 Blocks to simulate Roughness	Pressure distribution same as 68 study	$K_s/Y_c > 0.1$ - $Y_e/Y_c$ affected $K_s$ =Height of Roughness block
Hager (1983)	Analytical investigation	$F_o$ increased, Profile like Jet	Attempted to determine surface profile through analytical means
Christodoulou (1985)	Used rectangular channel with variable drop sections	$Y_e/Y_c$ decreased as Drop section increased	Drop section found to affect $Y_e/Y_c$
Nezu & Rodi (1986)	Channel dimensions $L=20m$ $V=0.6m$ , $D=0.65m$ Flume Hydraulically smooth Used LDA system	Friction velocity+Reynolds Stress increases near wall	LDA system obtained more accurate data
Keller Fong (1989)	Trapezoidal Flume  $L=3m$ $b=0.15m$ $m=1$	$nY_e/b$ vs $Q^2 n^3 / gb^3$ relation ship obtained $k=(4/3) \times \frac{(0.215+0.175Xe)}{(1+Xe)}$	Obtained value for pressure coefficient combined known values for traingle and Rectangular channels

Fig. 2.1(c): List of Previous Studies

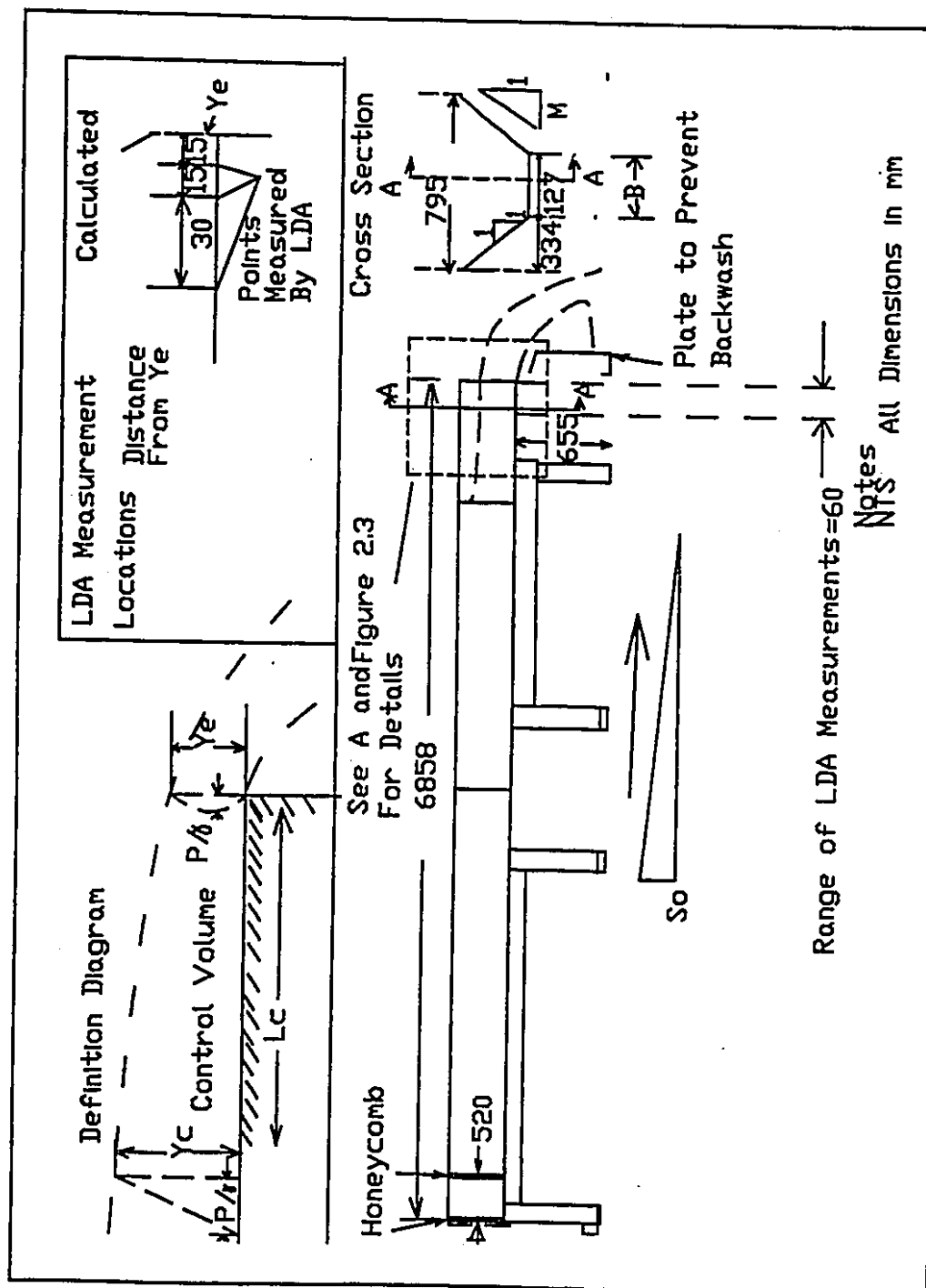
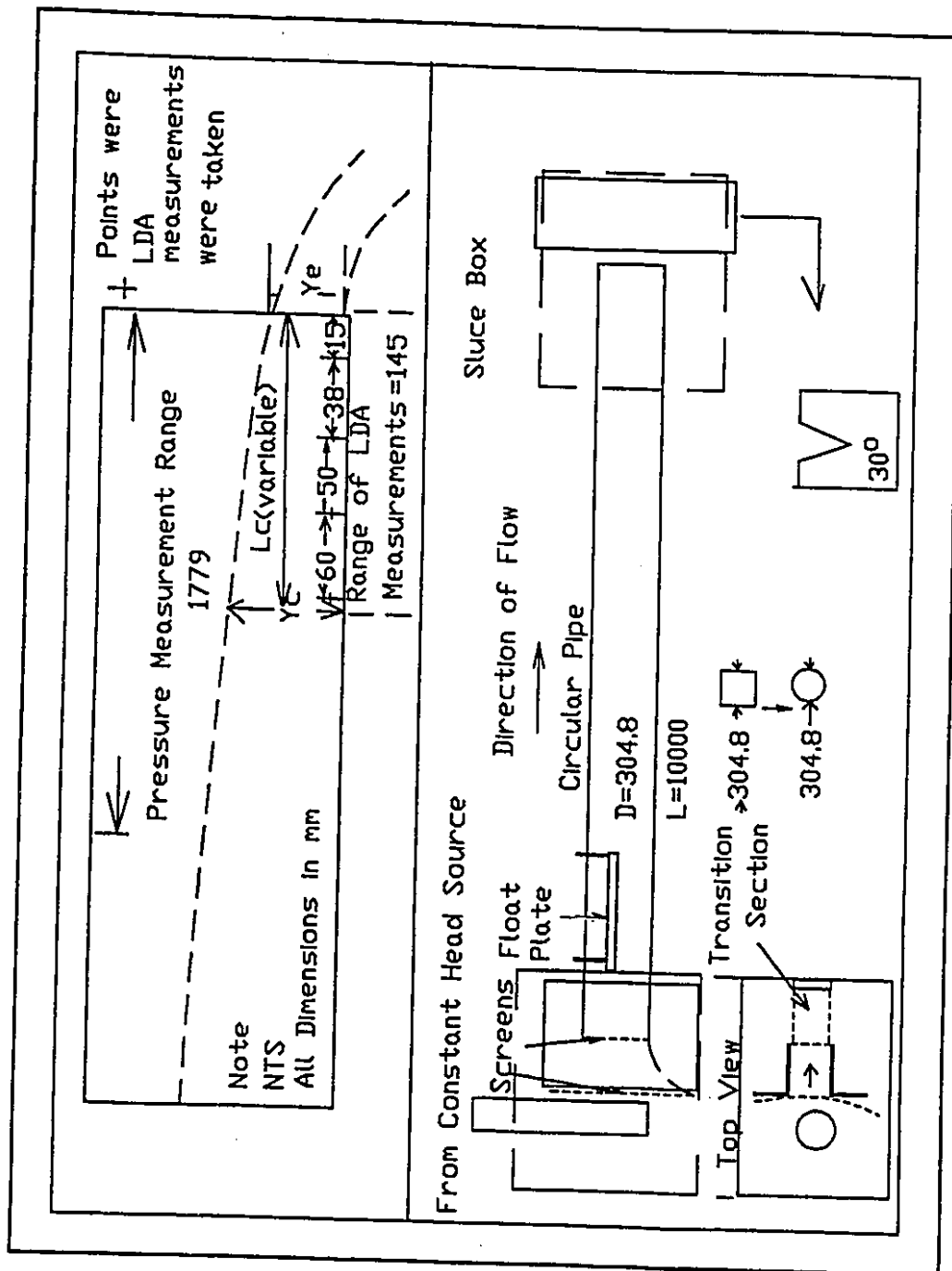
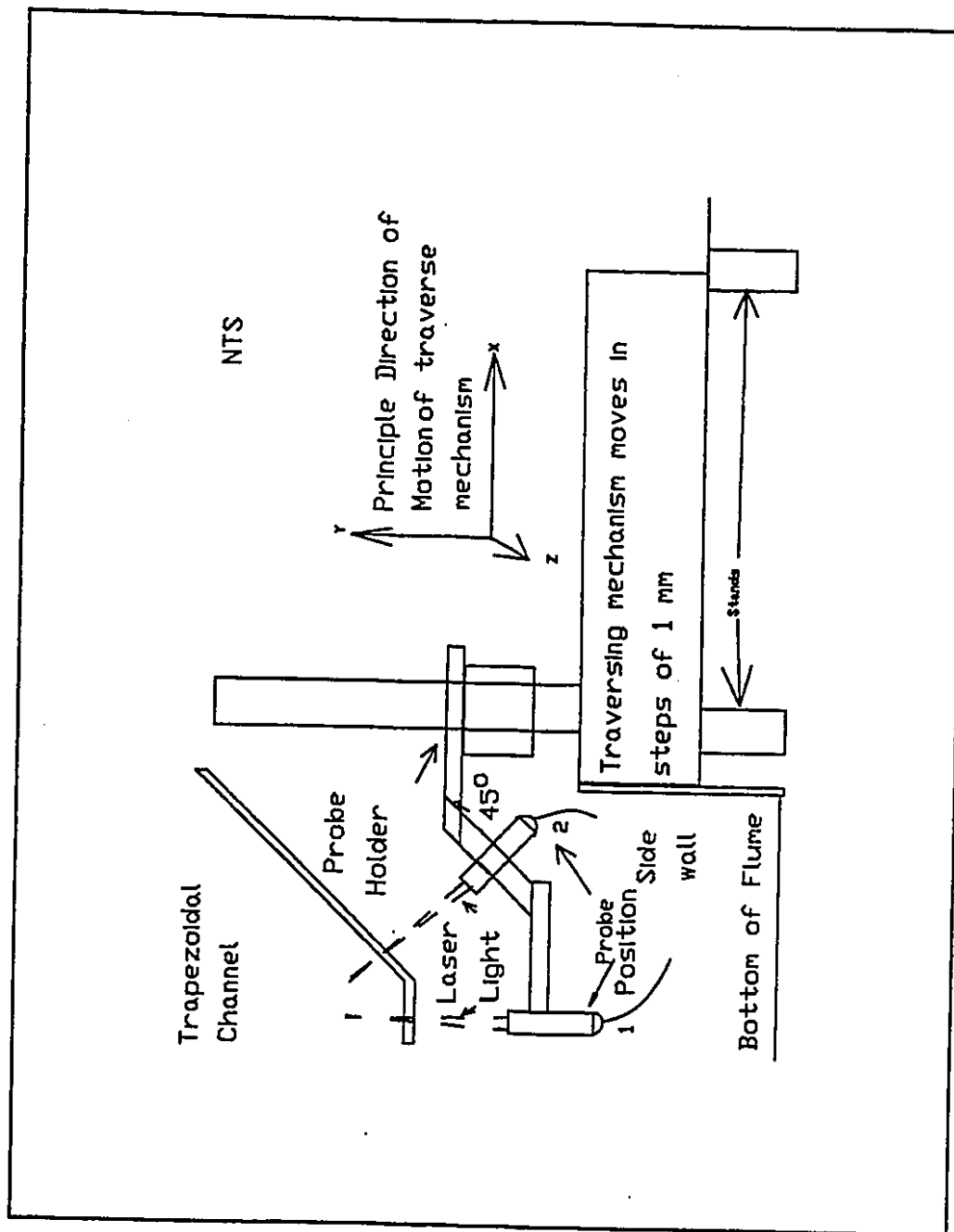


Fig. 3.1: Diagram of Trapezoidal Channel





**Fig. 3.2:** Diagram of Circular Channel



**Fig. 3.3:** Mount for Probe For Trapezoidal Channel

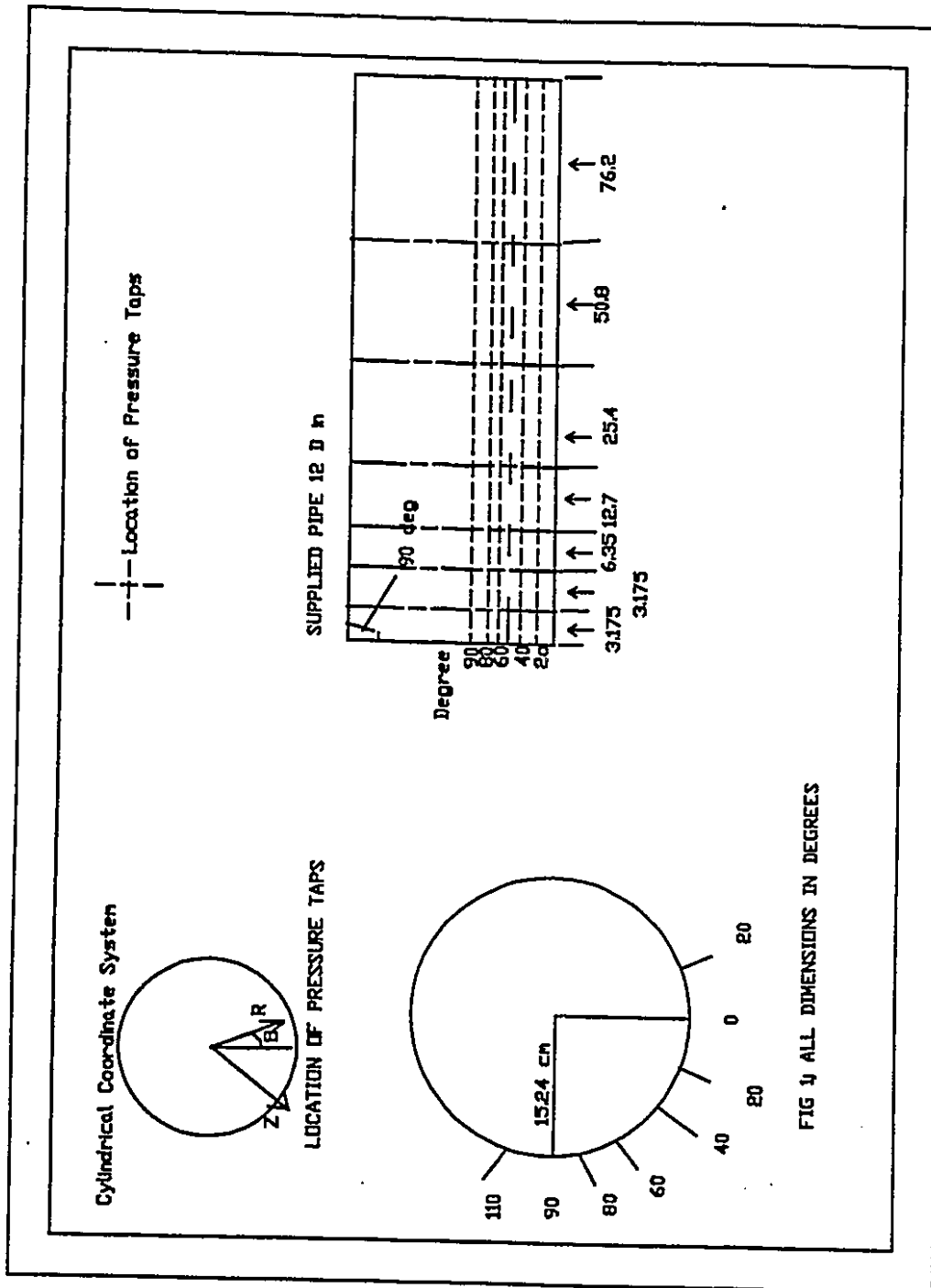
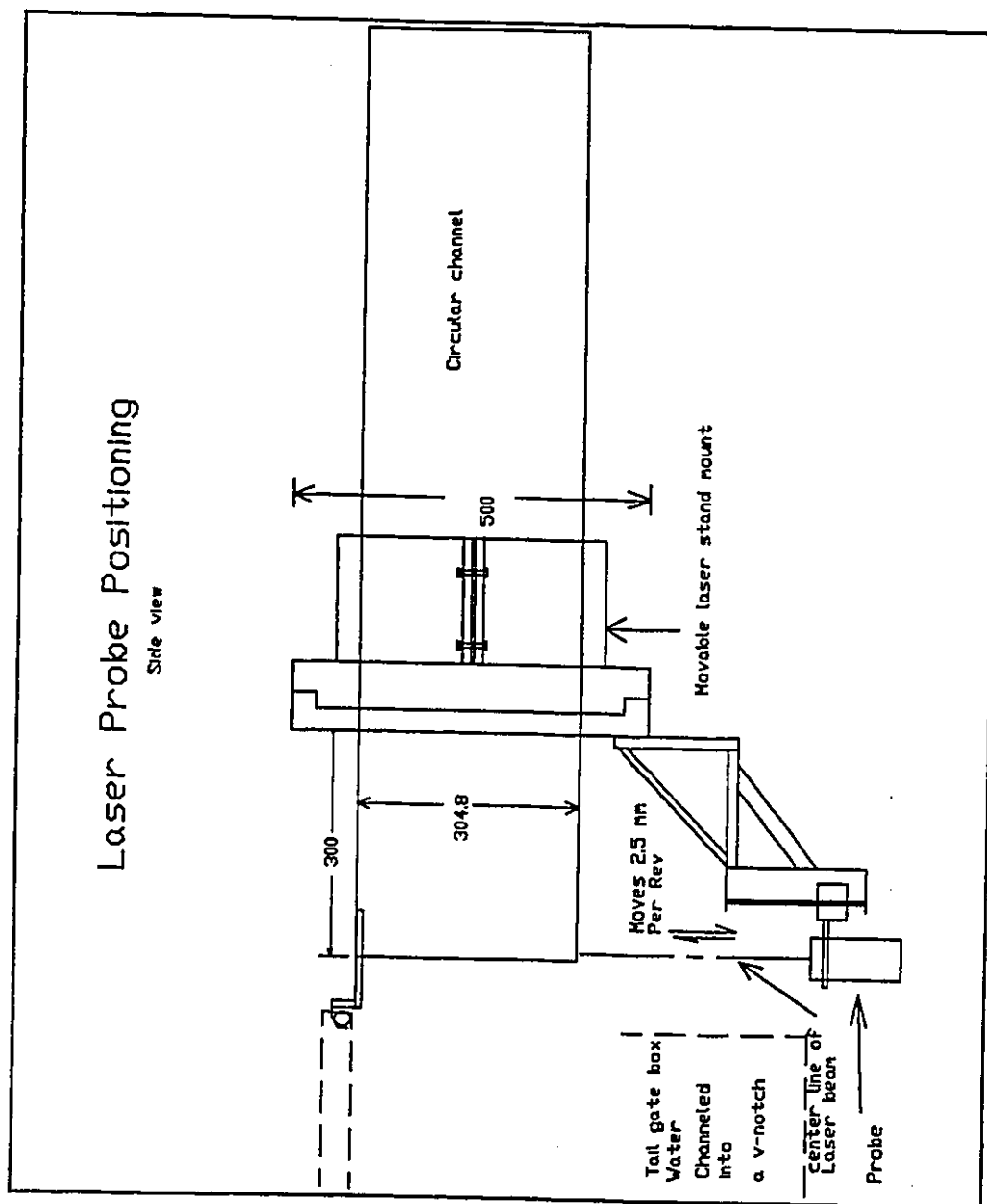


Fig. 3.4: Location of Pressure Tabs



**Fig. 3.5(a): Circular Laser Probe Positioning**

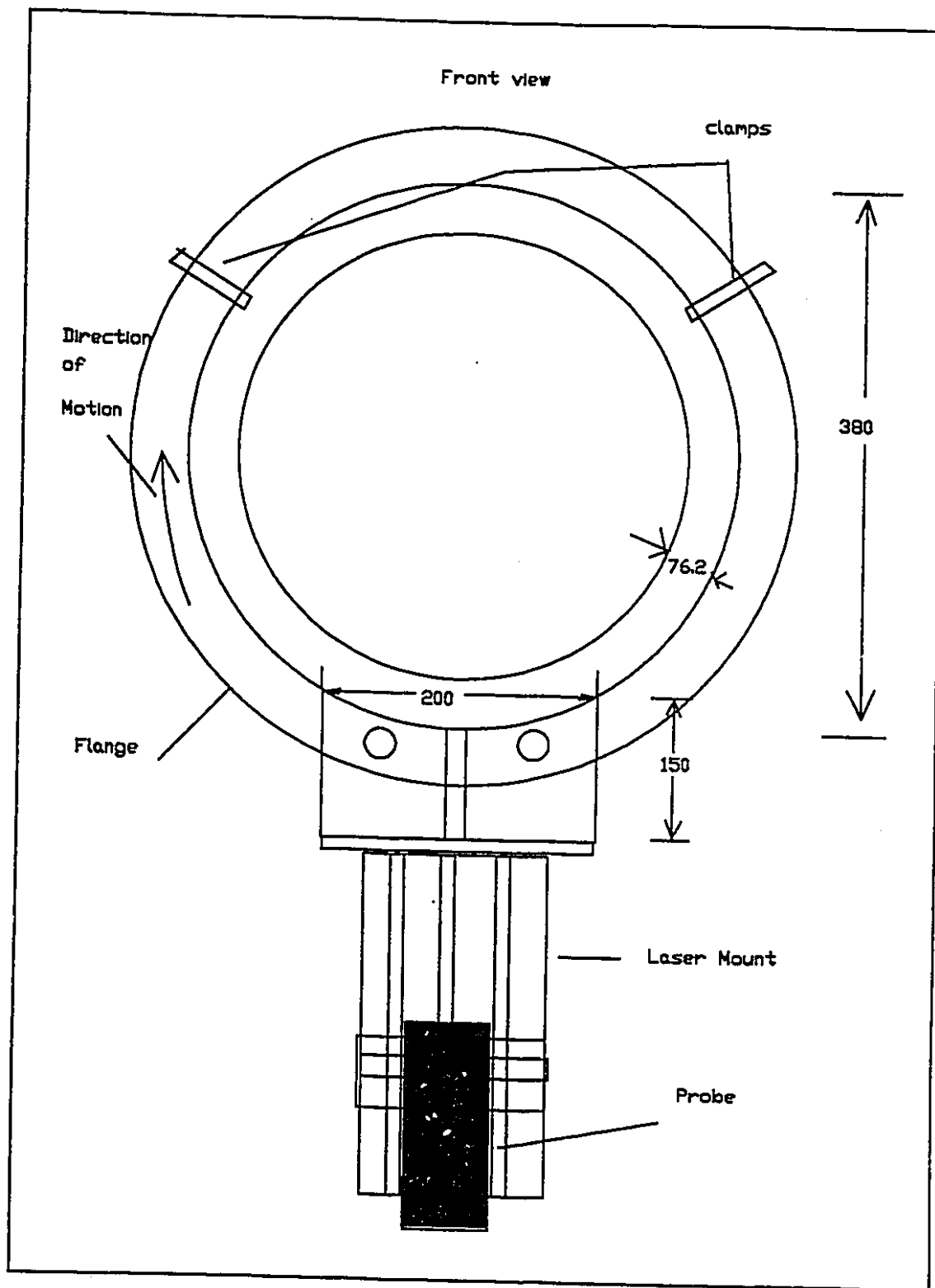


Fig. 3.5(b): Circular Laser Probe Positioning



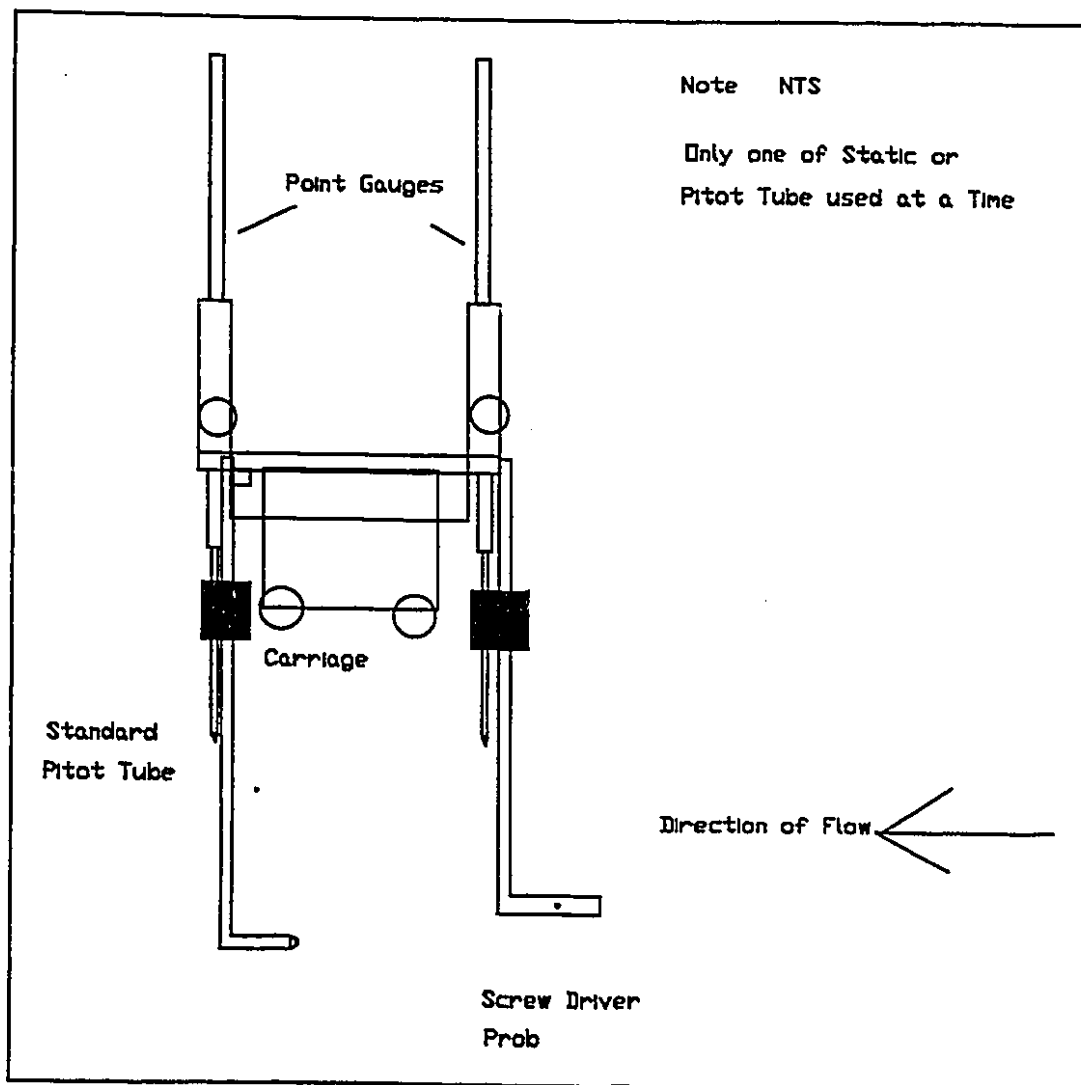
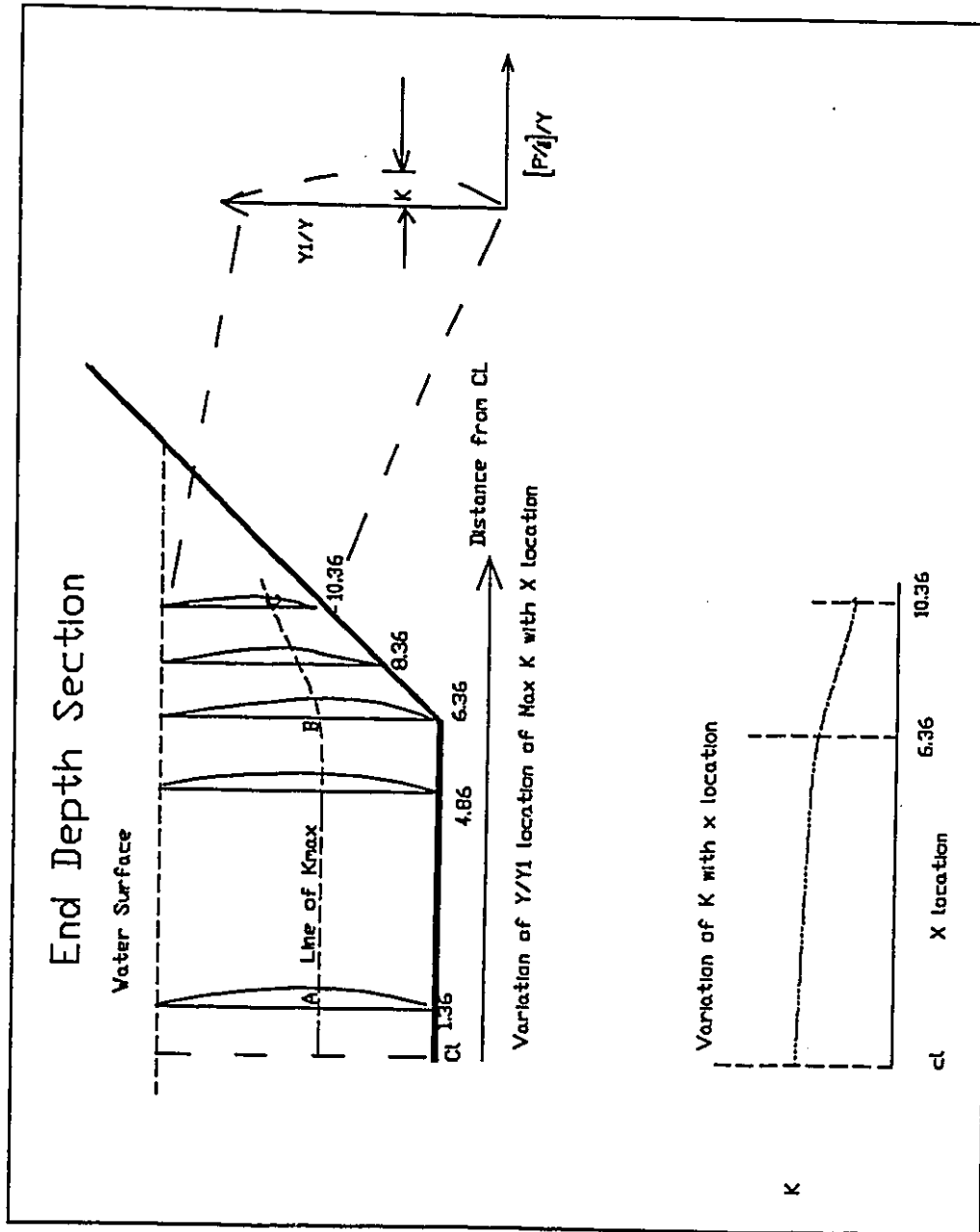
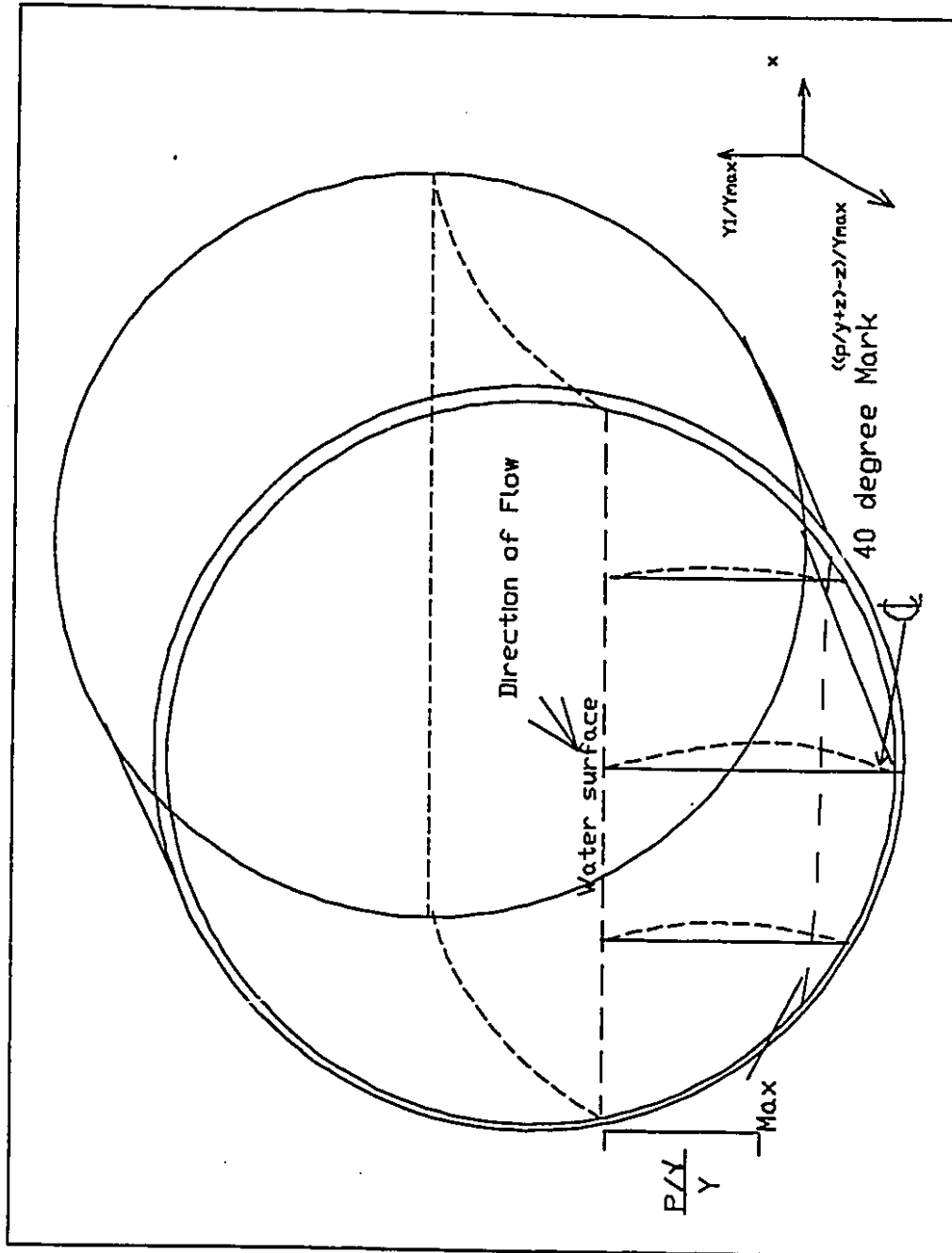


Fig. 3.7: Mounting for Pitot Tubes



**Fig. 4.1:** Pressure Distribution at Brink





**Fig. 4.2:** Pressure Distribution at Brink Depth

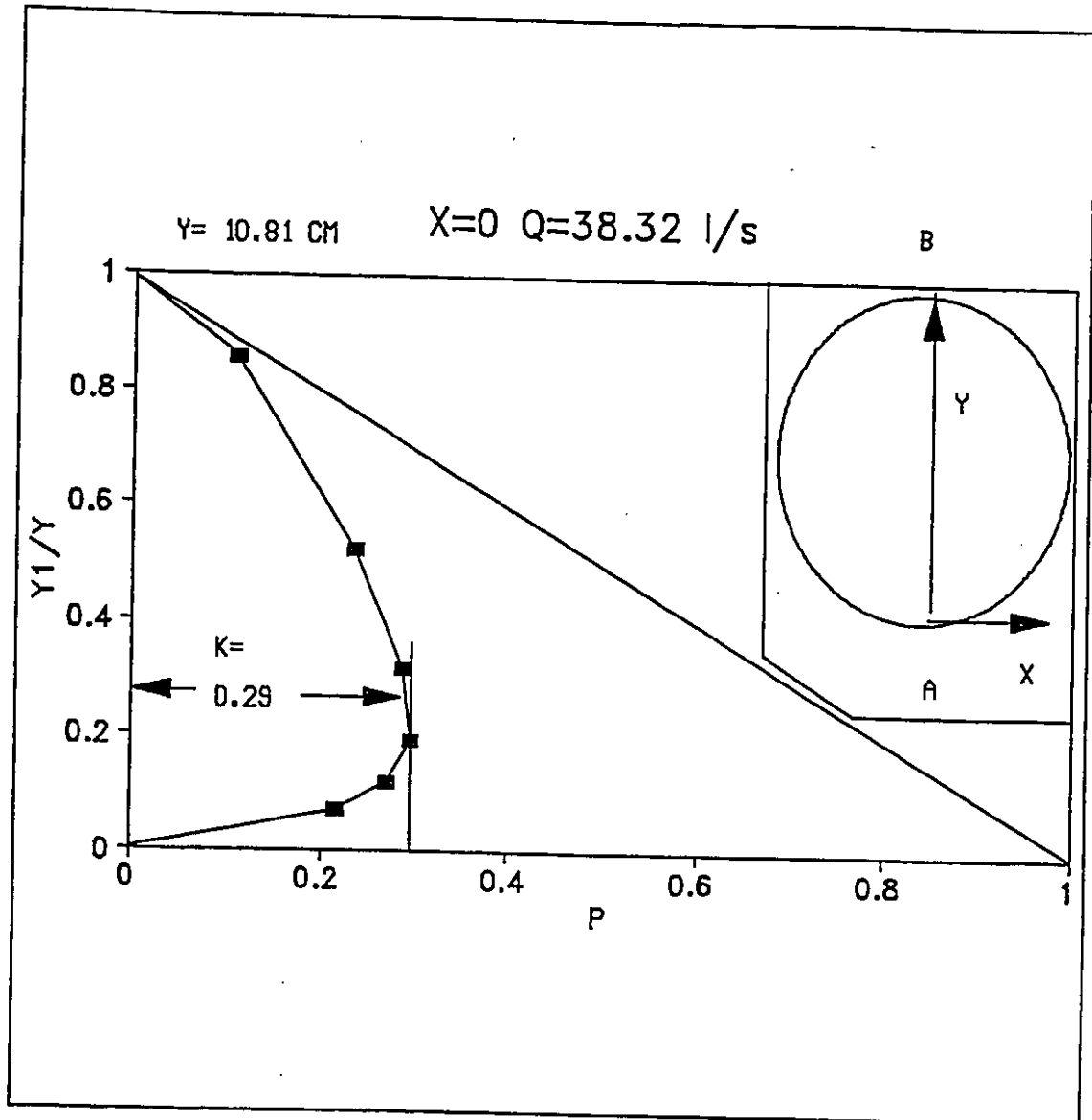


**Fig. 4.3:** Variation of  $P$  with  $Y1/Y$   
 $P = ((P/\gamma + z) - z) / y$ ; along center line (A-B)

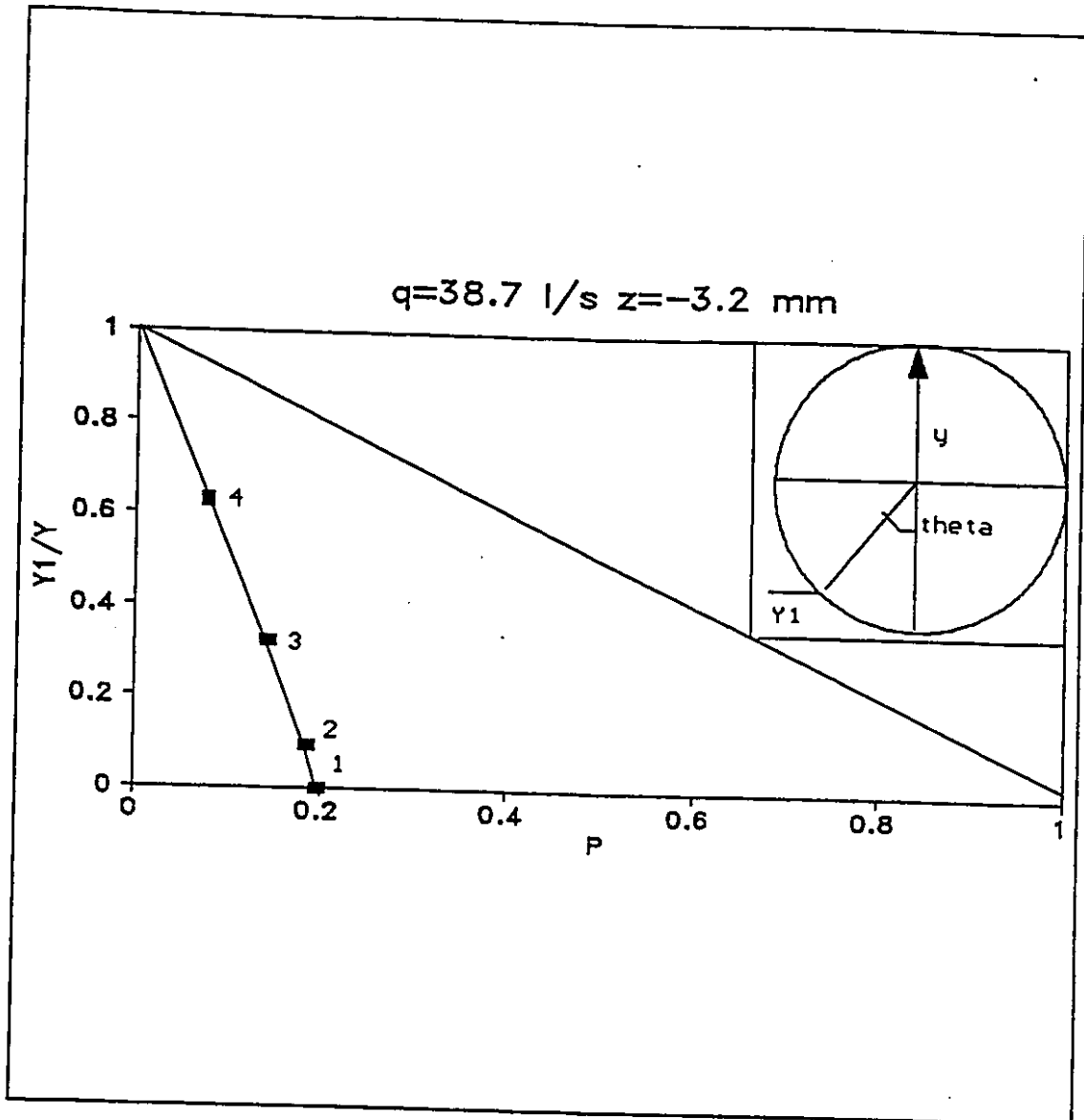


**Fig. 4.4:** Variation of  $P$  with  $Y1/Y$   
 $P = ((P/\gamma + z) - z)/y$ ; Instert: wall pressure tap  
 location :  $Y1=Y$  at Free Surface

Position	Theta	Height ( $Y1$ ) (mm)
1	0	0
2	20	10.16
3	40	36.1
4	60	76.2

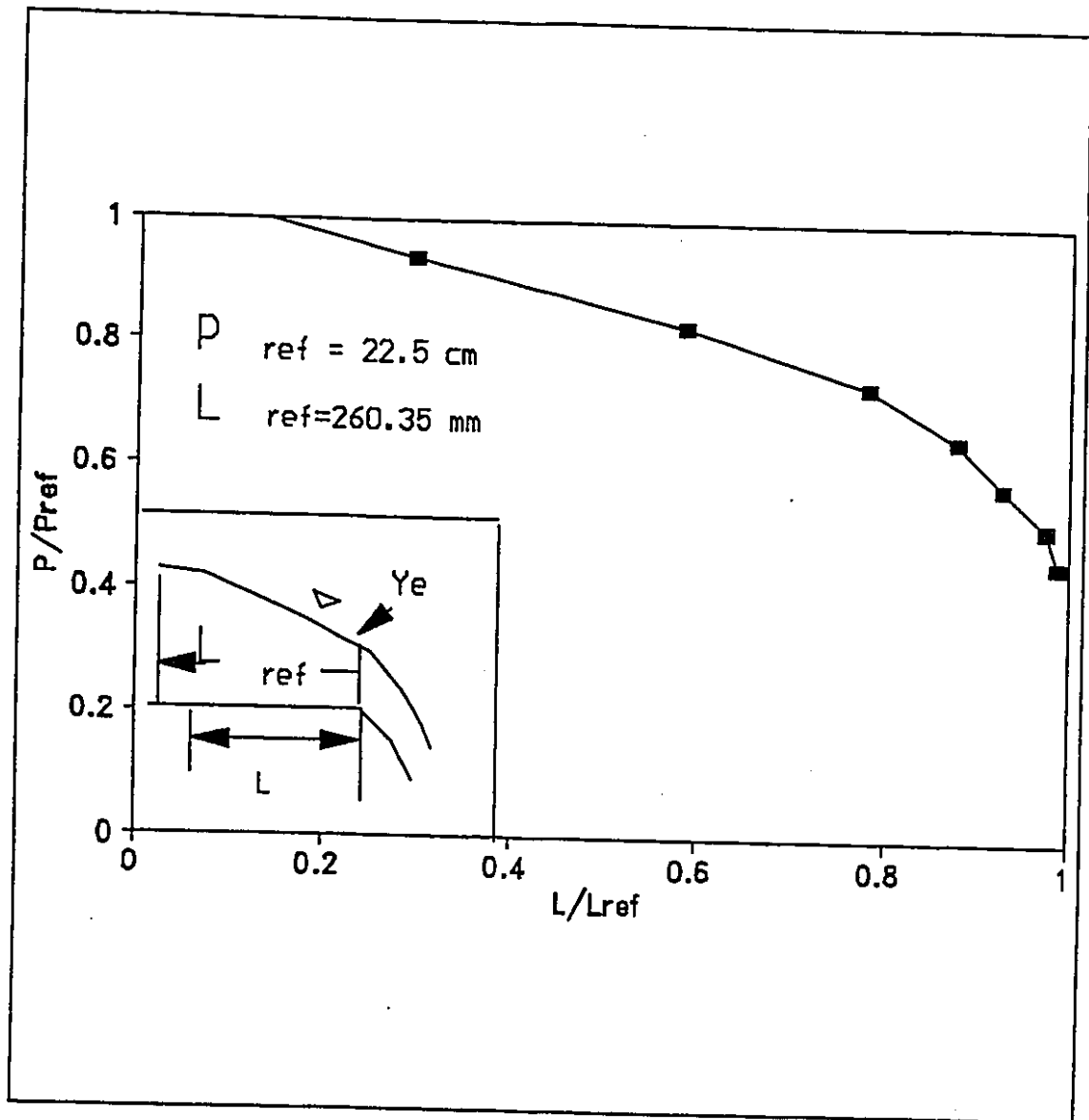


**Fig. 4.5:** Variation of  $P/P_{ref}$  with  $L/L_{ref}$  (Static Wall Profile along Channel Axis,  $X=0, Y=0$ )  $Q=38$  l/s,  $Y_e=11.2$  cm,  $P = P/\gamma =$  wall Pressures

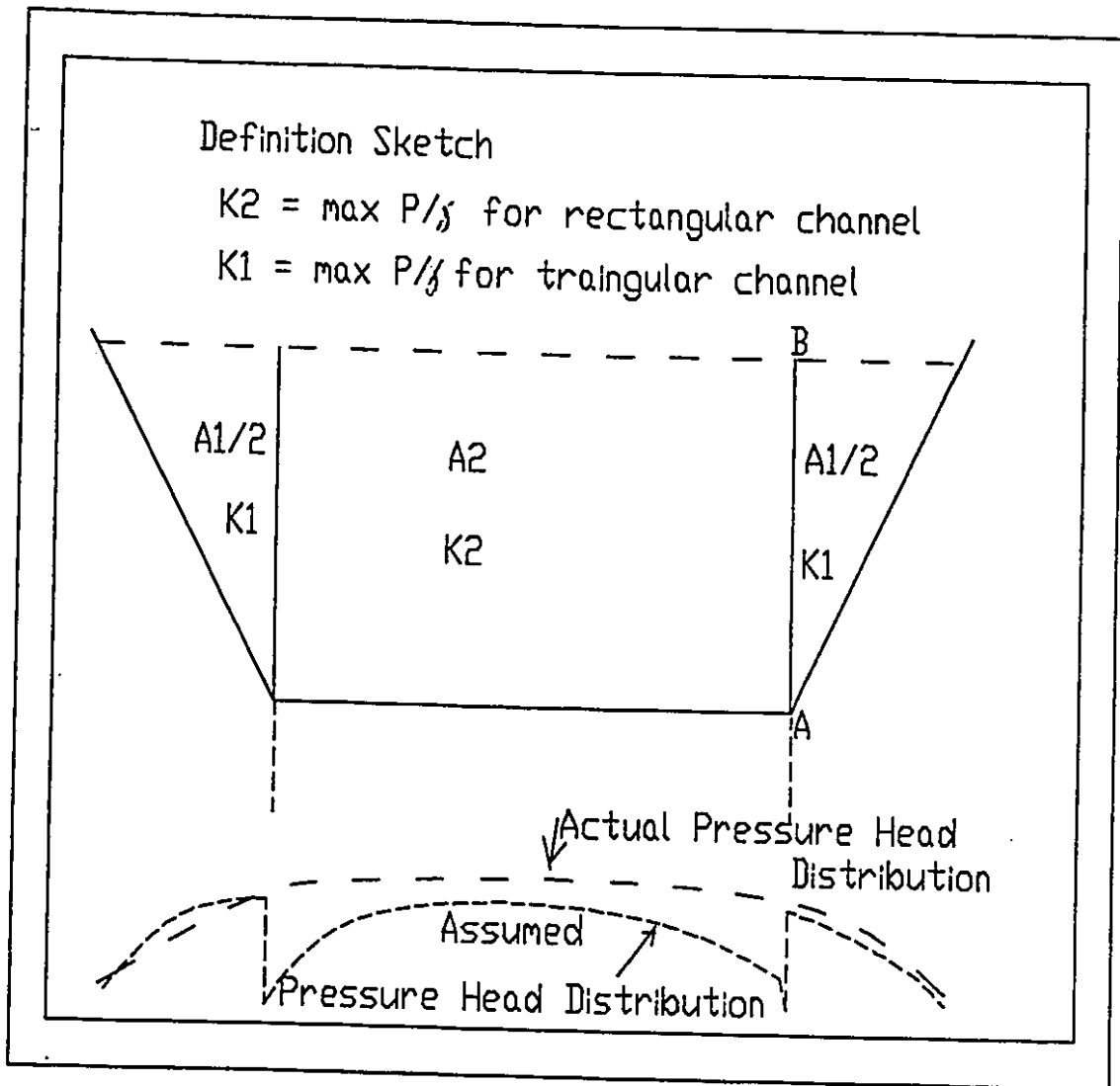


**Fig 4.6:** Definition Sketch used By Keller(1989) To calculated a pressure head coefficient.

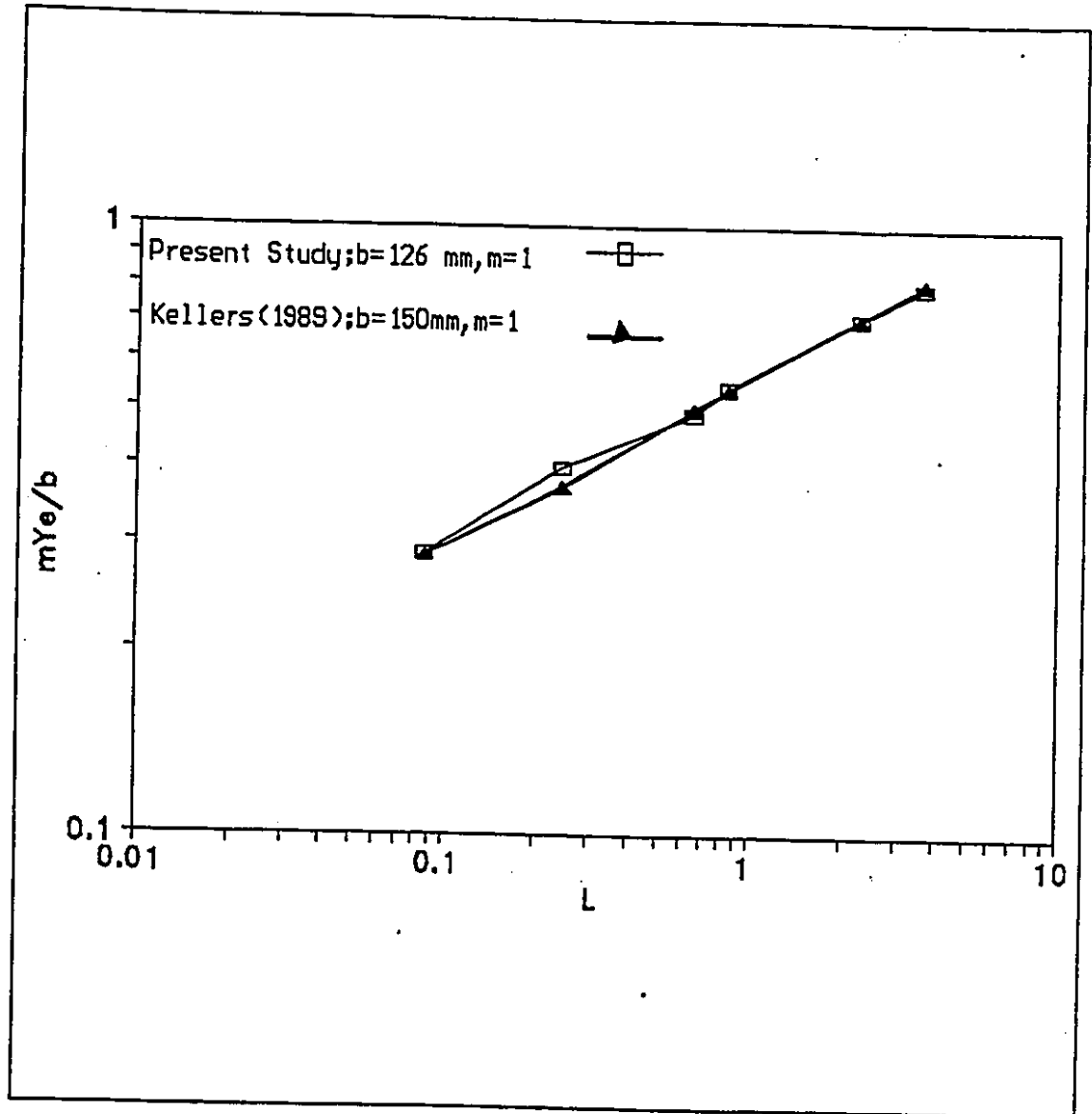


**Fig. 4.7:** Variation of  $mY_e/b$  vs  $L$   
 $L=Q^2m^3/gb^5$   
 $m$ =side slope of channel

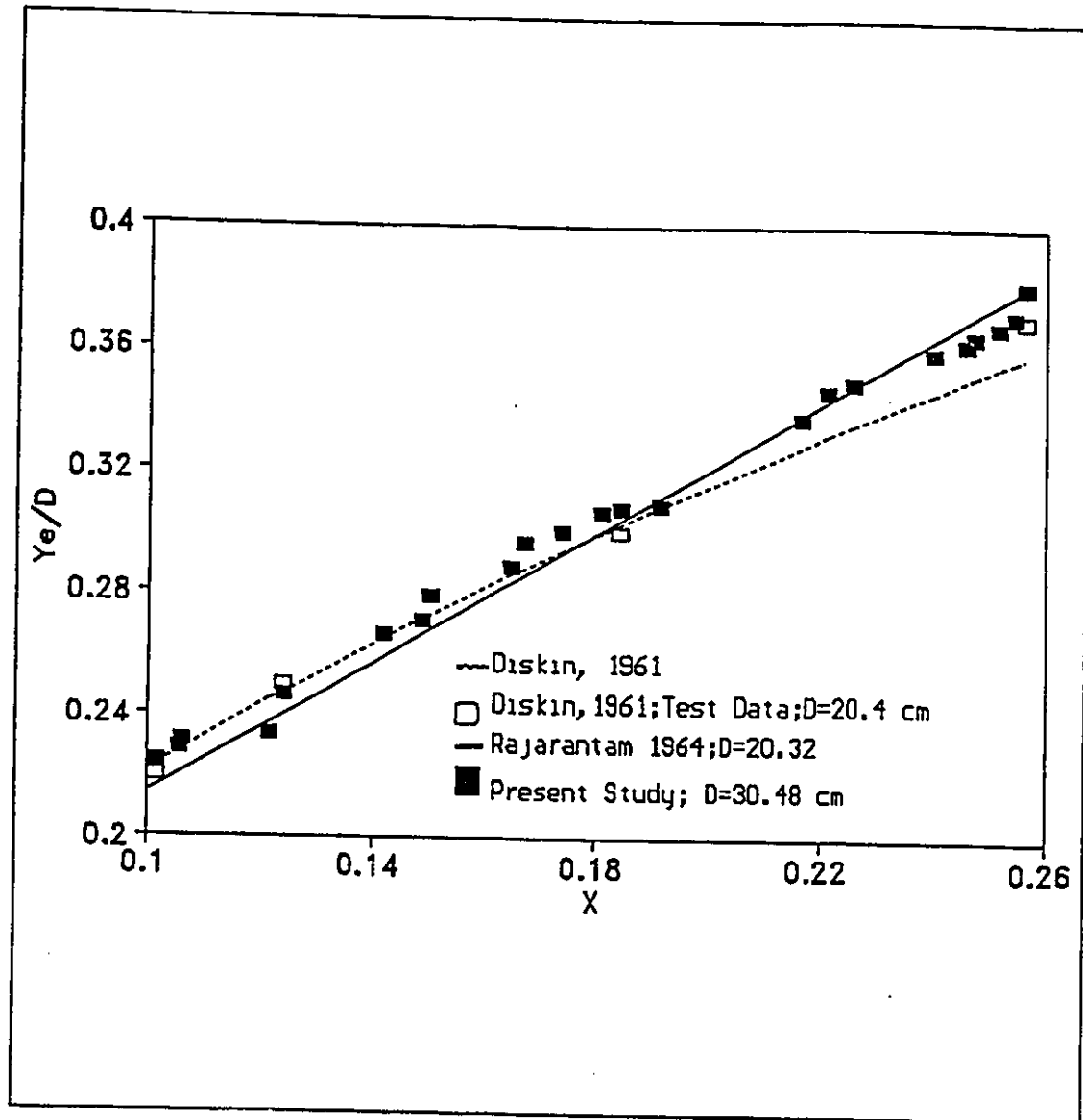


**Fig. 4.8:** Variation of  $Y_e/D$  with Parameter  $X$   
 $X = Q / (g^{0.5} D^{2.5})$

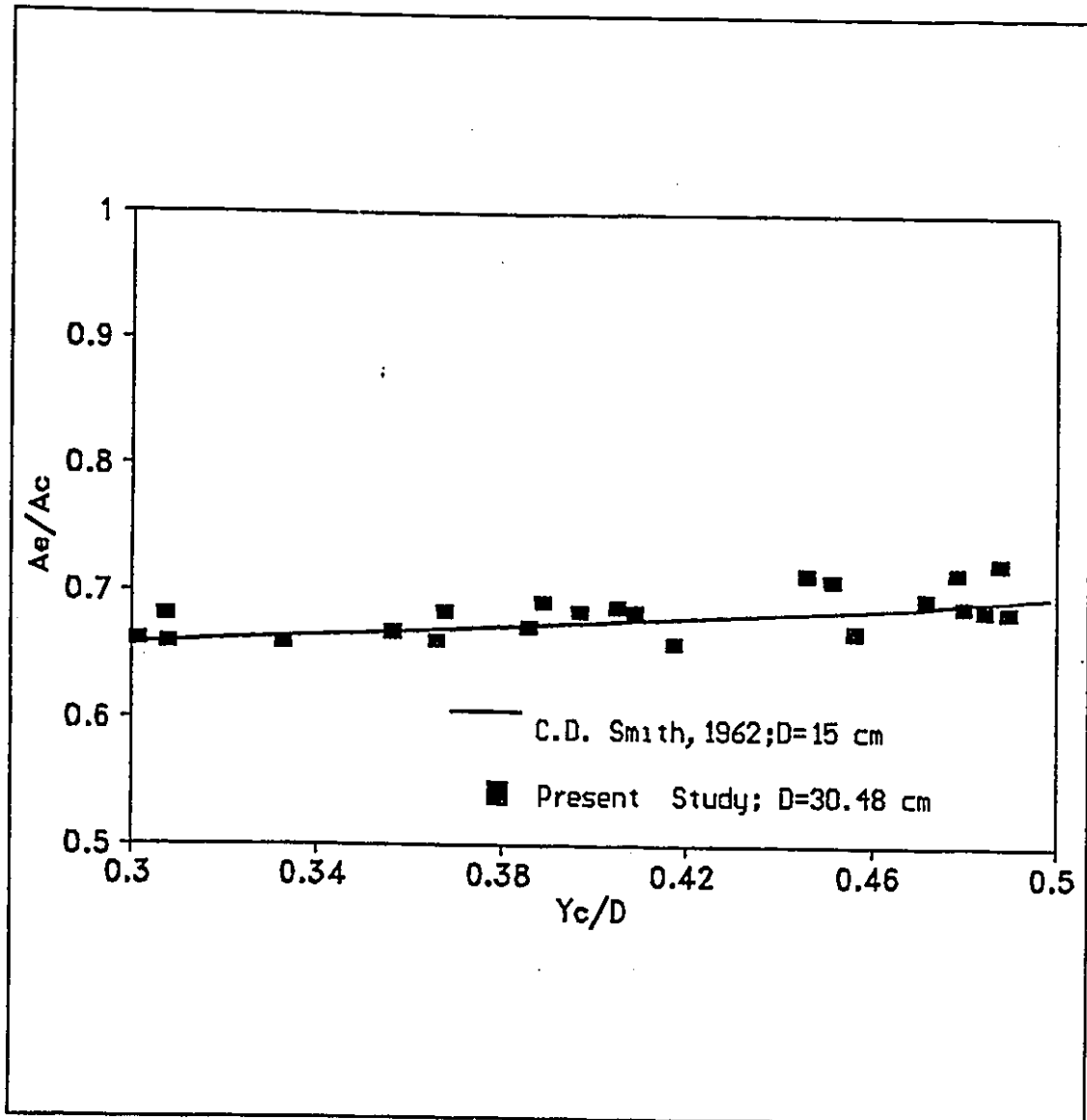
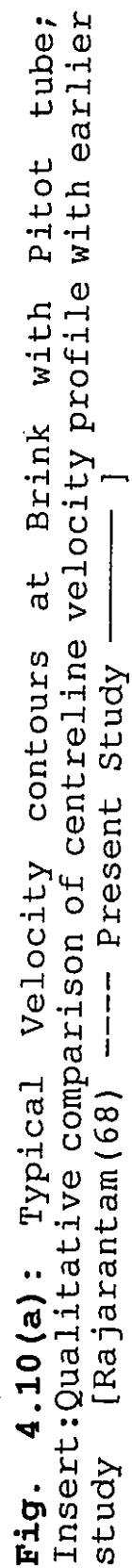


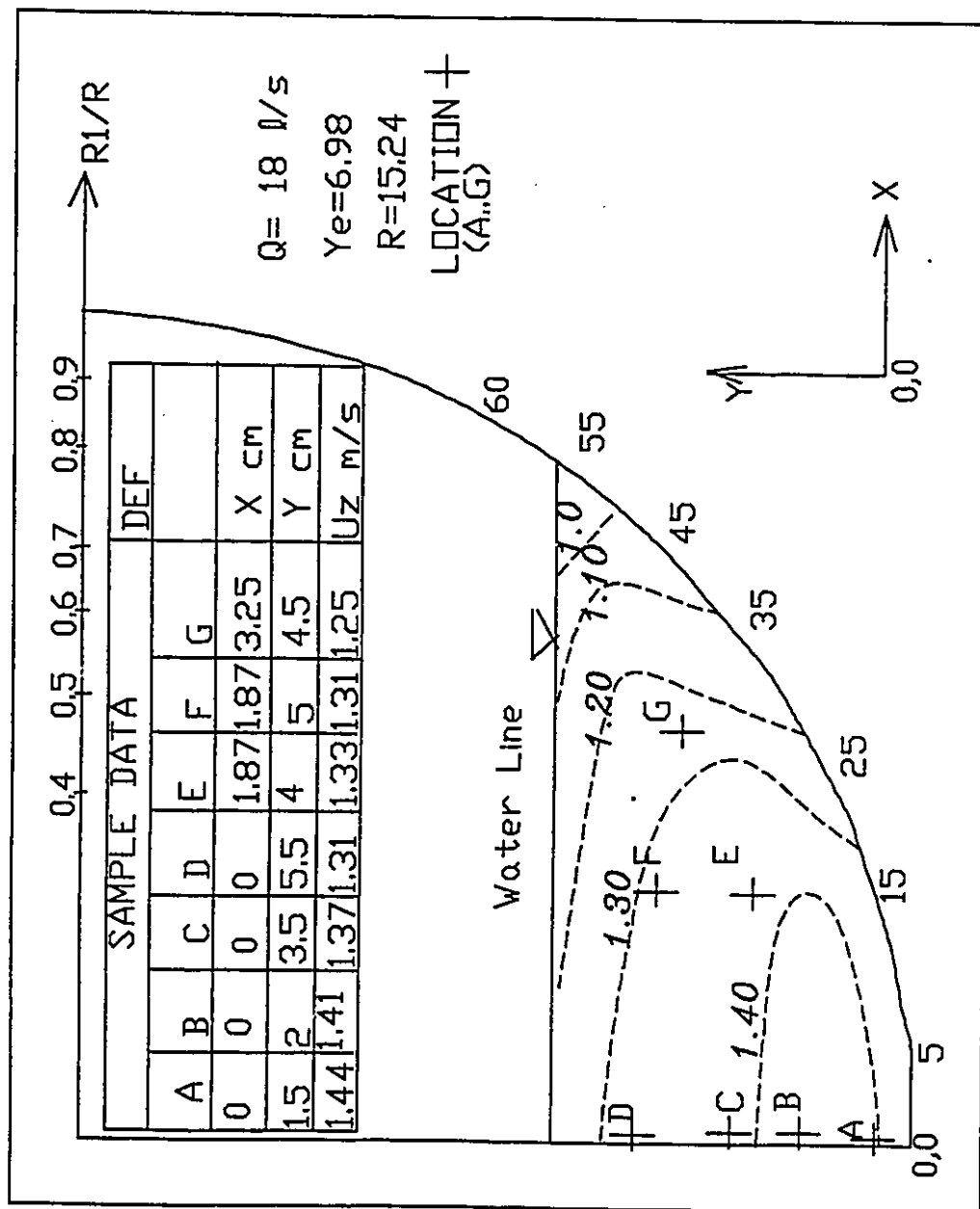
**Fig. 4.9:** Area Ratio vs  $Y_c/D$  Comparisons with Existing Data

$A_e$  = End depth area

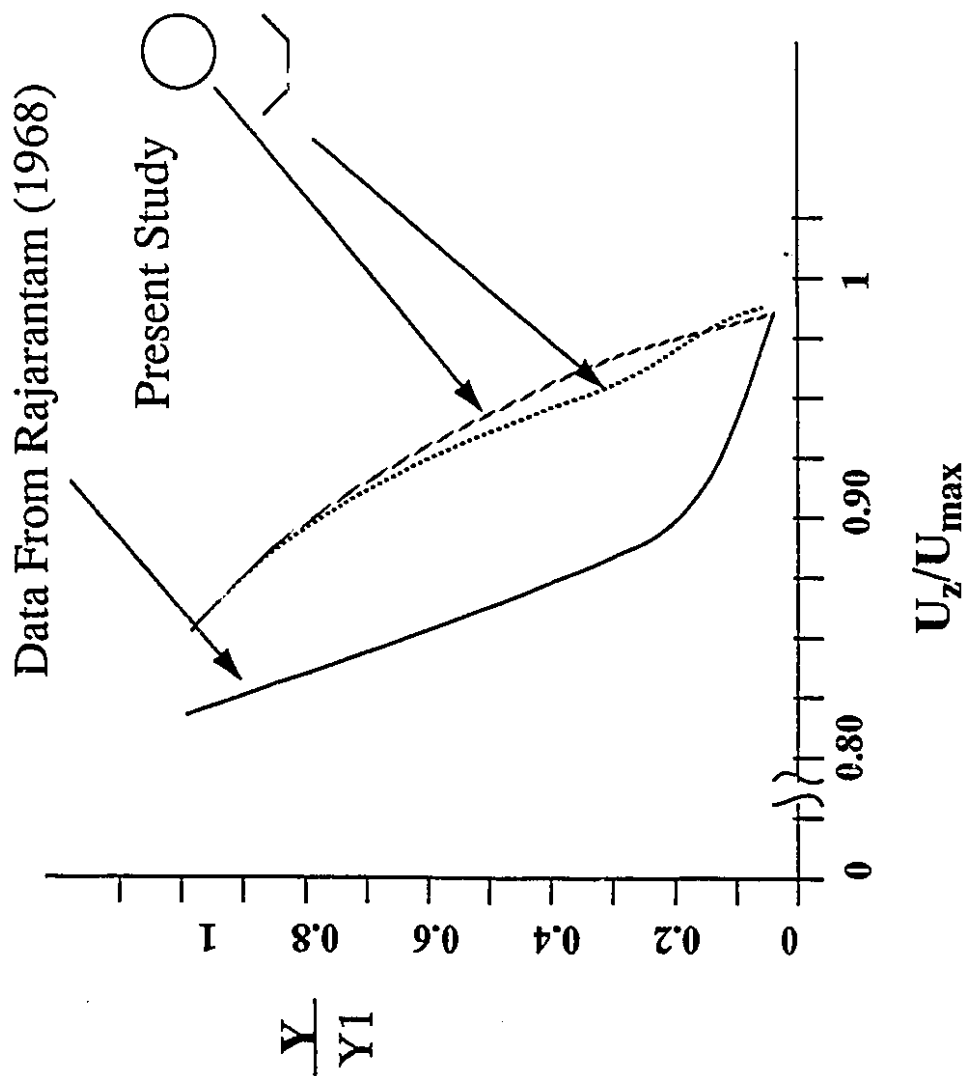
$A_c$  = Critical section area



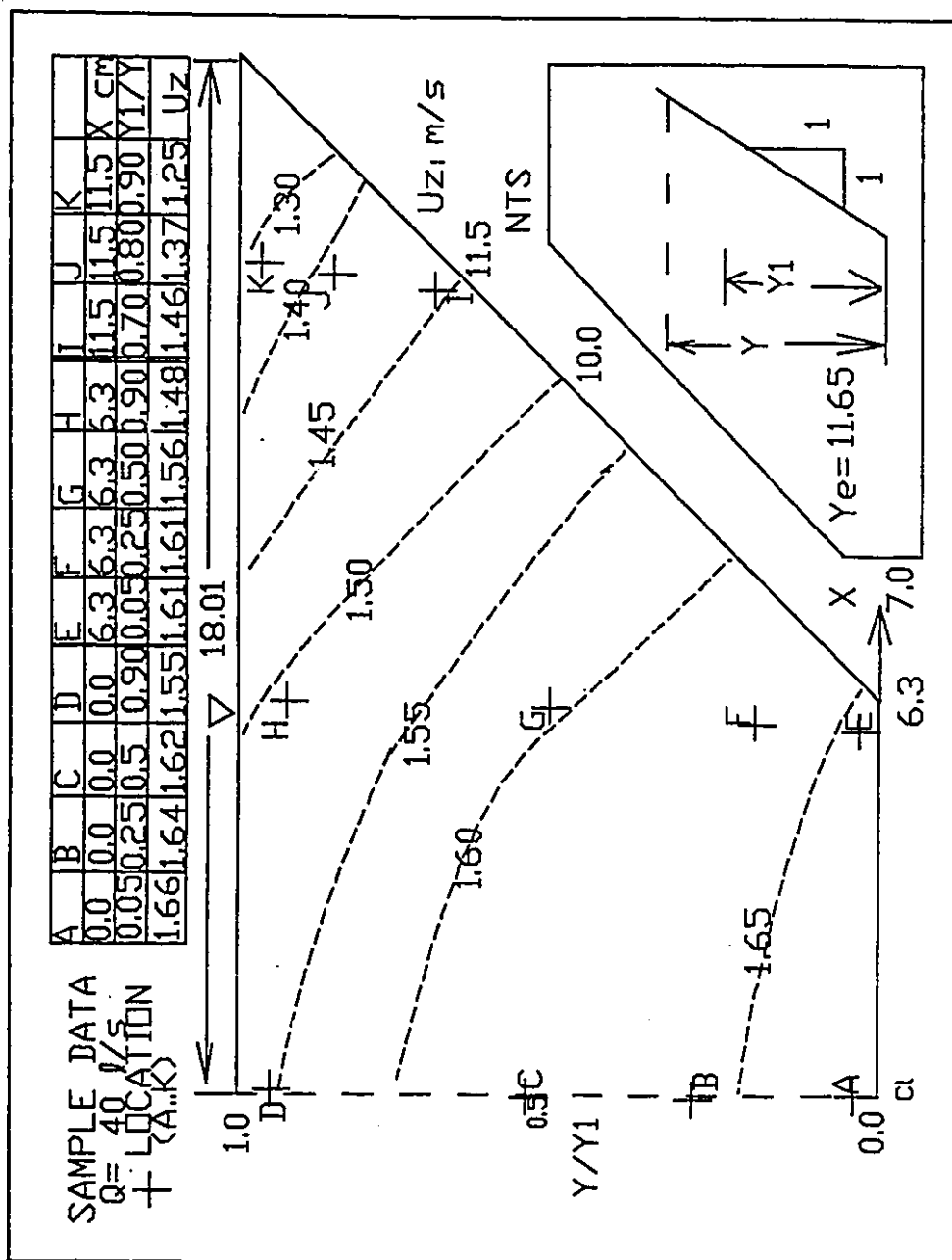




**Fig 4.10(b):** Pitot Tube Measurements  $U_z$  in Circular Channel



**Fig 4.10(c):** Comparisons of Velocity Profiles with Past Studies and Different Channel



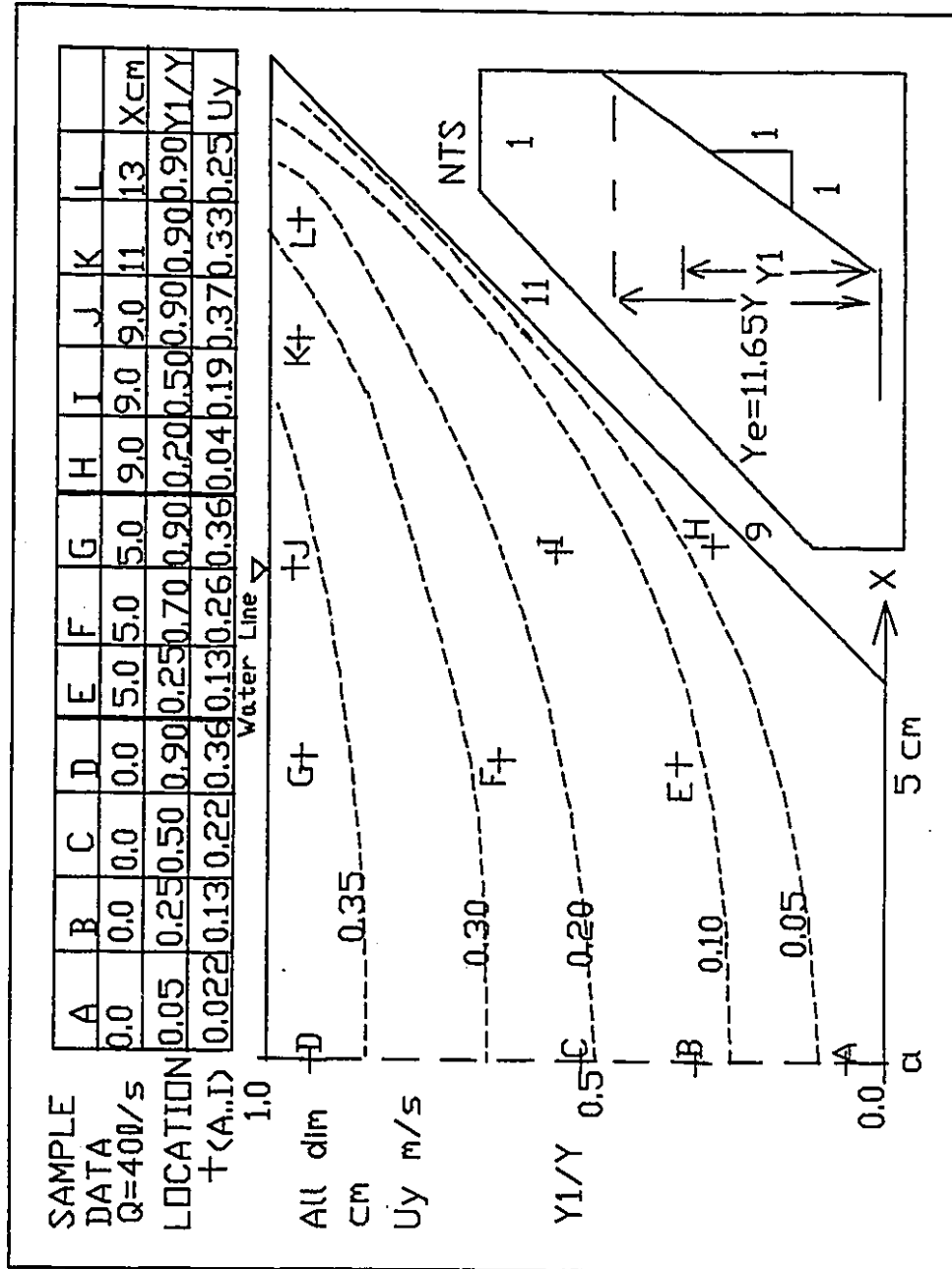


**Fig. 4.11(b):** Vertical Velocity ( $U_y$ ) contours for Laser Measurements;  
Insert: Definition Sketch

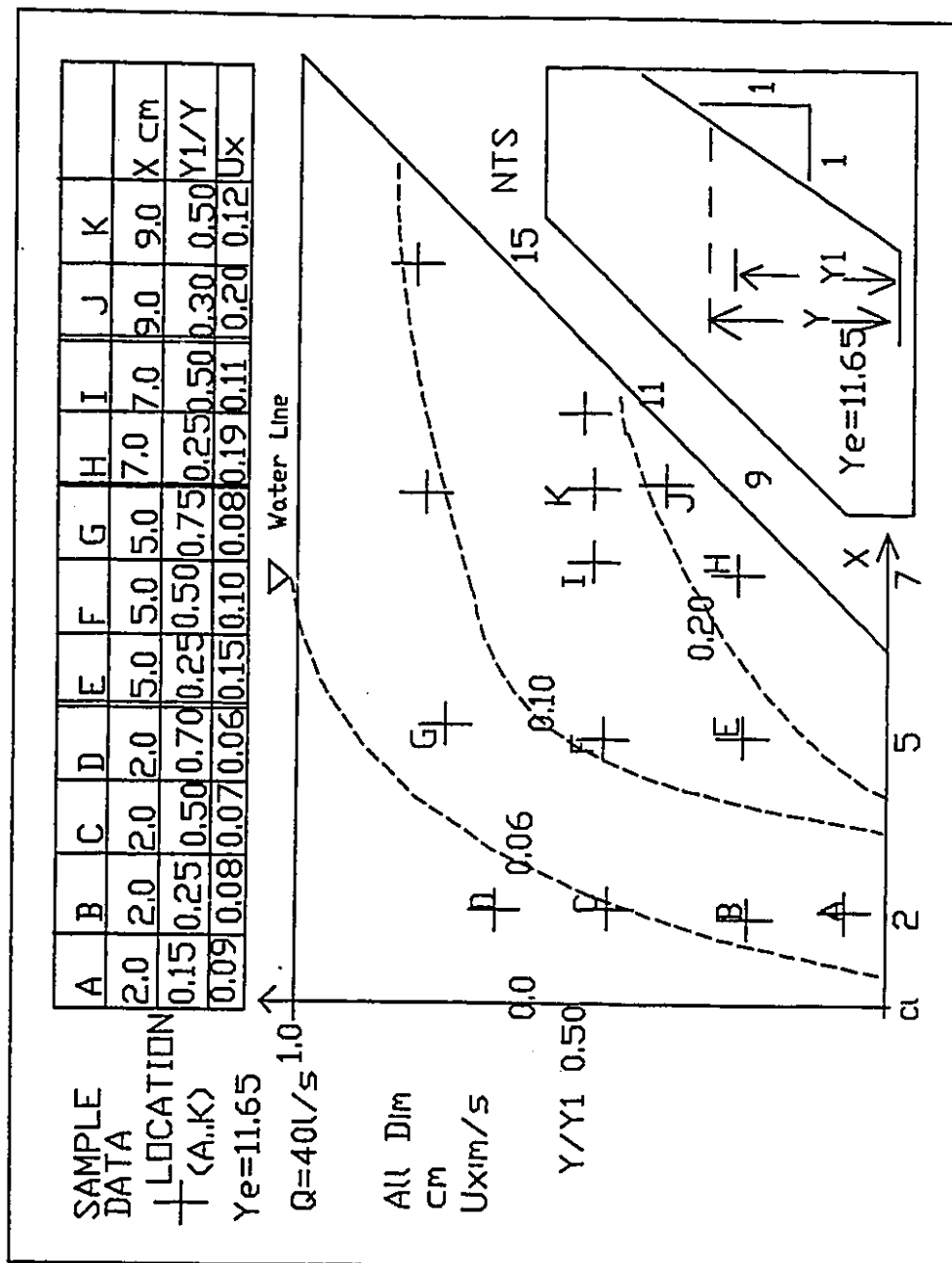


**Fig. 4.11(c):** Lateral velocity ( $U_x$ ) contours for Laser Measurements;  
Insert: Definition Sketch

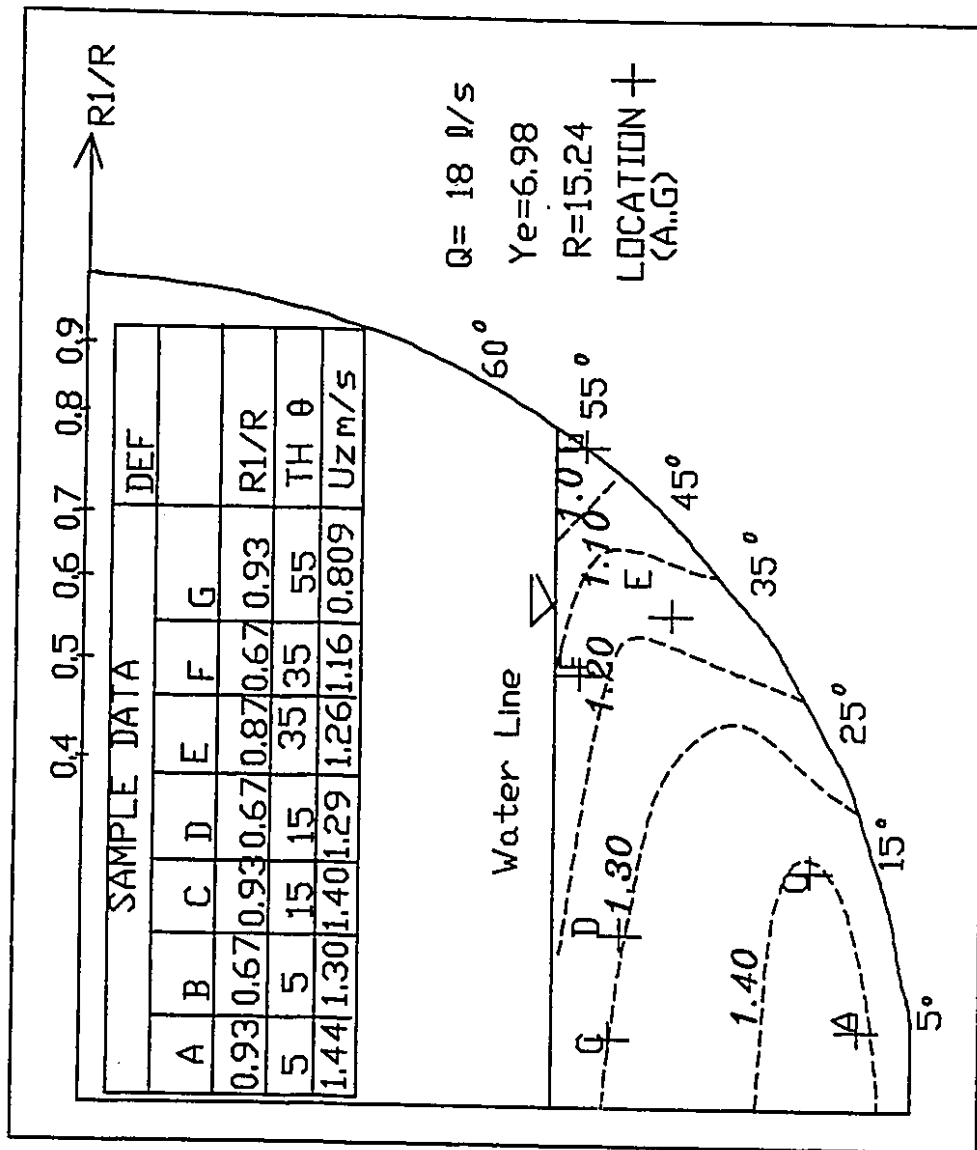
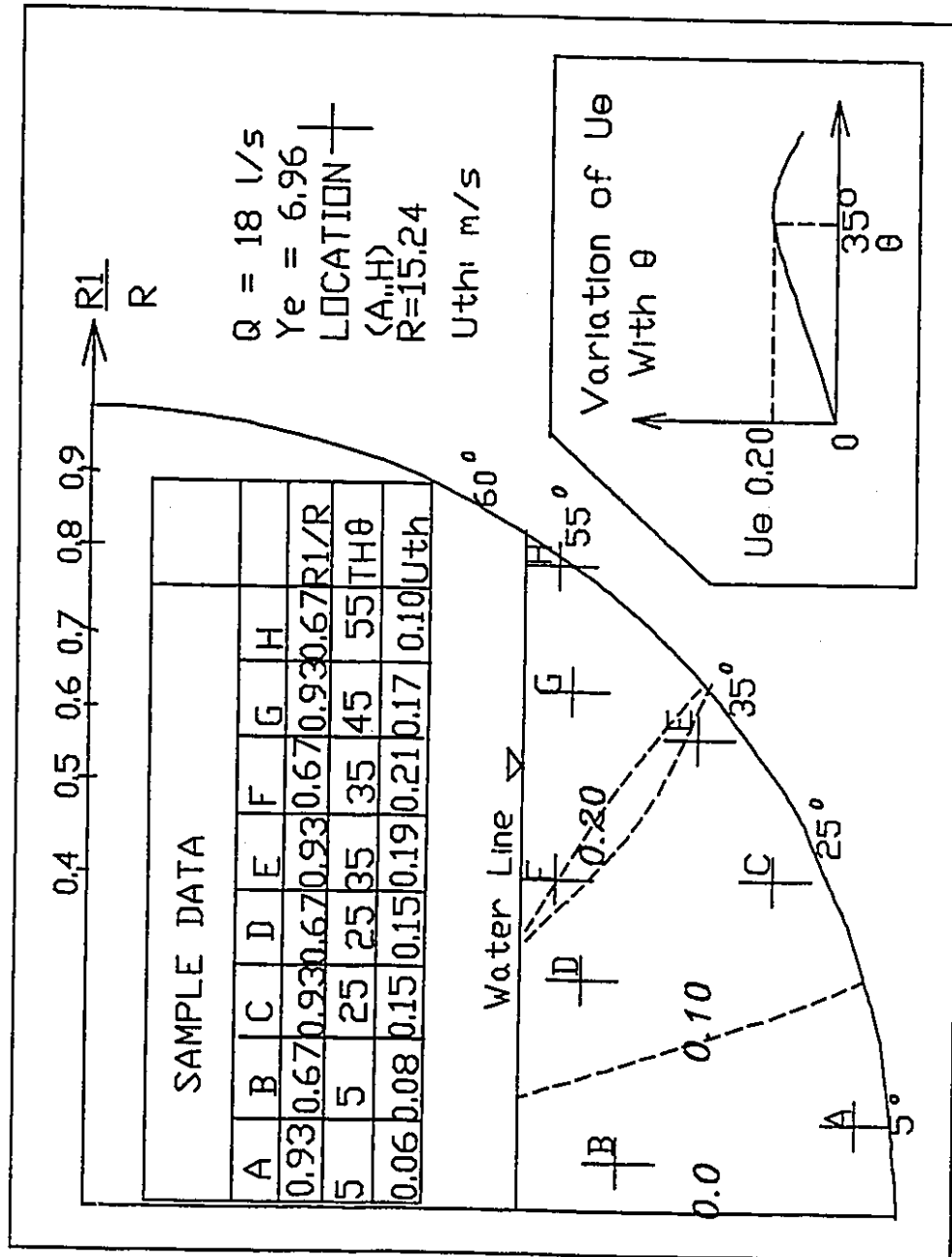


Fig. 4.12(a): Laser Measurements  $U_z$  in Circular Channel



**Fig. 4.12 (b):** Laser Measurements  $U_\theta$  in Circular Channel; insert variation of  $U_\theta$  with  $\theta$



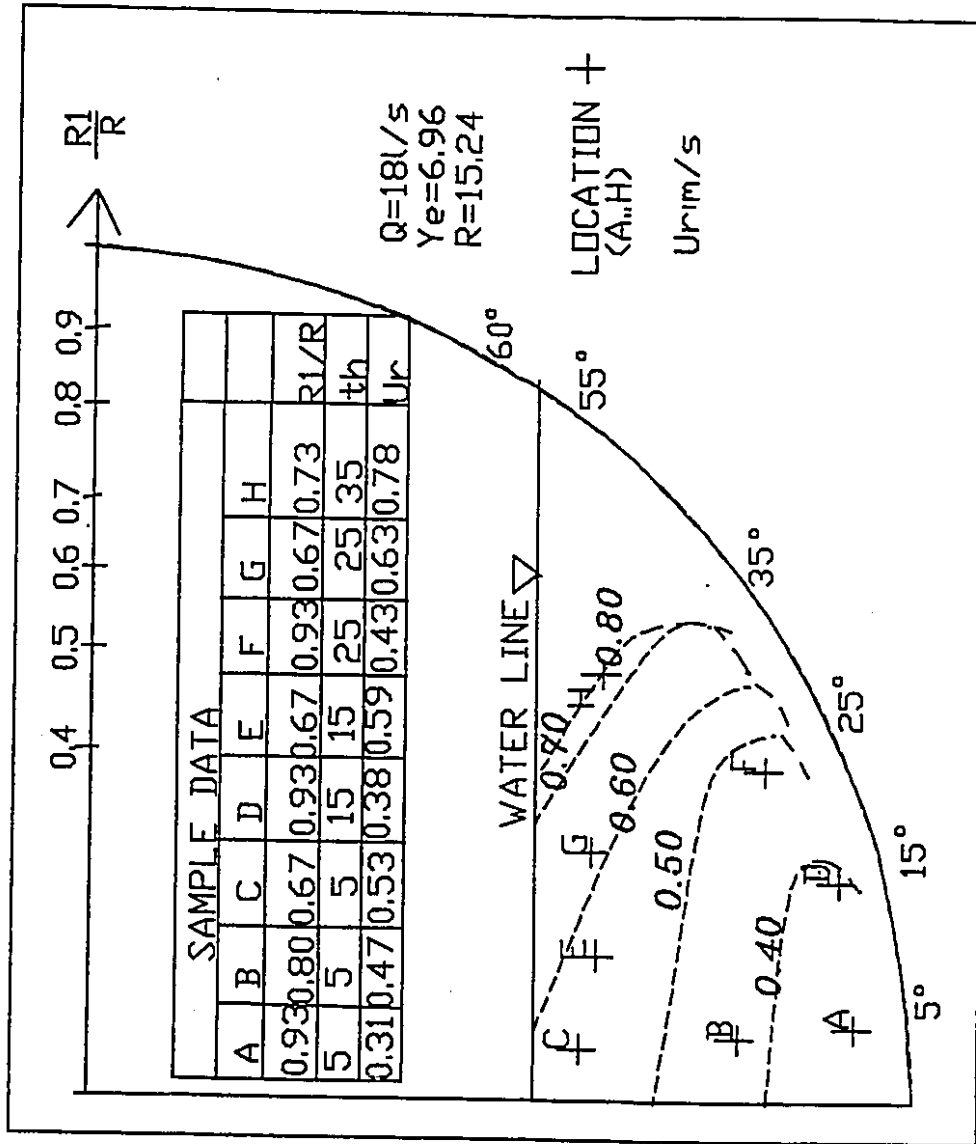
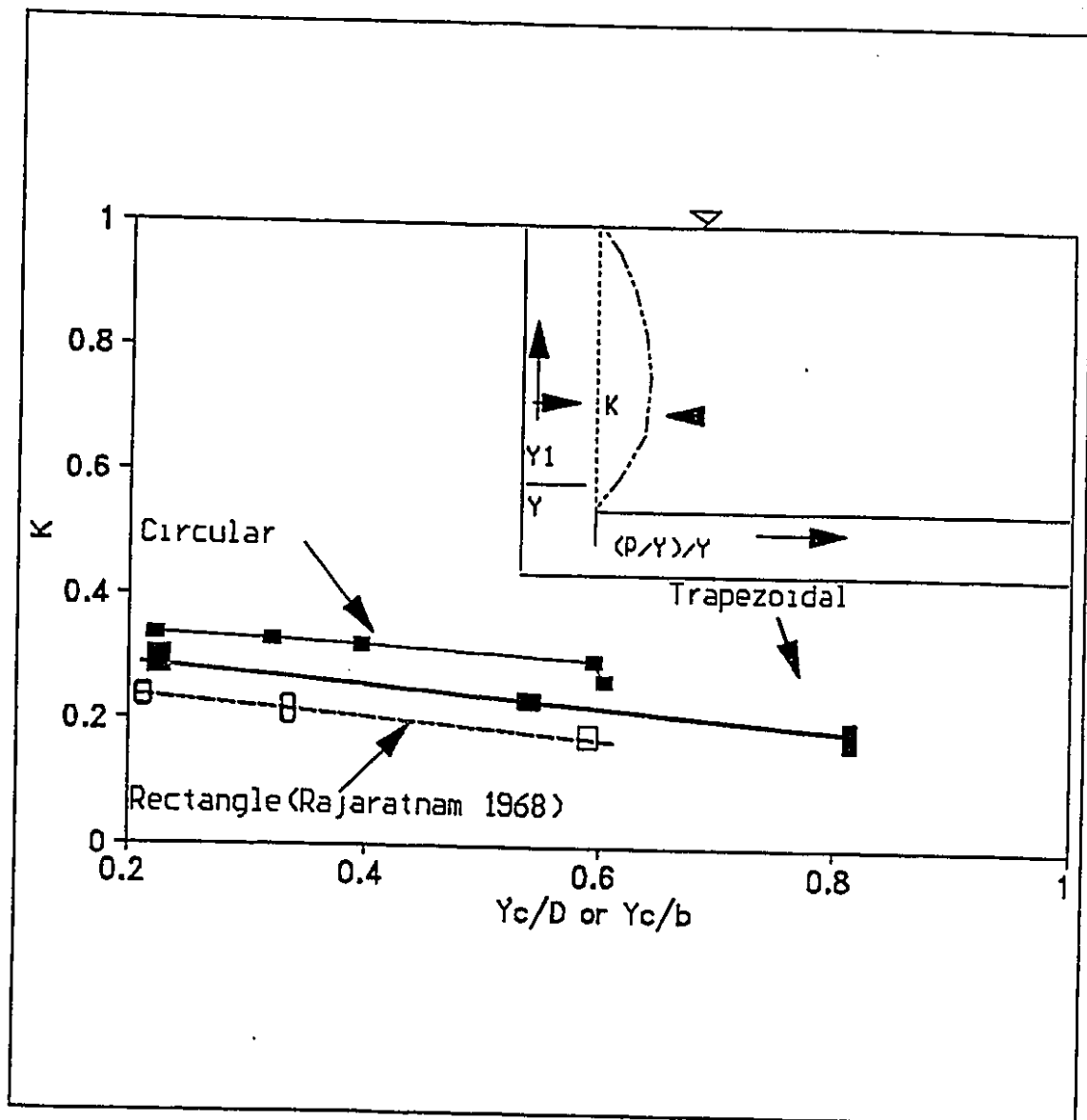
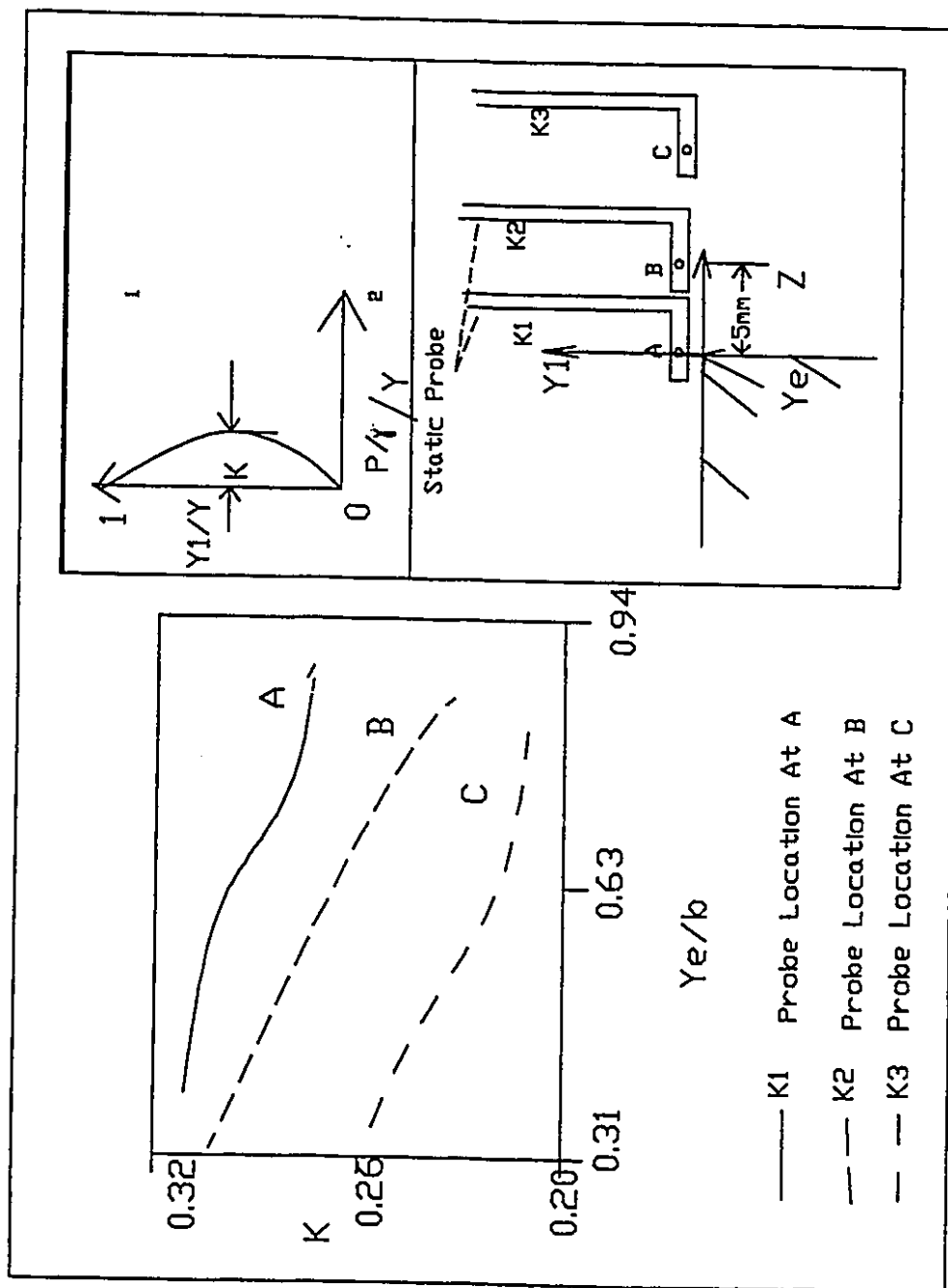


Fig. 4.12(c): Laser Measurements  $U_r$  in Circular Channel



**Fig. 4.13:** Comparing Maximum  $(P/\gamma)/Y$  values at end depth with different geometries  
Circular and Trapezoidal shapes  
determined in current study



**Fig. 4.14** Comparisons of  $K$  with Location of Probe;  
 Top insert: Definition of  $K$ ; Bottom insert: Position of static Probes.

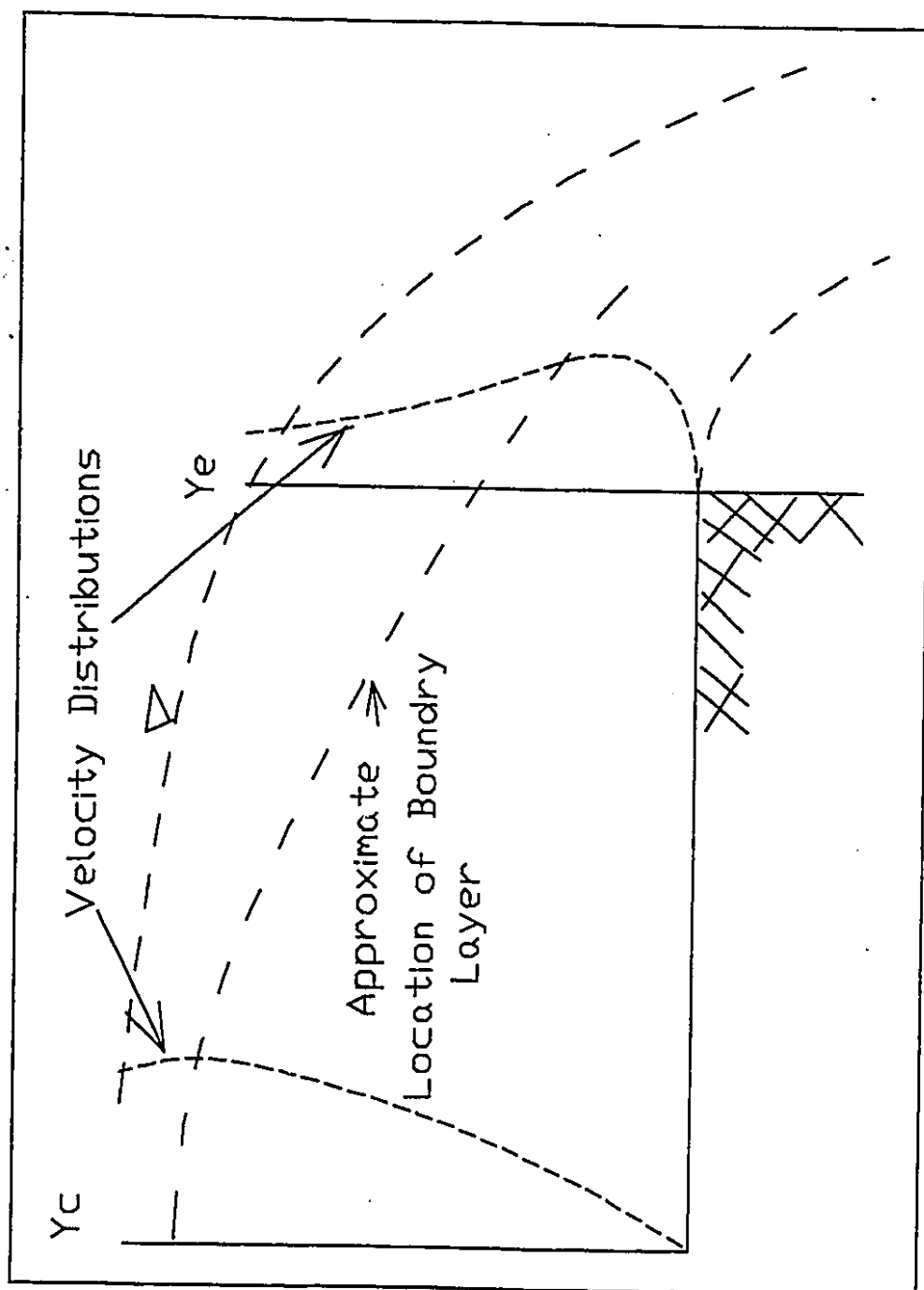


**Fig4.15:** Comparisons of velocity distributions at  $Y_e$  and  $Y_c$ .

## Appendix B

Flow chart for computer program to calculate Alpha and Beta coefficients

Input data in the following format  
One control Line  
# of Data Points, # of X points, # of Y Points  
  
Several information lines  
Xposition Yposition and Velocity

|  
  
Calculate the Average Velocity  
Sum all the Velocity Points, If a velocity point =0 then do not count it. Divide the sum of the velocities by the number of data points that did not have a velocity of 0.

|  
  
Calculate the Dx and Dy

Dx and Dy are  $1/2$  the difference between measurement points. Used to calculate the area around each point.

|  
  
Calculate alpha and beta Coefficients.

```

Program Alphabeta;
Uses Crt;
Var
  P : array[1..100,1..100] of real;
  x : array[1..100] of real;
  y : array[1..100] of real;
  v : array[1..100] of real;
  dy: array[1..100] of real;
  dx: array[1..100] of real;
  DeltaA:array[1..100] of real;
  corner:real;
  Y1: real;
  datapoints : integer;
  vave:real;
  v1:real;
  Xline:integer;
  Yline:integer;
  Xlineb:integer;
  Temp1:integer;
  Temp2:string;
  Vsum,Vtemp,Vtempl,a1,areal:real;
  Vtemp3,Vtemp2,Vsum1,Beta:real;
  alpha:real;

Procedure Input;
(*read data in from either the screen or a data file*)
var
  m:integer;
  j,i:integer;
begin
  datapoints := 9;
  xline :=3;
  Yline :=3;
  writeln('Input the values of x,y,v below');
  writeln(' x  y  v');
  for m := 1 to datapoints do
    readln(x[m],Y[m],v[m]);
    for i := 1 to datapoints do
      begin
        for j:=1 to 2 do
          P[i,j] := x[i];
          P[i,j]:=y[i];
        end;
      for i:=1 to datapoints do
        begin
          for j:=1 to 2 do
            write(p[i,j]:8);
            writeln;
          end;
        end;
      end;
end;
end;

```

```

Procedure Inputfile;

Var
  Filename:string;
  Samplefile:text;
  m,i,j:integer;
function fopened(var thefile: text; FName:string):boolean;
begin
  assign( Thefile,fName);
  (*$I-*)
  Reset (thefile);
  (*$I+*)
  -If IOresult = 0 then
    Fopened := True
  else
    Fopened := false;
end;

Begin
  Writeln('Input the name of the input file');
  readln(filename);
  If Fopened(Samplefile,filename) = true then
  begin
    readln(Samplefile,datapoints,xline,yline);
    for m := 1 to datapoints do
      readln(Samplefile,P[m,1],P[m,2],v[m]);
      close (samplefile);
    end
  else
    writeln('could not open file',filename);
  end;

```

```

Procedure Avelocity;
(*calculates average velocity*)
var
  i:integer;
  vtemp:real;
  count,count1:integer;
begin
  v1:=0;
  count1:=0;
  for i := 1 to datapoints do
  begin
    If v[i] = 0 then
      vtemp:=v1
    else
      begin
        count := count1 + 1;
        vtemp:=v1+v[i];
        count1:=count
      end
    end
  end;

```



```

        end;
        vl:=vtemp;
    end;
    vave:=vl/count1;
    writeln(vave,count1);
end;

```

Procedure dxdy;

```

var
    i,j:integer;
    m,m1:integer;
begin
    Dy[1] :=(p[2,2]-p[1,2])/2;
    for i := 2 to Yline do
        Dy[i] :=(p[i+1,2]-p[i,2])/2 +(p[i,2]-p[i-1,2])/2;
        If Dy[i] < 0 then
            Dy[i] :=(p[i,2]-p[i-1,2])/2;
        Dx[1] :=(p[1+Yline,1]-p[1,1])/2;
        m1:=Yline;
        for i:= 2 to xline do
            begin
                m := m1+Yline;
                D x [ i ]
                :=(P[m+1,1]-p[m,1])/2+(p[m,1]-p[m-(Yline+1),1])/2;
                m1:=m;
            End;
            If Dx[i] < 0 then
                Dx[i] :=(p[M1,1]-p[M1-(Yline+1),1])/2;
            For i := 1 to Yline do
                Writeln(dy[i]:8);
            For j:= 1 to xline do
                writeln(dx[J]:8);
            end;
end;

```

Procedure area;

```

var
    k,i,k1,j:integer;
begin
    K1:=0;
    for i := 1 to xline do
        begin
            for j := 1 to Yline do
                begin
                    k:=k1+1;
                    deltaA[k]:=dx[i]*dy[j];
                    K1:=k;
                end;
            end;
        for i:= 1 to datapoints do
            writeln(deltaa[i]:3:0,' ',v[i]:3:3);
        end;
    end;

```

```

end;

Procedure Calc;
var
i:integer;

begin
  al:=0;
  vtemp3:=0;
  Vtemp:=0;
  for i := 1 to datapoints do
    begin
      If v[i]=0 then deltaa[i] := 0;
      areal:= al + deltaa[i];
      al:=areal;
      vtemp1:=v[i]*v[i]*v[i]*deltaa[i];
      Vtemp2:=v[i]*v[i]*deltaa[i];
      vsum:=vtemp+vtemp1;
      vsum1:=vtemp2+vtemp3;
      vtemp3:=vsum1;
      vtemp:=vsum;
    end;
    writeln(al,vave);
    alpha:=vtemp/(al*vave*vave*vave);
    Beta:=vtemp3/(al*vave*vave);
    writeln('Alpha =',alpha:3:3,' Beta=',beta:3:3);

  end;

Procedure Output;
var
  i,j:integer;
  output:text;
  out1:string;
begin
  writeln('Input the name of the outputfile');
  readln(out1);
  Assign(output,out1);
  Rewrite(output);
  For i := 1 to Yline do

    Writeln(output,'Dy['',i,'']= ',dy[i]:8);
    For j:= 1 to xline do
      writeln(output,'Dx['',j,'']= ',dx[J]:8);
    for i:= 1 to datapoints do
      writeln(output,'delta    A['',i,'']= ',deltaa[i]:3:3,'
        ', 'V['',i,'']= ',v[i]:3:3);

    writeln(output,'Beta=',beta:3:3,' Alpha= ',alpha:3:3);

  Close (output);
end;

```

```
Begin
  clrscr;
  Writeln('Do you want to input data from the screen or
File?');
  Writeln(' (1)screen      (2)File');
  readln(temp1);
  If temp1 = 1 then
    Input
  else
    begin
      Inputfile;
    end;
  avelocity;
  dxdy;
  area;
  calc;
  output;
  readln;
end.
```

Flow chart for calculating the Pressure Coefficients

Input Data in the Following Format  
Q, Ye, Pressure head

Use Formulas in Table 2.1 to calculate coefficients

Output Results

```

Program pressure coefficient;
uses Crt;
Var
A:array[1..100] of real;{area of cross section}
V:array[1..100] of real;{average velocity}
q:array[1..100] of real;{flow rate}
c:real;{pressure head correction}
alphaprim,Betaprim:array[1..100] of real;{Pressure
coefficients chow}
Ye:array[1..100] of real;{end depth}
z:real;
H:array[1..100] of real;{measured pressure head}
K1:array[1..100] of real;{Raja coefficient}
P:array[1..100] of real; {real pressure}
Gamma:real;{specific weight of water}
K:array[1..100] of real;{kellers coefficient}
Xe:array[1..100] of real;
Ko:array[1..100] of real;{Chris coefficient}
I:integer;
Trails:integer;{How many trails need calculating}

Procedure Input;
var
Filename:string;
Sample:text;
Temp:integer;

Function Fopened(Var thefile:text;Fname:string):boolean;
Begin
Assign( thefile,fname);
(*$I-*)
Reset (thefile);
(*$I+*)
If IOresult = 0 then
Fopened := True
else
Fopened := false;
end;

Procedure Finput;
Var
Filename:string;
samplefile:text;
m:integer;

```

```

Begin
  Writeln('Input the name of the input file');
  Readln(filename);
  If fopened(samplefile,filename) = true then
    Begin
      Readln(samplefile,trails);
      For m := 1 to trails do
        readln(samplefile,q[m],Ye[m],H[m]);
      close (samplefile);
    end
  else
    writeln('could not open file',filename);
  end;

  Procedure screen;

  Var
    Filename:string;
    samplefile:text;
    m:integer;

  Begin
    Writeln('Input Name of input file to create');
    Readln(filename);
    Assign(samplefile,filename);
    Rewrite(samplefile);
    Writeln('Input number of trials');
    Readln(trails);
    Writeln(samplefile,trails);
    For m:= 1 to trails do
      begin
        Writeln('inpute Ye,Q,H');
        Readln(Ye[m],q[m],h[m]);
        writeln(samplefile,Ye[m],q[m],h[m]);
      end;
    Close (samplefile);
  end;

  Begin

    writeln('Input data by (1) file or by the (2) screen');
    Readln(temp);
    If Temp = 1 then
      Fininput;
    If temp = 2 then
      screen;
  end;

```

```

Procedure chow;
begin
  z:= (2/3)*Ye[i];
  a[i]:= (0.127+Ye[i])*ye[i];
  v[i]:=q[i]/a[i];
  c:= v[i]*v[i]/9.81;
  alphaprim[i]:= 1 + (1/q[i]*ye[i])*c*v[i]*a[i];
  betaprim[i]:= 1 + (1/a[i]*z)*c*a[i];
end;

Procedure Raja;
Begin
  gamma :=9810;
  p[i]:=h[i]*gamma*a[i];
  kl[i]:=p[i]/(a[i]* 0.5 * ye[i]*gamma);
end;

Procedure keller;
Begin
  xe[i]:=ye[i]/0.127;
  k[i]:= (4/3)*(0.215+0.175*xe[i])/(1+xe[i]);
end;

Procedure Chris;
var
  m:integer;
  Yc:real;{critical depth}
  r:real;
  D:real;
  Temp1,temp2,temp3,temp4:real;
  tol:real;
begin
  Q[i]:= q[i]/0.02831;
  Yc:=2.0927+16.009*q[i]-7.8757*q[i]*q[i]+2.1849*q[i]*q[i]*q[i];
  r:=ye[i]/(0.01*yc);
  d:=0.25;
  temp1:=1/r;
  Temp3:=(d/yc)*(d/yc);
  temp4:=(H[i]/d)*(h[i]/d);
  Ko[i]:= 0.01;
  repeat
    temp2:=1.5+0.5*(ko[i]*r*r+temp3*temp4);
    writeln(temp2,temp1);
    tol:=temp1-temp2;
    Ko[i]:= 0.01+ko[i];
  until ( abs(tol)<0.01);
end;

```

```

Procedure output;
Var
  Output:text;
  out1:string;
  i:integer;

begin
  Writeln('Input the name of the output file');
  readln(out1);
  Assign(output,out1);
  Rewrite(output);
  writeln(output,'Ye   alphaprim[i], ,betaprim[i],   ,k1,
,k,   ,ko');
  for i := 1 to trails do
    begin
      writeln(output,'Ye['',i,'']=','Ye[i]:3:3,','
',alphaprim[i]:3:8,','',betaprim[i]:3:8,','',k1[i]:3:8,','
',k[i]:3:8,','',ko[i]:3:8);
      writeln(alphaprim[i]:3:8,','',betaprim[i]:3:8,','
',k1[i]:3:8,','',k[i]:3:8,','',ko[i]:3:8);
    end;
  Close(output);
end;

Begin
  clrscr;
  input;
  For i:= 1 to trails do
    begin
      chow;
      Raja;
      Keller;
    (*  chris;*)
  end;
  output;
  writeln('Press enter to continue');
  readln;
end.

```



## Appendix C

## C.0 Using the Momentum Equation with Measured Pressure Heads

### C.0.1 Circular

Equations used in the analysis

$$\theta = 2\cos^{-1}\left(\frac{0.3048/2-H}{0.3048/2}\right) \quad \text{C.1}$$

$$A = 0.3048^2 \frac{\theta - \sin\theta}{8} \quad \text{C.2}$$

$$V = Q/A$$

$$M = \rho QV_c$$

$$P = 0.5HA\gamma$$

$$P_o = 1/2 (P/\gamma)_{\text{value measured}} \gamma A^*$$

$A^*$  = The sub area in the channel around which the  $(P/\gamma)_{\text{value}}$  value was measured. Refer to Fig C.1 for definition of sub areas used in circular channels when calculating the pressure force with measured values of  $P/\gamma$ .

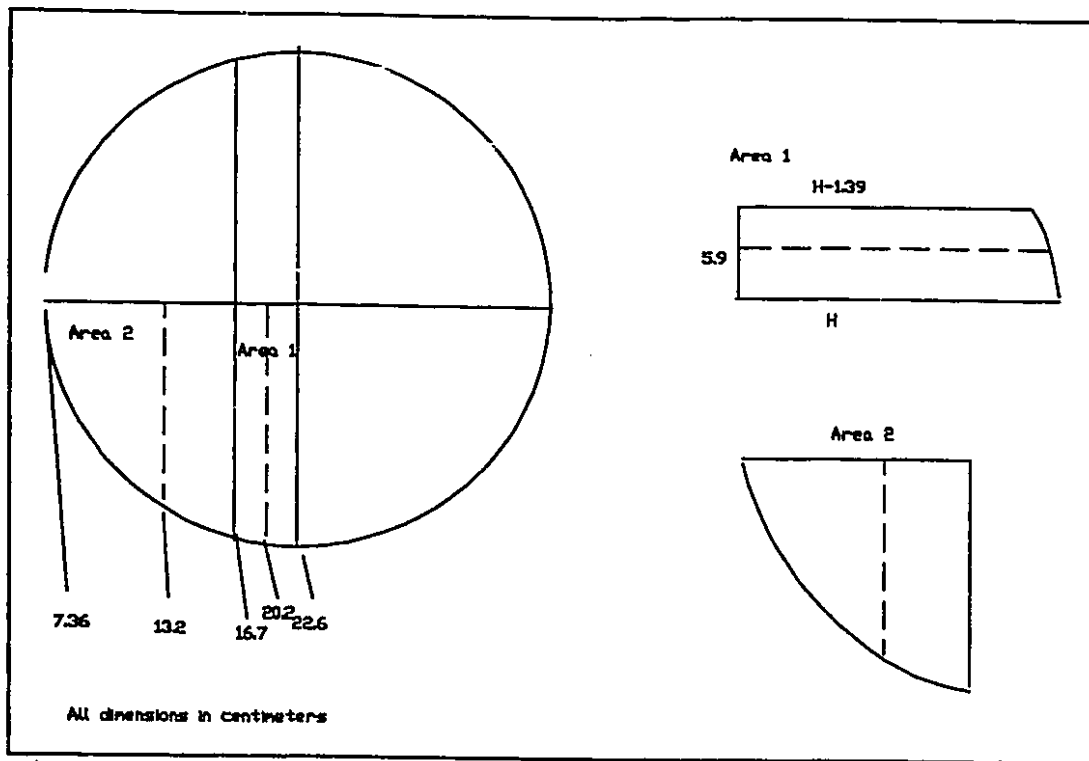


Figure C.1

Areas were calculated by the following method.

$$A1 = 5.9 * (h - 1.39) + 0.5 (5.9 * 1.39)$$

$$A2 = A/2 - A1$$

### C.0.2 Trapezoidal Channel

The same method was used for the trapezoidal channel. The only difference was the way the incremental areas were calculated.

The procedure for calculating each incremental area were as follows:

- (1) Took a line were vertical pressure head

measurements were performed.

- (2) Formed a rectangle around the line and calculate its area.
- (3) In the Triangle section the shape was a triangle plus rectangle.

The formula for calculating the area of a trapezoidal channel is shown below.

$$A = (b + y) y$$

### **C.1 Calculating $U_r$ in circular channels.**

Because the velocities were measured in two dimensions,  $U_r$  had to be calculated using the  $U_z$  and  $U_\theta$  data. To get the radial velocities, the following procedure had to be followed. Refer to Fig C.2 for definitions

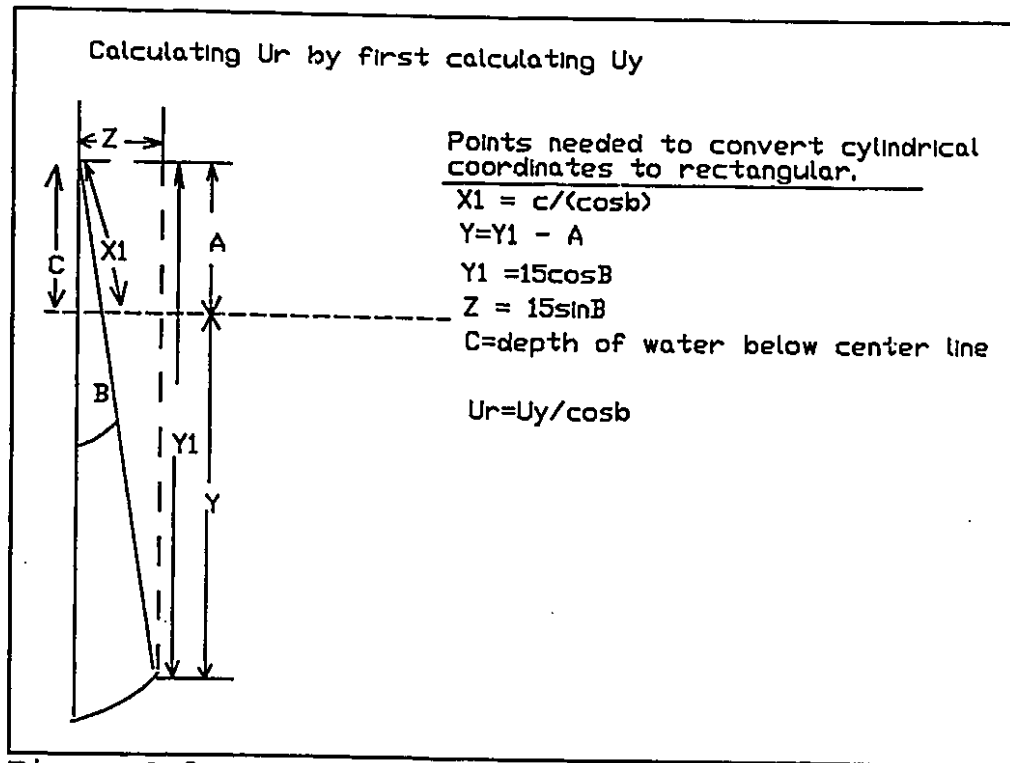


Figure C.2

First in calculating the  $U_r$  component, the position of the LDA measuring volume was located.

To accurately calculate the position and thus  $U_r$ , a table had to be set up. An example of such a table is shown in Table C.1. This table was generated for a flow rate of 40.71 l/s ( $Y_0 = 11.91$ ).

To obtain a value of  $dy/dz/y$ , had to first obtain an equation for the slope of the water surface. The slope of the water surface was obtained by measuring the water surface profile and using the least square method to generate an

equation. After an equation had been generated, the first derivative ( $dy/dz$ ) at the end depth ( $Y_e$ ) was taken. Then divided the first derivative by  $Y_e$ .

Table C.1 Calculation Table 1

B	Y1	Z	Y	$dy/dz/y$
5	14.94	1.3	11.84	0.0428
25	13.6	6.33	10.5	0.0483
35	12.3	8.6	9.2	0.0511
55	8.6	12.28	5.5	0.0589

Refer to Fig C.2 for Definitions

For B= 25 Degrees

$X_1 = 3.42$  cm (See Figure C.2)

Distance Below Water Surface

Along R coordinate position = 6.58 cm

$$Y = 6.58 \cdot \cos 25 = 6.58 \text{ cm}$$

$$Z = 10 \cdot \sin 25 = 4.22 \text{ cm}$$

$Y = 11.19$  and  $dy/dz/Y = 0.0455$  by interpolation from Table C.1

Distance from Bottom of channel =  $11.19 - 5.96 = 5.23$  cm

$$dy/dz = 0.0455 \cdot 5.23 = 0.238$$

Using the relationship of  $dy/dz = U_y/U_z$

$$U_z = 1.61 \text{ m/s (measured)}$$

$$U_y = 1.61 * 0.238 = 0.3804 \text{ m/s}$$

To Calculate  $U_r$ , use the following expression

$$U_r = U_y / \cos 25 = 0.419$$

For calculating the rest of the  $U_r$  values used Eq C.3.

$$\frac{\partial U_z}{\partial z} + \frac{1}{r} \frac{\partial U_r R}{\partial R} + \frac{1}{R} \frac{\partial U_\theta}{\partial \theta} = 0 \quad \text{C.3}$$

This equation was the continuity equation. Since  $U_z$  and  $U_\theta$  were measured, the components with those terms could be evaluated. For each radial, the  $U_r$  component was evaluated by the following forward difference formula as shown in Eq C.4.

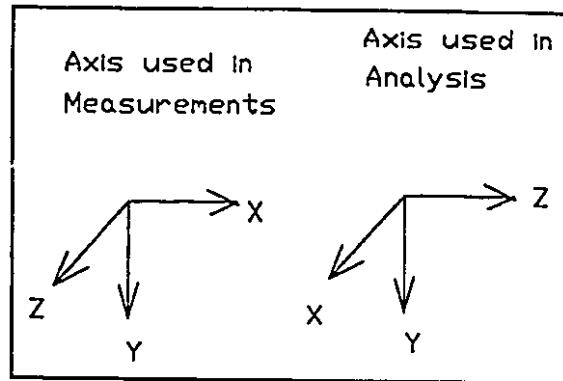
$$U_{r,i} R_i - U_{r,i-1} R_{i-1} = K * R * \Delta R \quad \text{C.4}$$

$$K = - \left[ \frac{\partial U_z}{\partial z} + \frac{1}{R} \frac{\partial U_\theta}{\partial \theta} \right] \quad \text{C.5}$$

## C.2 Check on Irrotationality in Circular Channels

Used two different sets of axis for measurements and to check on irrotationality. Fig. C.3 shows the orientation of the axis.

All analysis was done using rectangular coordinates. Circular coordinates were converted to rectangular coordinates with the help of Figure C.3 Qpro.



A sample of calculations for irrotationality are presented below. The data is for  $Y_e=11.91$  and  $Q=40.71$  l/s. Refer to Table C.2 for data used.

$$\frac{\partial V}{\partial x} = \frac{0.209 - 0}{0.09} = 2.22$$

$$\frac{\partial u}{\partial Y} = \frac{1.47 - 1.65}{0.057 - 0.1147} = 3.13$$

$$\frac{\partial u}{\partial z} = \frac{1.62 - 1.67}{0.0464 - 0.0688} = 2.23$$



Table C.2 Converting cylindrical coord to Reg coord for  $Y_e = 11.91$

Theta	R	Vz	Vr	Vth	V	Z	U	V	W
5	14	1.8	0.18	0.07	13.94678	1.219563		1.8	0.179316
5	13	1.78	0.21	0.07	12.95058	1.132452		1.78	0.209202
5	12	1.74	0.25	0.07	11.95438	1.04534		1.74	0.24905
5	11	1.66	0.3	0.07	10.95818	0.958228		1.66	0.29886
5	10	1.61	0.34	0.07	9.961986	0.871117		1.61	0.338708
						0			
25	14	1.76	0.26	0.17	12.68962	5.913849		1.76	0.235664
25	13	1.73	0.31	0.17	11.78322	5.491431		1.73	0.280984
25	12	1.71	0.36	0.17	10.87681	5.069013		1.71	0.326304
25	11	1.67	0.416	0.17	9.970414	4.646596		1.67	0.377063
25	10	1.63	0.419	0.17	9.064012	4.224178		1.63	0.379782
						0			0
35	14	1.65	0.36	0.19	11.47061	8.026518		1.65	0.294959
35	13	1.63	0.42	0.2	10.65129	7.453196		1.63	0.344118
35	12	1.62	0.47	0.2	9.831956	6.879873		1.62	0.385085
35	11	1.61	0.52	0.2	9.012626	6.30655		1.61	0.426051
35	10	1.6	0.52	0.21	8.193296	5.733227		1.6	0.426051
						0			0
55	14	1.46	0.65	0.26	9.03565	11.46422		1.46	0.373084
55	13	1.53	0.73	0.26	7.461675	10.64535		1.53	0.419002
55	12	1.5	0.8	0.27	6.8877	9.826474		1.5	0.45918
55	11	1.48	0.84	0.28	6.313725	9.007601		1.48	0.482139
55	10	1.47	0.89	0.3	5.73975	8.180728		1.47	0.510838
									0.172193

$$\frac{\partial w}{\partial x} = \frac{0.172-0}{0.09} = 1.19$$

$$\frac{\partial w}{\partial y} = \frac{0.172-0.155}{0.1147-0.1147} = 0.51$$

$$\frac{\partial v}{\partial z} = \frac{0.32-0.29}{0.0507-0.0087} = 0.79$$

Several other points at the same flow rate, and at different flow rates were checked for irrotationality

### C.3 Calculation of Pressure head Field

For calculating pressure head values at the end depth section , the following procedure was followed.

- (1) A position on the water surface point was used as a reference value since  $P/\gamma = 0$  and  $z$  and  $U^2/2g$  were known.
- (2) Used Eq C.6 for calculating the piezometric head for the entire end depth section out side the boundry layer. The end depth sections piezometric head were calculated with the use of Quattro Pro. A sample of the output for a circular channel with  $Y_0 = 6.98$  and  $R=5$  degrees is shown in Table C.3 for

Circular channels and Table C.4 for Trapezoidal channels at  $Y_e=11.91$ .

$$\left[\frac{P}{\gamma}+z\right]_a+\frac{U_a^2}{2g}=\left[\frac{P}{\gamma}+z\right]_b+\frac{U_b^2}{2g} \quad C.6$$

Table C.3 Sample Data for Calculated  $P/\gamma$  values for Circular channel

Theta	R	$U_z$ m/s	$U_r$ m/s	Uth	Y m	$U^2/2g$	$P/\gamma+Z$	$P/\gamma_m$
5	14	1.44	0.31	0.06	0.010	0.119	0.046	0.036
5	13	1.43	0.40	0.05	0.020	0.120	0.045	0.025
5	12	1.38	0.47	0.06	0.030	0.116	0.049	0.019
5	11	1.31	0.53	0.06	0.040	0.109	0.056	0.016
5	10	1.26	0.54	0.06	0.069	0.096	0.069	0

Table C.4 Sample Calculated  $P/\gamma$  values for trapezoidal channel

$U_z$ (m/s)	$U_y$ (m/s)	Y (m)	$U_z/2g$	$P/\gamma$ (m)
1.81	0.022	0.005	0.165	0.069
1.73	0.10	0.03	0.153	0.056
1.67	0.22	0.056	0.145	0.038
1.60	0.26	0.07	0.135	0.03
1.52	0.35	0.115	0.124	0

#### C.4 Momentum Analysis With Calculated Pressure Data for Circular Channel.

The same procedure was used in the momentum analysis as was used with measured data. The only difference was in the method for calculating the incremental areas. Refer to Figure C.4 for definitions of areas used. For the particular case in question, used data for the Flow Rate = 40.71 l/s and  $Y_e = 11.91$  cm.

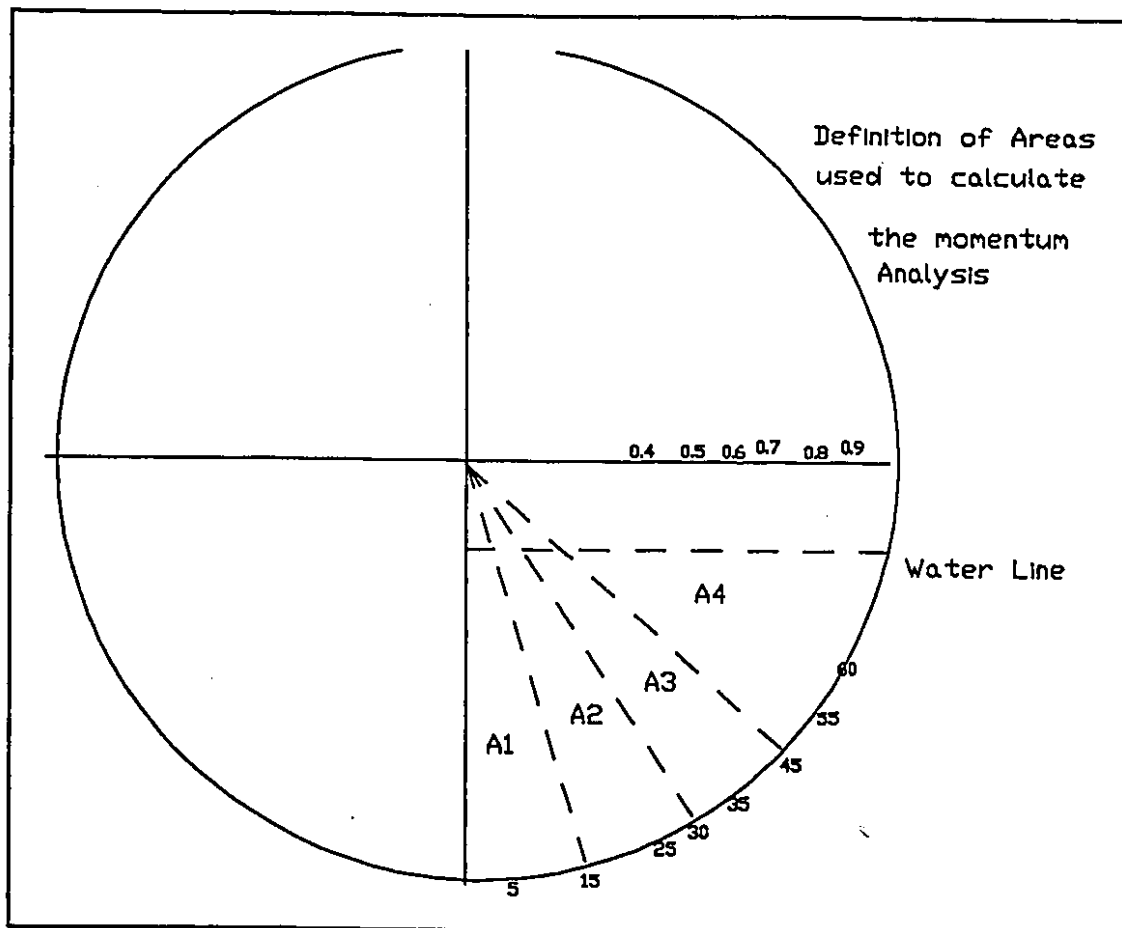


Figure C.4

$$A_1 = 1/2R^2\Theta - (0.031*0.031\tan15)*0.5$$

$$A_2 = 1/2r^2\Theta - (0.031*0.031\tan30)*0.5 - (0.031*0.031\tan15)*0.5$$

$$A_3 = 1/2r^2\Theta - (0.031*0.031\tan45)*0.5 - (0.031*0.031\tan30)*0.5$$

$$A_e = \frac{A_e}{2} - \sum_1^3 A_i$$

When calculating the end depth pressure force, used equations in section C.0. Data in Table C.3 was for calculating the pressure force for  $Ye = 11.91$ .

Table C.5 Pressure Force Calculation

A (m <sup>2</sup> )	P <sub>ave value</sub> (m)	P <sub>e</sub> (N)
0.00281	0.035	0.9715
0.00279	0.027	0.737
0.00281	0.031	0.86
0.0189	0.011	1

For end depth section

$$P_e = 3.56 \text{ N} \quad M_e = \rho Q V \beta = 63.50 * 1.03 = 65.41 \text{ N}$$

$$V_{ave} = 1.56 \text{ m/s (average velocity from laser measurements)}$$

For critical section, use standard formulas for pressure force and momentum and calculation of area..

$$Y_c = 15.88 \text{ cm}$$

$$P_c = 30.74 \text{ N} \quad M_c = 42.40 \text{ N}$$

$$T_c = 73.12 \quad T_e = 72.52$$

### **C.5 Calculating $U_y$ for Trapezoidal channel.**

Followed the same procedure as was used in the circular pipe.

## C.6 Checking Irrrotationality for Trapezoidal Channel

Used same procedure as was used for circular channels

Some sample calculations for  $Y_e=11.65$  (Results shown in Table E.1) are listed below

Location:  $Y1/Y=0.5, x=0, z=0$

$$\frac{\partial u}{\partial Y} = \frac{1.66-1.55}{0.09} = 1.11$$

$$\frac{\partial v}{\partial x} = \frac{0.20-0.0}{0.20} = 1$$

Location:  $Y1/Y=0.5, x=0, z=0$

$$\frac{\partial u}{\partial z} = \frac{1.64-1.56}{0.64} = 1.25$$

Location:  $Y1/Y=0.5, x=0.0476, z=0.015-.03$

$$\frac{\partial w}{\partial x} = \frac{0.10-0.08}{0.015} = 1.35$$

Location:  $Y1/Y=0.3, x=0.05, z=0$

$$\frac{\partial v}{\partial z} = \frac{0.13-0.04}{0.09} = 1$$

$$\frac{\partial w}{\partial Y} = \frac{0.15-0.08}{0.05825} = 1.2$$

Other points were also checked and irrotationality was confirmed. Continuity was also confirmed with several points. One of those points is shown below.

$$\frac{\partial u}{\partial x} = \frac{1.615-1.415}{0.015-0.06} = -4.44$$

$$\frac{\partial v}{\partial y} = \frac{0.13-0.22}{0.034-0.058} = 3.86$$

$$\frac{\partial w}{\partial Y} = \frac{0.10-0.08}{0.0526-0.0286} = 0.83$$

If the resultants all three equations s are added up, the result is 0.25. This value is close enough to zero to satisfy continuity.



## Appendix D

## Uncertainty Analysis

### Uncertainties in measured variables

Discharge using standard (ASME) V-notch	Q ±3%
Depth gauge	Y ±0.1mm
LDA measurements	V ±0.5%
P/γ	±0.5mm

### Trapezoidal positioning

X±1mm
Y±0.1mm
Z±3mm

### Circular Measurements

Θ±1 degree
r±2mm
Z±3mm

### Calculated variables

Y/Y1	
([p/γ+z]-z) from measured P/γ data	±5%
([p/γ+z]-z) from calculated P/γ data	±2.5%
Ur	±5%
Uy(trapezoidal channel)	±5%
α	±2%
β	±2%

### Sample Calculations

In estimating the error for  $U_y$ , the same procedure would apply for  $U_r$  since similar procedures were used.

$U_y$  is a Function of ( $U_z, Y, dy/dz$ )

The uncertainty in  $U_z \gg Y$  or  $dy/dz$  so neglect  
Uncertainty in Y and X with average values  
are  $Y \pm 1\%$  and  $X \pm 5\%$

By the following equation uncertainty in  $dy/dz$  is determined

$$W_r = \sqrt{\left(\frac{1}{100}\right)^2 + \left(\frac{5}{100}\right)^2}$$

$W_r \pm 5\%$  for  $dy/dz$  and  $U_y \pm 5\%$

## Appendix E

Units for all Tables are as follows

- (1) Locations(X,Y,Z) are in cm.
- (2) Velocities are in m/s
- (3)  $P/\gamma$  and manometer readings are in cm of water
- (4) End depth elevations ( $Y_1, Y_{max}$ ) are in cm

Table E.1 Results from laser Readings for Trapezoidal Channel  
 $Y_e=11.65$  and  $Q=40.71$  l/s, Probe at 90 degrees

Y	X	Uz	Ux	P/ $\gamma$
1.43	2.36	1.571	0.09	7.4
3.11	2.36	1.611	0.08	8.4
4.43	2.36	1.620	0.07	9.2
7.21	2.86	1.584	0.08	10.2
7.21	5.26	1.567	0.10	10.1
4.93	4.76	1.615	0.10	9.1
2.33	.86	1.597	0	
4.63	-.64	1.580	0	
6.58	-.14	1.576	0	
3.48	-.14	1.598	0	
1.99	-.64	1.600	0	
.33	-.64	1.61	0	
3.48	4.86	1.646	0.15	7.6
8.49	5.36	1.572	0.08	10.6
Pos2 3.0 cm from $Y_e$				
8.49	5.36	1.56	0.07	11.4
6.48	4.86	1.556	0.08	10.7
4.94	6.16	1.534	0.08	10.1
3.08	4.56	1.550	0.09	9.4
2.29	5.56	1.531	0.11	9.1
Pos3 6.0 cm from $Y_e$				
2.29	5.96	1.415	0.09	10.8
5.59	6.26	1.448	0.09	11.4
8.18	5.36	1.513	0.01	12.1
9.03	5.36	1.5	0.08	12.4
9.03	3.86	1.502	0.09	12.4

Table E.1 C'ont (Probe at 45 degrees)

Y	X	Uz	Uy*	P/y
6.66	8.76	1.483	0.41	9.8
7.24	6.26	1.562	0.36	10.3
3.98	6.26	1.551	0.34	8.5
1.38	6.86	1.23	0.24	6.7
5.94	8.56	1.477	0.36	9.4
7.33	10.16	1.468	0.39	9.9
9.59	9.86	1.474	0.36	11
9.7	12.76	1.414	0.36	11.4
9.63	13.86	1.366	0.38	11.4
8.59	10.86	1.46	0.37	10.7
7.93	12.86	1.367	0.37	10.4
4.44	7.56	1.515	0.37	8.7
4.88	5.56	1.57	0.37	
4.33	8.36	1.44	0.36	
7.56	8.36	1.474	0.29	
1.83	7.36	1.564	0.36	
4.03	9.16	1.552	0.44	
6.29	9.86	1.47	0.35	
3.27	8.16	1.509	0.36	7.8
5.33	9.36	1.489	0.36	8.6
Pos2				
5.08	5.36	1.513	0.27	10.1
4.05	8.26	1.419	0.3	10.3
7.34	7.66	1.438	0.34	10.9
8.54	12.16	1.416	0.31	11.6
6.99	10.16	1.456	0.33	10.8
Pos 3				
10.43	14.16	1.29	0.24	13.1

Table E.1 Probe at 45 degrees con't

10.87	8.36	1.441	0.26	12.9
7.23	3.16	1.505	0.25	12.1
4.54	3.76	1.486	0.23	11.4
4.98	5.56	1.43	0.21	11.5

Table E.2 Velocity at the critical section

Y	X	$(P/\gamma + z + V^2/2g)$	Uz
9.9	4.35	29.4	1.17
7.9	4.35	28.5	1.09
4.9	4.35	27.5	1.00
1.9	4.35	25.9	0.829
0.4	4.35	24.8	0.686
9.9	6.35	29.2	1.155
7.9	6.35	28.3	1.08
4.9	6.35	27.3	0.981
1.9	6.35	25.8	0.816
0.4	6.35	25	0.714
11.9	11.35	29	1.13
9.9	11.35	28.2	1.07
7.9	11.35	27	0.95
4.9	11.35	24.8	0.686

Table E.3 Laser readings For Q=40.71 and Ye=11.91

Pos 1

theta	distance From Center (cm)	Uz	Uth
5	15	1.630	0.070
	14	1.746	0.070
	13	1.743	0.070
	12	1.710	0.070
	11	1.640	0.070
	10	1.610	0.070
25	15	1.580	0.150
	14	1.700	0.170
	13	1.690	0.170
	12	1.675	0.170
	11	1.652	0.170
	10	1.625	0.180
35	15	1.484	0.200
	14	1.632	0.190
	13	1.610	0.200
	12	1.610	0.200
	11	1.600	0.200
	10	1.600	0.210
55	15	1.270	0.250
	14	1.500	0.260
	13	1.510	0.260
	12	1.480	0.270
	11	1.470	0.260
60	15	1.370	0.210
	14	1.490	0.240
	13	1.470	0.250
	12	1.470	0.240
	11	1.450	0.270
70	15	1.300	0.230
	14	1.400	0.200
	13	1.380	0.200
	12	1.360	0.240
75	15	1.130	0.170
	14	1.340	0.190

Pos 2

theta	distance From Center (cm)	Uz	Uth
5	15	1.370	0.000
	14	1.575	0.000
	13	1.640	0.000
	12	1.620	+++++
	11	1.620	+++++
	10	1.610	+++++
55	15	1.219	0.256
	14	1.430	0.200
	13	1.450	+++++
	12	1.480	+++++
	11	1.470	+++++
Pos3			
5	15	1.200	0.000
	14	1.400	0.000
	13	1.490	0.000
	12	1.490	+++++
	11	1.500	+++++
55	15	1.221	0.090
	14	1.360	0.050
	13	1.390	+++++
	12	1.400	+++++
	11	1.400	+++++
Furthest			
	15	1.077	+++++
	14	1.227	+++++
	13	1.364	+++++
	12	1.400	+++++
	11	1.420	+++++
	10	1.420	+++++

Actual

Readings

Ye	V-notch	Ye	Q(cfs)
31.9	40.71	11.91	1.41419
Y1	32.37	Y1	12.38
Y2	32.91	Y2	12.92
Y3	33.54	Y3	13.55

Table E4 Laser Readings for Flow Rate Q=31.74 l/s Ye=9.65

Pos 1			
theta	distance From Center (c)	Ux	Uy*
5	15	1.475	0.078
	14	1.620	0.080
	13	1.630	0.074
	12	1.600	0.060
	11	1.570	0.060
25	10	1.550	0.067
	15	1.480	0.191
	14	1.550	0.158
	13	1.560	0.162
	12	1.540	0.150
35	11	1.530	0.160
	10	1.500	0.160
	15	1.250	0.273
	14	1.500	0.220
	13	1.500	0.220
55	12	1.480	0.230
	11	1.460	0.220
	10	1.430	0.230
	15	1.120	0.270
	14.5	1.270	0.250
47.25	14	1.340	0.270
	13.5	1.320	
	13	1.310	0.270
	12	1.300	0.290
	surface	1.290	
60	15	1.200	
	14	1.260	0.200
	13	1.200	0.230
65	15	1.012	0.180
	14	1.081	0.120

\*Measured at End Depth Section

Pos 2			
theta	distance From Center (c)	Ux	Uy
10	15	1.330	
	14	1.480	0.000
	13	1.510	0.000
	12	1.520	+++++
	11	1.480	+++++
55	10	1.480	+++++
	15	1.110	0.078
	14.5	1.250	0.086
	14	1.330	0.072
	13.5	1.370	0.080
Pos3	13	1.370	
	12.5	1.340	
	12	1.320	
	15	0.900	0.000
	14	1.290	0.000
10	13	1.340	0.000
	12	1.413	+++++
	11	1.400	+++++
	15	0.964	0.026
	14.5	1.150	0.000
55	14	1.218	0.000
	13.5	1.270	0.000
	13	1.320	0.000
	15	0.940	+++++
	14	1.142	+++++
Furthest	13	1.190	+++++
	12	1.270	+++++
	11	1.300	+++++
	10	1.300	+++++
			Actual

Readings		Actual	
Ye	V-notch	Ye	Q(cfs)
30.8	37.1	9.65	1.121217
Y1	31.14	Y1	9.99
Y2	31.73	Y2	10.58
Y3	32.55	Y3	11.4



Table E.5 Pressure Field Data For Circular Pipes

Flow Rate	Z	Y1	P/Y	Ymax
38.5	Center	0.6	1.9	11.61
		1.6	3	
		2.6	3.1	
		3.6	2.9	
		5.6	2.3	
		8.6	0.9	
	40° Line	4.6	1.4	
		5.6	1.3	
		6.6	1	
		7.6	0.8	
		8.6	0.5	
38.3	Center	0.6	2.4	11.11
		1.6	3	
		2.6	3.3	
		3.6	3.2	
		5.6	2.6	
		8.6	1.2	
	40° Line	4.6	1.4	
		5.6	1.6	
		6.6	1.5	
		7.6	1.3	
		8.6	0.9	

Table E6 sample Monometer Data

Monometer	Reading	Actual Reading	P/y	Y1	Ymax
11	10.4	2.9	1.884	1.016	11.03
12	9.7	2.2	2.2	0	
13	10.4	2.9	1.884	1.016	
14	12.3	4.8	1.1932	3.61	
15		-7.5	-15.12	7.62	
21	11.6	4.1	3.084	1.016	11.24
22	11.25	3.75	3.75	0	
23	11.6	4.1	3.084	1.016	
24	13	5.5	1.8932	3.61	
25	16.2	8.7	1.08	7.62	
31	13	5.5	4.484	1.016	11.34
32	12.8	5.3	5.3	0	
33	13	5.5	4.484	1.016	
34	14.5	7	3.3932	3.61	
35	16.5	9	1.38	7.62	
41	15	7.5	6.484	1.016	11.57
42	14.7	7.2	7.2	0	
43	15	7.5	6.484	1.016	
44	16.3	8.8	5.1932	3.61	
45	17.2	9.7	2.08	7.62	
51	17.1	9.6	8.584	1.016	11.93
52	17	9.5	9.5	0	
53	17.1	9.6	8.584	1.016	
54	18	10.5	6.8932	3.61	
55	19.2	11.7	4.08	7.62	
61	19.5	12	10.984		
62	19.2	11.7	11.7		
63	19.5	12	10.984		
64	19.8	12.3	8.6932		
65	20.4	12.9	5.28		
72	20.8	13.3	13.3		
75	21	13.5	5.88		
82	21.5	14	14		
85	21.9	14.4	6.78		
92	22	14.5	14.5		
95	22	14.5	6.88		
e1	22.1	14.6	14.6		

Table E.7 Pressure Field Measurements For Trapezoidal Channel

x	z	Y*	Y	P/y+z	Y1	Y1real	P/y (p/y+z)r
1.36		4.4	0.4	7.55	0.491	10.27176	1.95
		5	1	8.8			3.2
		5.5	1.5	9.7			4.1
		6	2	10.4			4.8
		7.5	3.5	11.9			6.3
		9.5	5.5	13.5			7.9
		11.5	7.5	14.9			9.3
		13	9	15.65			10.05
6.36		4.4	0.4	7.6			2
		5	1	9			3.4
		5.5	1.5	9.7			4.1
		6	2	10.5			4.9
		7.5	3.5	12			6.4
		9.5	5.5	13.5			7.9
		11.5	7.5	14.85			9.25
		13	9	15.7			10.1
8.36		6.5	2.5	9.3			3.7
		7	3	10.5			4.9
		7.5	3.5	11.2			5.6
		8	4	11.9			6.3
		9.5	5.5	13.4			7.8
		11.5	7.5	14.8			9.2
		13	9	15.7			10.1
10.36		8.5	4.5	11.1			5.5
		9	5	12.2			6.6
		9.5	5.5	12.9			7.3
		10	6	13.5			7.9
		11	7	14.4			8.8
		11.5	7.5	14.8			9.2
		13	9	15.7			10.1
							-5.6

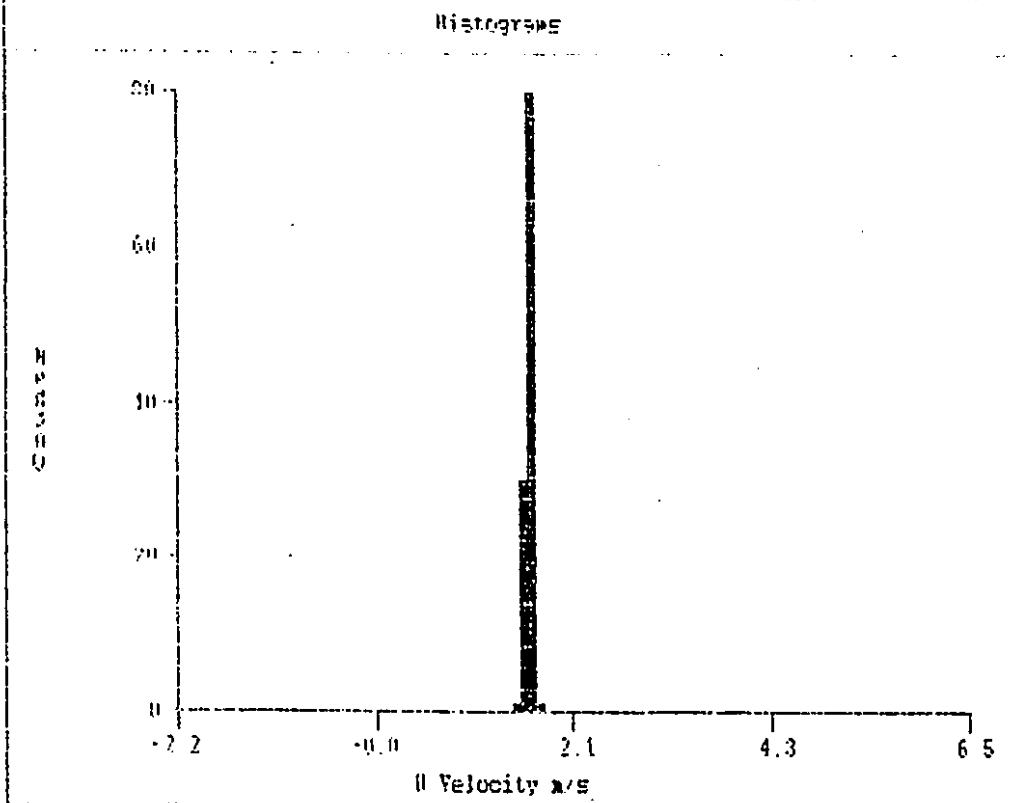
Table E.8  $Q=34.32$  l/s and  $Y_e=9.67$  cm

Mon #	Reading	Actual Reading	Monometer #	Reading	Actual Reading
1	7.8	1.8	31	14	8
2	7.8	1.8	32	14	8
3	7.8	1.8	33	14	8
4	7.8	1.8	34	14	8
5	7.8	1.8	35	14	8
6	7.8	1.8	36	14	8
7			37	14.2	8.2
8	10.4	4.4	38	14.6	8.6
9	11.4	5.4	39	15.4	9.4
10	14.0	8	40	16.6	10.6
11	9.5	3.5	41	16	10
12	9.5	3.5	42		
13	9.5	3.5	43	16	10
14	9.5	3.5	44		
15	9.5	3.5	45	16	10
16	9.6	3.6	46	16	10
17	10.2	4.2	47	16	10
18	11.4	5.4	48	16.8	10
19	12.4	6.4	49	16.8	10.8
20	15.2	9.2	50	17.2	11.2
21	11.6	5.6	51	17.6	11.6
22	11.6	5.6	53	17.6	11.6
23	11.6	5.6	55	17.6	11.6
24	11.6	5.6	56	17.6	11.6
25	11.6	5.6	57	17.6	11.6
26	10.8	4.8	58	17.6	11.6
27	12.0	6	59	17.6	11.6
28	12.8	6.8	60	18	12

Table E.8 Con't

29	13.2	7.2	u1	18.8	12.8
30	16	10	u2	18.8	12.8

KARLIV.004 10-5-93 01:56:54 X: 110 000 mm Y: 0 000 mm Z: 0.000 mm  
Mean: 1.660 RMS: 0.0379 Skew: 0.1344 Flat: 7.0067



CARLY 001 19-5-93 01:40 10 X: 0 000 km Y: 0 000 km Z: 0 000 m  
 Resn. 1.6842 RMS: 0.0895 Elev: 0.0760 Flt: 3.7878

